

*Soft Elastic Fibrous Polyurethane
based Scaffolds for Muscle Tissue
Engineering*

DISSERTATION

zur Erlangung des akademischen Grades eines
Doktors der Naturwissenschaften (Dr. rer. Nat.)
im Promotionsprogramm „Polymer Science“
in der Bayreuther Graduiertenschule für Mathematik und
Naturwissenschaften
(BayNAT)
der Universität Bayreuth

vorgelegt von

Juan Manuel Uribe Gómez

aus Bogotá, Kolumbien

Bayreuth, 2021

The work presented in this dissertation began in January 2018 in Biofabrication group at the university of Bayreuth and was finished in July 2021 under supervision of Prof. Leonid Ionov.

Date of submission: 09.11.2021

Date of defense: 09.03.2022

Acting Director: Prof. Dr. Hans Keppler

Doctoral committee:

Prof. Dr. Leonid Ionov	(reviewer)
Prof. Dr. Seema Agarwal	(reviewer)
Prof. Dr. Holger Ruckdäschel	(chairman)
Prof. Dr. Ruth Freitag	

Dedication / motto

Perdida la esperanza
Perdida la ilusión
Los problemas continúan
Sin hallarse solución.

Nuestras vidas se consumen
El cerebro se destruye
Nuestros cuerpos caen
rendidos
Como una maldición.

El pasado ha pasado
Y por él nada hay que hacer
El presente es un fracaso
Y el futuro no se ve...

Eskorbuto

Table of Contents

Summary.....	1
Zusammenfassung.....	4
1. Introduction.....	9
1.1 Muscle tissue.....	9
1.2 Biofabrication.....	11
1.2.1 Biofabrication of tubular structures.....	12
1.2.2 Fabrication of tubular structures.....	12
1.3 Fiber formation for cell guidance.....	15
1.3.1 Uniaxial fiber formation techniques.....	15
1.3.2 Commonly used material for fibers production.....	16
1.3.3 Parameters of Melt electro-writing.....	17
1.3.4 Parameters of Touch-spinning.....	19
1.4 Conclusion.....	22
2. Aims.....	24
3. Synopsis.....	25
3.1 Shape-Morphing Fibrous Hydrogel/Elastomer Bilayers.....	25
3.2 Soft Elastic Fibrous Scaffolds by Touch Spinning.....	26
3.3 Touch-spinning poly(ester-urethane) elastomer synthesized in solvent-free conditions.....	27
4. Literature references.....	29
5. Publication list.....	38
6. Individual contribution to joined publications and manuscripts presented here.....	39
7. Manuscripts.....	41
Manuscript 1.....	41
Manuscript 2.....	57
Manuscript 3.....	83
8. Conclusion.....	106
Acknowledgements.....	107

Summary

Tissue engineering, the multidisciplinary field of medical, material and engineering sciences, attempts to meet the goal of increasing life expectancy and quality of individuals that require a tissue or organ transplant. Tissue engineering could improve the accessibility of these implants, as well as the acceptance of the patient's immune system. However, the fabrication of complex organ structures that consist of specific, uniaxial, and complex cell patterning remains as a challenge. With the aim to contribute with solutions for these problems, biofabrication emerged as an innovative science for production of tissues and organs. By definition, biofabrication is "the production of complex biologic products from raw materials such as living cells, matrices, biomaterials, and molecules" [1]. As a novel technique part of biofabrication emerged 4D biofabrication, that is the fabrication of complex 3D structures by shape-transformation of constructs made by stimuli-responsive materials. One of the main advantages of this technique is that allows high resolution and does not require any sacrificial material.

The specific aim of this thesis was to develop new biocompatible, biodegradable polymeric materials suitable for biofabrication with specific mechanical properties for muscle tissue engineering. It is envisioned that those materials must be able to provide high processability in terms of fibers production, and suitable topography to promote cell alignment and growth, and elasticity is needed to emulate muscle behavior. The novelty of this work is the investigation of a family of different polyurethanes in terms the cell-material interaction, biodegradability, and biocompatibility.

Two different methods for fiber production were tested by using different synthesized thermoplastic elastomers. The first one, melt electro-writing (MEW), and the second one, touch spinning (TS). In the first approach MEW fibers were deposited directly on top of self-folding polymer. Self-folding polymer-based systems are polymeric actuators capable to change their shape responding to external stimulus such as pH, temperature, or immersion in water, etc. Here, crosslinked polymer was used to generate self-rolling tube-shape structures with fibers inside. The MEW fibers, after shape-transformation, remains inside the tubular construct providing structure and enhance cell alignment. The second approach consist in the fabrication of fiber scaffolds

by using TS where the cells were seeded on the top of the fibers to provide the pattern and cell support.

First, we established an approach for the fabrication of shape-changing bilayered scaffolds, which allow the growth of aligned skeletal muscle cells, using a combination of 3D printing of methacrylated hyaluronic acid (HA-MA) hydrogel, melt electrospinning writing (MEW) of thermoplastic polycaprolactone-polyurethane elastomer (PCL-PU), and further shape transformation (**Figure 1**). The combination of the selected materials and fabrication methods allows several important advantages such as biocompatibility, biodegradability, and suitable mechanical properties like the important components of extracellular matrix (ECM), which allow proper cell alignment and elasticity. Myoblasts demonstrate excellent viability on the surface of the shape-changing bilayer, where they occupy space between fibers and align along them, promoting efficient cell patterning inside folded structures. The bilayer scaffold can undergo a controlled shape transformation and form multilayer scroll-like structures with cells encapsulated and aligned inside. Overall, the importance of this approach is the fabrication of tubular constructs with a patterned interior that can support the proliferation and alignment of muscle cells for muscle tissue regeneration [2].

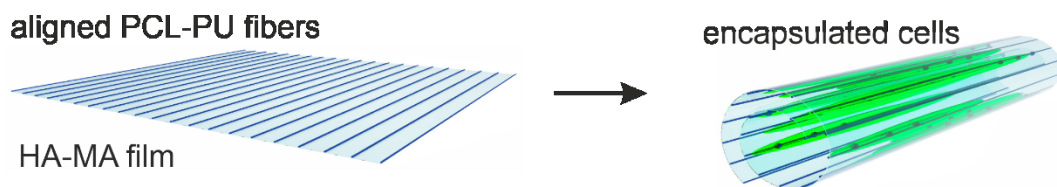


Figure 1. Scheme of fabrication of tubular structures with MEW fibers and cells inside

Furthermore, with the aim to fabricate highly aligned soft elastic fibrous scaffolds for muscle tissue engineering using a new technique, touch spinning, utilizing a family of thermoplastic elastomers (**Figure 2**). A family of polyester–polyurethane soft copolymers based on polycaprolactone and poly(1,4-butylene adipate) with different molecular weights and different chain extenders such as 1,4-butanediol and polyethylene glycols with different molecular weight were synthesized. By varying the molar ratio and molecular weights between the segments of the copolymer, different physicochemical

and mechanical properties were obtained. The polymers possess elastic modulus in the range of a few megapascals and good reversibility of deformation after stretching. The combination of the selected materials and fabrication methods allows several advantages such as biocompatibility, biodegradability, suitable mechanical properties (elasticity and softness of the fibers), high recovery ratio, and high resilience mimicking the properties of the extracellular matrix of muscle tissue. Myoblasts demonstrate high viability in contact with the scaffolds, where they align along the fibers, allowing efficient cell patterning on top of the structures. Altogether, the importance of this approach is the fabrication of highly oriented fiber constructs that can support the proliferation and alignment of muscle cells for muscle tissue engineering applications [3].

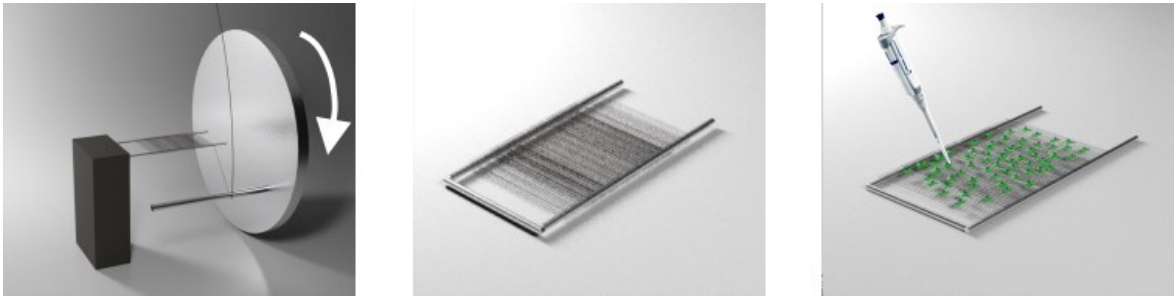


Figure 2. Scheme of fabrication of touch spinning fibrous scaffolds and seeding cells on top of the scaffold

Overall, through this work, it was shown that using novel 4D biofabrication techniques we could engineer uniaxial scaffolds and induce the alignment of skeletal muscle cells. In particular, the thermoplastic-polyurethane-based elastomers are promising for use as shape-morphing materials for muscle microtissue formation.

Zusammenfassung

Der Forschungsbereich der Gewebezüchtung (engl.: Tissue Engineering, TE) entstand als interdisziplinäres Feld zwischen Medizin und Materialforschung, mit dem Ziel die Lebenserwartung und Lebensqualität von Erkrankten zu verbessern und die steigende Diskrepanz zwischen Organspendern und benötigten Spenderorganen zu verringern. Eins der größten Probleme der Gewebetransplantation, die Abstoßung des Spenderorgans durch das Immunsystem des Patienten, soll durch Tissue Engineering gelöst werden. Auch wenn Tissue Engineering verspricht, viele aktuelle Probleme zu lösen, ist die Herstellung von komplexen organischen Strukturen mit spezifischer Zellanordnung und Ausrichtung immer noch eine große Herausforderung.

Darauf folgend wurde die Biofabrikation ins Leben gerufen um als innovatives Forschungsfeld, neue Lösungen für die Produktion von Gewebe und Organen zu bieten. Definiert wird die Biofabrikation als „die Herstellung komplexer biologischer Produkte mit Hilfe von Ausgangsmaterialien wie lebenden Zellen, Matrizen, Biomaterialien und Molekülen“ [1]. Als Ableger der Biofabrikation entwickelte sich die 4D Biofabrikation, welche die Herstellung komplexer 3D Strukturen durch die Verwendung von formändernden Materialien ermöglicht. Die größten Vorteile dieser Methode sind die hohe Auflösung und die Unabhängigkeit von Stützmaterial.

Das Ziel dieser Arbeit war die Entwicklung neuer, biokompatibler und bioabbaubarer Polymere, die in der Biofabrikation von Muskelgewebe eingesetzt werden können und die erforderlichen mechanischen Eigenschaften aufweisen. Diese Polymere müssen mehrere Voraussetzungen erfüllen, einfache Prozessierbarkeit für eine gute Faserproduktion, Elastizität um Muskelgewebe zu simulieren und eine geeignete Topografie, die eine Ausrichtung der Zellen unterstützt. Das Novum in dieser Arbeit ist die Untersuchung mehrerer neuer Polymere aus der Familie der Polyurethane unter Berücksichtigung der Zell-Material Interaktion, Bioabbaubarkeit und Biokompatibilität.

Zwei verschiedene Methoden zur Faserherstellung wurden für die unterschiedlich synthetisierten thermoplastischen Polymere angewendet. Die erste Methode ist elektrostatisch unterstütztes Schreiben mit Polymerschmelzen (engl.: melt electrospinning writing, MEW), die zweite ist Verspinnen durch Berührung (engl.:

touch spinning, TS). Im ersten Ansatz werden durch MEW erzeugte Fasern direkt auf dem formändernden Polymer abgelegt. Formändernde Polymersysteme sind gekennzeichnet durch polymere Aktuatoren die durch externe Stimuli, wie Änderung des pH-Werts, der Temperatur oder durch Immersion in Wasser, in der Lage sind ihre Form zu verändern. In dieser Arbeit wurde ein vernetztes Polymer verwendet um eine sich selbst zusammenrollende Röhre mit Fasern im Inneren zu erschaffen. Die MEW Fasern bleiben auch nach dem Zusammenrollen im Inneren der Röhre erhalten um Struktur zu geben und die Zellorientierung zu verbessern. Im zweiten Ansatz wurden Fasermatten mittels TS hergestellt und anschließend auf der Oberfläche mit Zellen in definierten Mustern besiedelt

Zuerst entwickeln wir einen Ansatz für die Herstellung von formändernden Doppelschicht Gerüsten, die ein ausgerichtetes Wachstum von Skelettmuskelzellen erlauben. Dazu wird eine Kombination von 3D Druck von Hyaluronsäure (HA-MA) Hydrogel, MEW von thermoplastischen Polycaprolacton-Polyurethan Elastomeren (PCL-PU), und zusätzliche induzierte Formänderung durch äußere Stimuli verwendet (Abbildung 1). Die Kombination der ausgewählten Materialien und Prozessierungsmethoden generiert mehrere Vorteile, unter anderem Biokompatibilität, Bioabbaubarkeit und mechanische Stabilität, vergleichbar zur Extrazellulären Matrix (ECM), die eine Zellausrichtung und gleichzeitige Elastizität erlaubt. Myoblasten zeigen eine exzellente Viabilität auf der Oberfläche der formändernden Doppelschicht, wo sie den Raum zwischen den Fasern besetzen und sich daran ausrichten, was zu einer effizienten Verteilung der Zellen im Inneren der gefalteten Strukturen führt. Die Form des Doppelschicht Gerüsts kann kontrolliert verändert und zu einer mehrlagigen zylindrischen Struktur aufgerollt werden, in deren Inneren sich ausgerichtete Zellen befinden. Zusammengefasst ist das Hauptziel dieses Ansatzes die Herstellung von rohrförmigen Konstrukten, die eine definierte innere Struktur besitzen und die Proliferation und die Ausrichtung von Muskelzellen für die Muskelzellregeneration unterstützen [2].

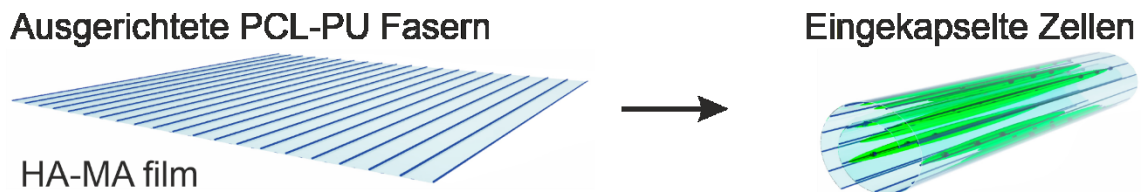


Abbildung 1. Schematische Darstellung der Herstellung von rohrförmigen Strukturen mit MEW Fasern und Zellen im Inneren

In dieser Studie wurde ein Ansatz für die Herstellung von präzise orientierten, weichen und elastischen Fasergerüsten durch TS erarbeitet und anhand eines Vertreters aus der Familie der thermoplastischen Elastomere auf die Anwendung zur Herstellung von Muskelgewebe hin untersucht (Abbildung 2). Eine Familie von weichen polyester-polyurethan Copolymeren, basierend auf Polycaprolacton und Poly(1,4-butylene adipate) mit verschiedenen Molekulargewichten und verschiedenen Kettenverlängerern, wie 1,4-Butanediol und Polyethylenglykol mit unterschiedlichen Molekulargewichten, wurden synthetisiert. Durch Anpassung der molaren Verhältnisse und des Molekulargewichtes zwischen den einzelnen Segmenten des Copolymers konnten verschiedene physikochemische und mechanische Eigenschaften erzeugt werden. Die Polymere besitzen Elastizitätsmoduli in der Größenordnung einiger Megapascal und eine gute Erholung der Deformation nach Streckung. Die Kombination der ausgewählten Materialien und Herstellungsmethoden ergibt diverse Vorteile wie Biokompatibilität, Bioabbaubarkeit, gute mechanische Eigenschaften (Elastizität und Weichheit der Fasern), gute Erholung nach Stress und hohe Belastbarkeit, was den Eigenschaften der Extrazellulären Matrix von Muskelgewebe entspricht. [3].

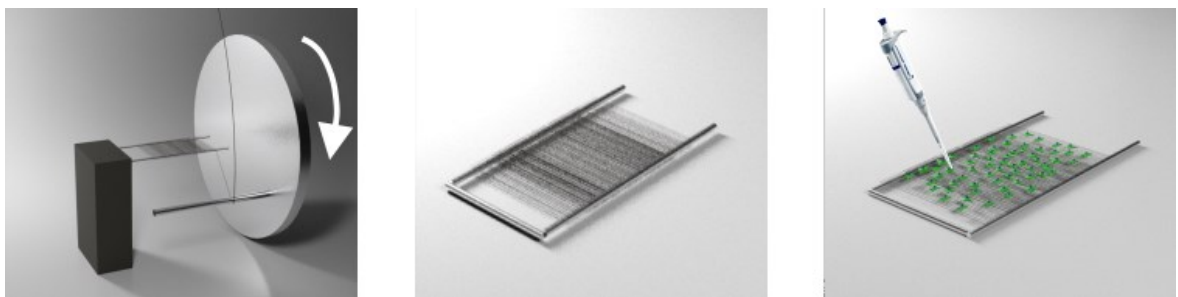


Abbildung 2. Schematische Darstellung der Herstellung von Fasergerüsten mittels Touch Spinning und Besiedelung mit Zellen auf der Oberfläche

Alles in allem konnte in dieser Arbeit gezeigt werden, dass die entwickelten Materialien und Verarbeitungsprozesse für die Herstellung von uniaxial orientierten Gewebekonstrukten mit Skelettmuskelzellen geeignet sind. Es konnte gezeigt werden, dass thermoplastische, auf Polyurethan basierte Elastomere das Potenzial haben in der Muskelgeweberekonstruktion eingesetzt zu werden und durch ihre induzierbare Formänderung auch muskuläre Mikrostrukturen formen können.

1. Introduction

1.1 Muscle tissue

Decades of research in skeletal muscle physiology have provided deep insights into the structural and functional complexity of anatomical muscle tissue, from macro- to nanoscale. Designed to accomplish the tasks of contraction, force, movement and structural body support, skeletal muscle can be viewed as a biomechanical device with diverse, carefully synchronized components. These components include nerves for impulse transmission, vasculature for oxygenation, and homogeneous distributed apparatus for regulation and metabolic activity for maintaining cellular homeostasis [4]. Muscles are divided in three types: cardiac, skeletal, and smooth muscle. Cardiac muscle consists of a set of self-stimulating, non-fatiguing, highly organized muscle cells with an intermediate energy requirement for function. Skeletal muscle consists of a set of nerve supplied, voluntary muscle cells that present fatigue and high energy requirements. Smooth muscle consists of mononucleate fibers that are not striated. A quick look at the cellular and molecular structure allows to appreciate the composition complexity, the specific structure and function of striated muscle types (cardiac and skeletal) that is designed to accomplish the contraction, force, and movement. Striated refers to the arrangement of cytoskeletal proteins that appear as striations in the muscle fibers when viewed at the microscopic scale. Skeletal muscle is an aligned tissue that contains several bundles of muscle fibers (myofibers) with a specific arrangement. Each myofiber (containing several myofibrils), represents a muscle cell with its basic cellular unit named sarcomere. Bundles of myofibers form the fascicles, and bundles of fascicles form the muscle tissue, with each layer successively encapsulated by the extracellular matrix (ECM) and supported by the cytoskeletal networks [5].

ECM is the extracellular part of the tissue that usually provides structural support to the cells and additionally performs various important functions. ECM is composed of an interlocking mesh of collagen, glycosaminoglycans and fibrous proteins which promote and benefit the cell adhesion. The elastin in ECM provides elasticity to tissues, allowing it to be stretched when needed and to return to its original shape. The nonlinear elasticity of biopolymers can affect cell structure and function [6, 7], and biomaterials that would

qualify to replace elastin should also have a nonlinear elastic behavior. Moreover, the topology of ECM has also been found to affect cell structure, functionality, and physiological responsiveness. An ideal tissue repair material should be able to mimic the mechanical and biological functionality of the ECM [8, 9].

Skeletal muscle is highly vascularized and innervated tissue and embedded with components of the metabolic and regulatory machinery, that supports and transfer efficiently energy production and cellular homeostasis (Figure 3). Highly coordinated activity between all the components is essential for keeping the healthy state of muscular tissue and the motor activity. Any perturbations (e.g., genetic, or environmental) to this delicate equilibrium, result in health and function loss of muscle, typically characterized by muscle fiber loss, reduced motor output and in some cases death [4].

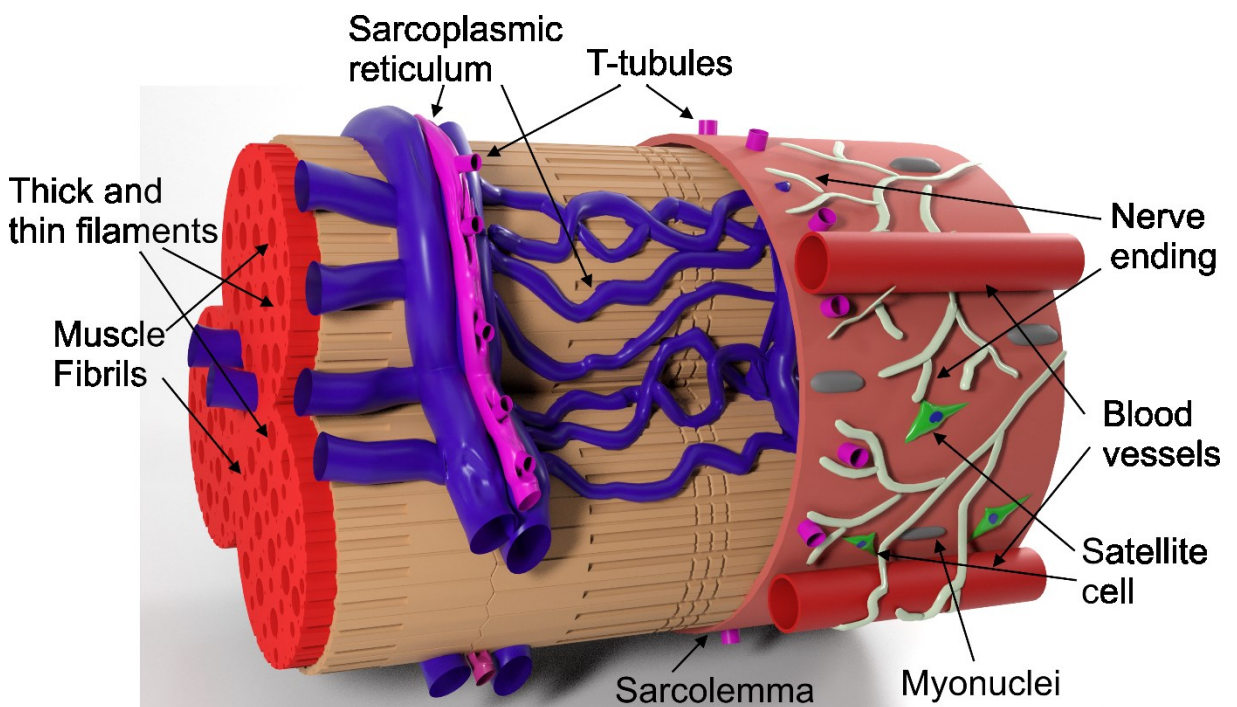


Figure 3. Schematic representation of skeletal muscle fiber—single mature muscle fiber as a bundle of myofibrils, encased by the sarcolemma. The sarcoplasmic reticulum enmeshes fibrils with transverse (T) tubules intersecting them. Bundles of myofibers form fascicles, which further group together to form the muscle tissue. Satellite cells reside along the host muscle fiber, directly above the sarcolemma under the basal lamina of muscle and in proximity of myonuclei. Innervating nerve fibers and local capillaries extend along the length of the muscle fiber [4].

1.2 Biofabrication

The term biofabrication is extensively used by many scientific communities and disciplines to describe different processes and phenomena. There have been several attempts to formulate a clear definition of biofabrication that would accept its use within these different areas. One example is “*Regardless of the slight emphasis of the definitions, there are several unique features of Biofabrication: first, the building blocks are cells or biologics; second, the fabrication processes are bio-inspired or bio-friendly; and finally, the products are biological systems, models or devices with transformative properties*” [10]. This definition does not include some biological processes such as biomineralization, because these are considered as not bio-inspired but natural processes. Hence, since biofabrication intrinsically means to fabricate products, it could broadly be described as “*a process that results in a defined product with biological function*”. This would involve all the different and novel aspects of biofabrication; however, it would also include several other fields of research and natural processes. Taking into account the dynamic and evolving research activities and developments of the different technological aspects, J. Groll *et al.* suggest a definition of biofabrication for tissue engineering and regenerative medicine as “*the automated generation of biologically functional products with structural organization from living cells, bioactive molecules, biomaterials, cell aggregates such as micro-tissues, or hybrid cell-material constructs, through Bioprinting or Bioassembly and subsequent tissue maturation processes*” [11].

There are two major approaches for creating bio-scaffolds. In the first approach the cells and material are processed together, allowing high control on terms of cell distribution among the scaffolds. Furthermore, it is possible to realize several kinds of co-culture of cell lines, increasing its applications potential. Finally, it offers the possibility to generate micro- and macro-architectural such as vascular networks and precise positioning of cell clusters. In the second approach, the scaffold is generated first and then cells are seeded onto them. Generally, the bio-scaffolds are made by biodegradable and biocompatible polymers, synthetic or natural, which allow the cell attachment and proliferation. However, this approach also presents disadvantages, two of the main disadvantages are the nonhomogeneous cell distribution inside the scaffolds, due to the slow cell migration, and the difficulty to recreate complex inner microstructural features [12].

1.2.1 Biofabrication of tubular structures

With the aim to mimic the ECM, one of the big challenges is to mimic natural tubular structures present in the human body, such as veins, arteries, osteons, etc. Structures that show in their architectures high ordination and composition in terms of cell types, and chemistry [13] as well as different diameters that can be from micrometers to few centimeters.

1.2.2 Fabrication of tubular structures

There are several methods for the fabrication of scaffolds, both with cells (vital) and without cells (non-vital). One of the most promising methods for preparing non-vital, 3D scaffolds is 3D printing, which allows the construction of complex structures using computer aided design, which can be seeded with cells post-fabrication. Fairly recently, the evolution of the method has led to 3D bio-printing, which is 3D printing of non-vital and vital materials together [11, 13, 14]. Both methods are based in automatized deposition of controllable amounts of materials. Even though they offer many advantages such as local deposition, multi-materials extrusion, automatization, and individual adjustments, they still presenting intrinsic limitations, such as lack of cues for cell orientation and mechanical anisotropy. To resolve some of these drawbacks, several fabrication methods had been developed, all of them with advantages and disadvantages. For example, although digital light processing–stereolithography allows good resolution, it is not well compatible with printing of cells. Two-photon polymerization allows even higher resolution in the order of nanometers, however, does not allow patterning of cells of different types and mixing of different cell-containing materials is highly challenging. Extrusion can achieve average resolutions around 100 μm , however, these vary greatly depending on the printed material, considering that printing conditions can damage cells. Melt electrospinning allows very high resolution [15], down to approximately 1 μm , but it is not compatible with cells because high temperature and high voltage are used. Ink-jet printing allows high resolution (10–20 μm) but it operates with diluted cell suspensions, which require mechanical stabilization. Thus, there is always a gap between

resolution, compatibility with cell deposition, cell viability and mechanical stability, and no one of the existing 3D printing/bioprinting methods can provide all advantages [12, 13, 16].

Notwithstanding the tremendous potential of the printing techniques toward the biofabrication and the recently achieved progress in 3D printing, one of the most challenging current approaches is the printing of tubular and vascular structures [17]. For instance, the printing of vascular system or microfilaments of muscles is a major problem, limiting the use of 3D printing for complex tissues or organs [18-20]. Tubular structures are typically achieved through either direct or indirect bioprinting techniques. Direct bioprinting results in interconnected internal channels of hollow structures [20-23], however, the tubular structures obtained through this method presents high wall thickness and requires high shear forces that tend to damage printed cells. Indirect bioprinting, on the other hand, uses the printing of sacrificial templates that later needs to be removed to generate the channels in the construct [24-26].

Although some approaches of tubular structure bioprinting have been developed, they still lack resolution and versatility, which is high enough to produce tubes with very small internal diameters and sufficient complex architecture in a controlled manner to fulfill all the intricate tissue and organ engineering demands. However, the formed structures are not tight. Development of methods for fabricating shape-changing structures, which form tightly tube-and sphere-connected structures and multiple connected functional tubes, is essential for the fabrication of multiple tissues and organs. Fabrication of tubes can be achieved by using 3D Printing, which could be either as low viscosity inks/bioinks or inside self-healing gel that provides support for printed structures [27].

4D biofabrication, a recently developed technology with the intrinsic ability of shape transformation upon response to stimuli, has shown great potential for the fabrication of tubular structures for tissue engineering [28-31]. Different biofabrication techniques can be used to achieve 4D biofabrication such as solvent casting, spin/dip coating, photolithography, printing, etc. by using shape transformation and is not limited exclusively to shape transformation of 3D printed/bioprinted objects. The term 4D is used because of the time necessary to shape transformation, moreover, the fourth dimension contributes and plays a big role in this fabrication technique. This technology offers great

potential for the creation of advanced, sophisticated and dynamic structures with high resolution, impossible to achieve by using other biofabrication techniques. The main concept of 4D biofabrication of tubular structures is illustrated in Figure 4. There are three general techniques to obtain cell-laden 4D biofabricated structures. In the first approach (Figure 4a), a 3D construct is first fabricated and then its shape is changed, followed by the cell deposition. In the second approach (Figure 4b), a 3D construct is fabricated and then the cells are seeded on top of the structure, followed by shape transformation. In the third approach (Figure 4c), the 3D construct is fabricated with cells, followed by shape transformation. Every approach presents advantages and disadvantages depending on the applications [12].

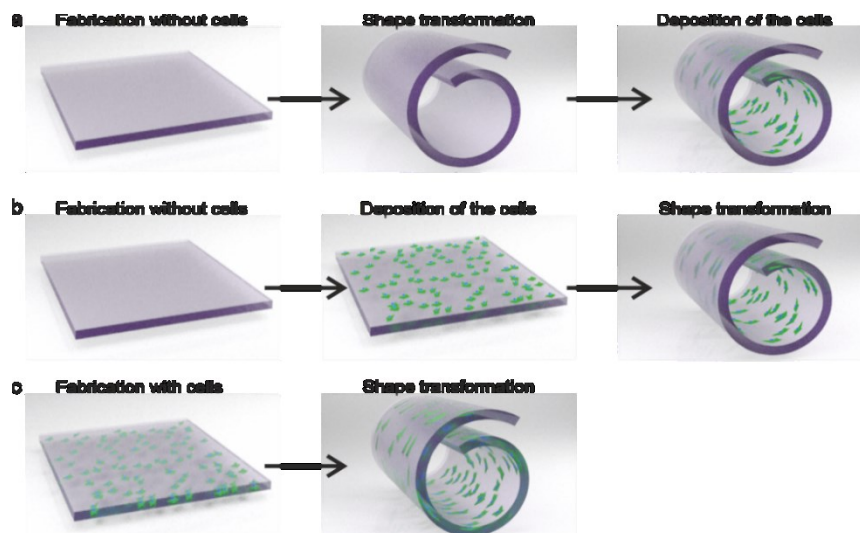


Figure 4. 4D biofabrication of tubular structure: a) fabrication of non-vital construct, shape transformation, and deposition of cells inside the construct (cells in green); b) fabrication of non-vital construct, deposition of the cells on top of the construct, and shape transformation of the cell-filled tubular structure; c) fabrication of the vital construct with cells encapsulated inside, and its shape transformation [6, 12].

Although shape transformation allows the fabrication of a variety of complex structures, tubes and spheres are the two main geometric forms needed in tissue engineering. The entire vascular system is based on the tubular elements and many glands are based on a combination of spherical and tubular elements. One of the main features of 4D biofabrication is the ability to form a variety of hollow shapes. For instance, tubes can be formed by rolling rectangular films (Figure 5a), and spherical shapes can be formed by folding films in the shape of a lotus flower (Figure 5b). Furthermore, more complex

combinations of 2D films can result in complexes of tubes or tubes with valve-like elements (Figure 5c,d) [32-34].

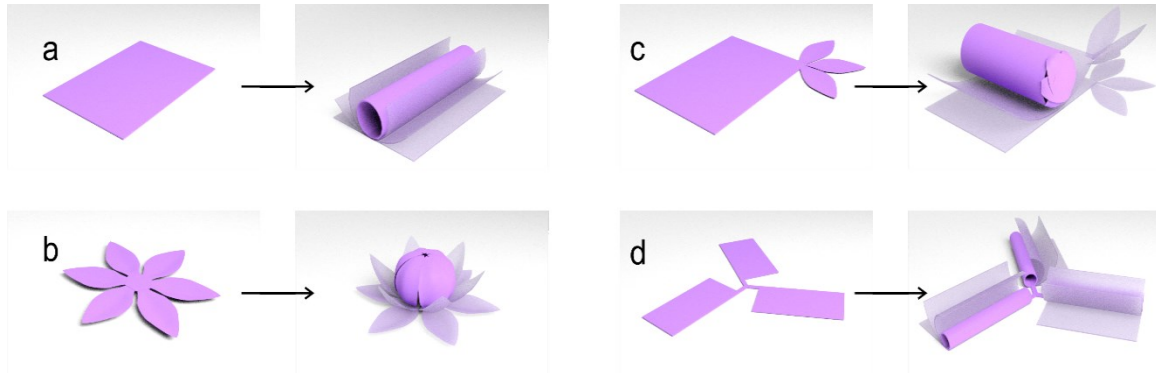


Figure 5. 4D biofabrication of different 3D forms by shape transformation of 2D layers with different shapes: a) formation of tubes by folding of rectangular film; b) capsule formation by folding of lotus flower-like film; c) combination of rectangular and lotus flower-like elements allows the fabrication of more complex alveolar structures; d) branched tubular structure allows obtained by the folding of interconnected films [12, 32-34].

1.3 Fiber formation for cell guidance

Fibrous scaffolds can be used to provide cell guidance and patterning, the main characteristics of suitable fibrous scaffolds are the cell attractive and biocompatible chemistry surface, as well as the porosity and mechanical properties. In recent years many techniques for fibers production have emerged for micro and nano-fibers production with the aim to mimic the structure of ECM.

1.3.1 Uniaxial fiber formation techniques

The fiber formation process is called spinning and can be divided into several types: wet, gel, blow, melt and electrospinning. Small diameter fibers are commonly fabricated using solution electrospinning, but aiming for larger fibers involves fabrication techniques as melt spinning and fused deposition modeling (FDM) [35-37].

Melt electro-writing, or melt spinning, is one of the electrohydrodynamic based additive manufacturing (AM) techniques that was first described in a 1936 patent [38]. It is used to fabricate fibers at micron and sub-micron scales [39]. Figure 6 displays the MEW device along with its main components, including pneumatic or air pressure, a translating spinneret housing the polymer melt that is heated by the copper coils or heater, applied

voltage, and the collector, connected to the ground, which could be of planar or cylindrical configuration. The key parameters applied are pressure and voltage, polymer melt temperature, set temperature, volumetric flow rate, tip-to-collector distance, and the translational speed. The key measurements are fiber diameter and the alignment of fibers which are affected by the air pressure and critical translational speed (CTS), respectively [40-42].

1.3.2 Commonly used material for fibers production

Melt electrowriting (MEW) has been developed as a technique that allows a high precision of fiber deposition, allowing programmed patterns as requirement for the fabrication of complex patterned scaffolds with controlled topography. Many recent studies have been performed using the MEW technique to spin fibers from various thermoplastic materials with low melting points such polycaprolactone [41], poly hydroxymethylglycolide-co- ϵ -caprolactone [43], polylactide-poly-(ethylene glycol) [44], and most recently Poly(vinylidene fluoride-co-trifluoroethylene) [45] among others. Although the MEW scaffolds can be used to print complex structures with varied patterns and high resolution, it cannot be used to print cell-laden structures alone [46, 47], but in combination with 3D printing [48, 49]. The fabrication of complex multilayered 3D structures with aligned cells can be addressed using 4D biofabrication. For example, the biofabrication of skeletal muscle microtissue using shape-changing double-layer electrospun mesh- polycaprolactone (PCL)/methacrylated alginate (AA-MA) [50]. Aligned PCL nanofibers were able to support the alignment of myoblasts cells, whereas the electrospun mesh still lacked porosity, proper size and contained random fibers. Moreover, the bottom layer was made of electrospun random AA-MA fibers, which did not induce cell adhesion. The main problem with the typically used PCL for fibers production is that they are stiff and plastic semicrystalline polymers [51-53]. The PCL fibers cannot be deformed by cells even via buckling mechanism upon cell contraction because the fibers generate a highly dense network with small mesh size [54]. The second component of the bilayer was alginate, which is biodegradable but not a component of ECM [50].

1.3.3 Parameters of Melt electro-writing

Various configurations of thermoplastic polymers are delivered to the charged nozzle, or translating syringe or spinneret, which is positioned over a stage connected to the ground, via applying air pressure, delivering the polymer melt to the charged nozzle and directly writing it on the collector plate as a molten fluid column. The heater heats the polymer converting it to a melt. Then the voltage is applied to the syringe creating a potential difference between the grounded collector and spinneret, causing the charges within the melt to separate. The voltage is applied to prevent Raleigh-Plateau instabilities. The charges with the same polarity travel towards the fluid's exposed bead surface increasing the surface charge density leading to the Taylor-cone projection. The electric field at the tip pushes out the melt at high electrostatic stresses overcoming the Taylor-cone and ejecting the polymer melt towards the collector plate connected to the ground. Once the polymer melt reaches the collector plate, it solidifies into a continuous filament. Once the speed of the spinneret is higher than the CTS, corresponding to the velocity of the polymer jet and collector, the MEW of direct fibers is achieved [55].

A polymer melt only requires enough cooling to solidify during direct-writing. This happens after, or just prior to, the molten jet touching the collector. This essentially depends on the processing parameters, and there is a minor embossing underneath many MEW scaffolds from the collector [41]. In addition, electrohydrodynamic quenching occurs during melt electrospinning, where the movement of charged water vapor induces a cooling effect over the jet [56]. Figure 6 shows the patterns from a molten jet, demonstrating its liquid properties. When the spinneret (or collector) speed is increased further, straight lines of fibers are possible (Figure 3a) that accurately are able to stack upon each other [41]. One important aspect of MEW is introduced here: the term “critical translation speed” (CTS). The CTS is the speed at which the spinneret (or collector) matches the jet, and a linear fiber is produced. With this repeated layering approach, a fibrous scaffold with microscale features can be fabricated (Figure 6a-c).

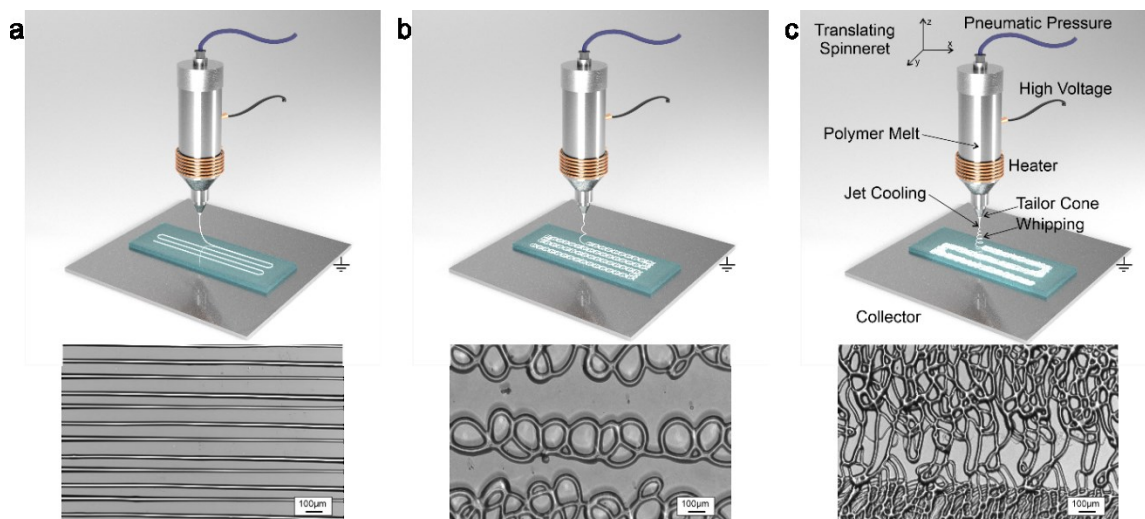


Figure 6. Three different modes of melt-electrowriting. a) the melted polymer (PCL2000-HDI-BDO 1:2:1) there is no whipping, and the speed is at CTS or above, a linear fiber is direct-written, b) there is no whipping, and the speed of the collector is lower than the CTS, mechanical buckling of the fibers occurs, c) When properties allow whipping, a line of electro-spun fibers is observed.

Melt temperature is also another parameter that influences fiber formation, with a strong effect on diameter. Considering the viscoelastic property of polymer melts, an increase in temperature above the melting temperature of the polymer causes the viscous part of the polymer to be more prevalent to the elastic part, with a decreased viscosity. Hence, higher CTS is required for direct writing [57]. Temperature should be limited when processing thermally sensitive polymers, such as aliphatic polyesters, which can degrade quickly at relevant processing temperatures within the melt reservoir, or the syringe [58]. The diameter of the spinneret plays a role in limiting the melt flow rate, in reference to the polymer rheology and extrusion limitations. Small-sized spinnerets produce small diameter fibers, but with a decreased manufacturing throughput. Melt flow rate also influences fiber diameter, which is adjusted via the feeding pressure, and it is an efficient way to control fiber diameter. Higher melt feed produces large fiber diameters, accompanied with instabilities. This depends on the polymer properties as well, such as their functional groups and molecular weight [41]. Rheological behavior is determined by the molecular weight (and PDI) of the polymer. Low M_w results in low viscosity, and in turn, decreased polymer chain entanglements in the jet. Fiber diameter and CTS are controlled by the length, configuration, and constitution of the macromolecules [59].

Electrical field strength influences the stretching force, where an increase in field strength results in an increased stretching force with thin and faster jets. During the process where

the Taylor-cone goes towards the collector plate, the molten polymer jet goes through quenching and partial or full solidification, and any increase in the electric field, causes faster solidification [60]. MEW is a solvent-free technique, making it preferable, where toxicity and volatility issues can be avoided. It also has reduced electrical instabilities and is a safer method in comparison to electrospinning, notable is that it is non-toxic to mammalian cells [39]. Due to its solvent-free processing characteristics, it has been applied in biological fields to print porous microarchitecture scaffolds, which are mainly used as engineered tissue models [55].

1.3.4 Parameters of Touch-spinning

Electrospinning is the most popular fabrication technique used for producing nanofibers [61, 62]. In electrospinning, nanofibers are generated from a droplet of polymer solution, which is stretched upon the application of a high-voltage electric field, which is usually between 20 – 30 kV, depending on the dielectric properties of the material [61]. For fabricating 2D and 3D fibrous non-woven structures, the fibers could be deposited on collectors (plane electrodes or frames) or rotating electrodes (which are of cylindrical shape) [63]. This technology has been used a lot for the fabrication of nanofibrous scaffolds in regenerative medicine, but the use of high voltage on the loaded biomolecules has reported several detrimental effects [64-66]. Therefore, alternative technologies were developed to fabricate nanofibrous scaffolds to induce the inclusive guidance of cells with tissue-engineered grafts [67, 68].

Touch-spinning is one of the recently developed technologies, where nanofiber-production does not involve the usage of high-voltage electric fields, but fibers are drawn out from polymer solutions or melts using mechanical forces. This technique was developed due to the increased interest in nanofiber-fabrication, aiding in forming bones and tissues in combination with cells [69]. With this technique, fiber diameters within the range of 40 nm to 5 μ m have been achieved [68]. This technique is not limited by the needs of the spatial arrangement of oppositely charged electrodes, therefore more flexibility is present in the design and geometry of drawing out the fibers, manipulating their deposition and their alignment. One of the key advantages of this fabrication technique is the ability to generate fibers with a well-controlled fiber alignment, diameter, crystallinity, and polymer chain alignment in amorphous phase [69-71].

The simple setup of the touch-spinning device is depicted in Figure 7. The main components are the syringe, where a polymer solution or melt is supplied, air pressure, the rotating disk with rods, the collector plate, and a stepper motor (for controlling the movement in XYZ direction). The process of fiber collection in touch-spinning starts with supplying the polymer solution or melt into the syringe and applying pressure for extrusion. If a polymer melt was to be supplied, both a heater and a cooler would be needed; one to melt the polymer and the latter to cool down the formed fiber. Once the polymer solution/melt is extruded, the droplet formed at the nozzle needs to touch the rods on the rotating disk, which is ensured via adjusting the Z-axis. As the rotation of the rotating disk is initiated, a liquid bridge forms between the rod and the nozzle, and as the rotation proceeds, the liquid bridge stretches and forms a fiber. Due to mass conservation, the fiber diameter decreases with an increase in fiber length. The fibers are collected in the frame or collector plate, placed at the center of the disk [68]. Fiber diameter is controlled by adjusting the rotational speed, flow rate, and the concentration of the polymer solution [69].

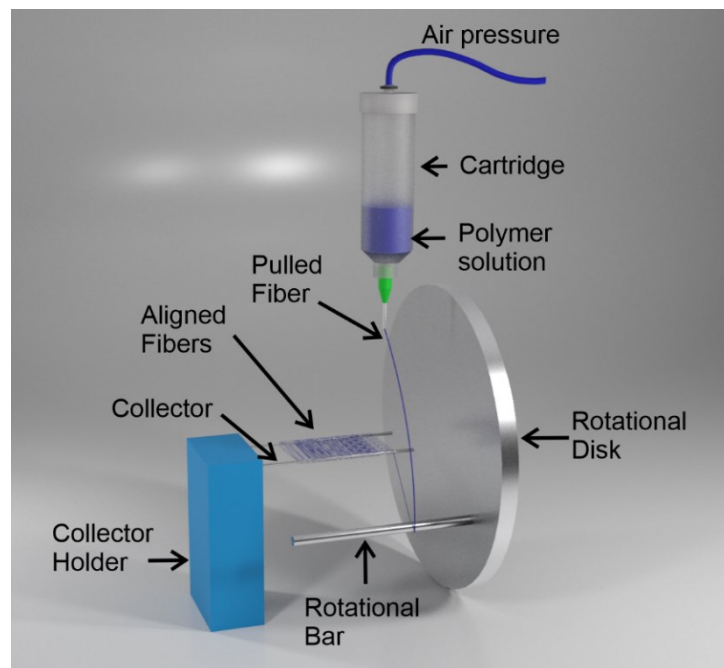


Figure 7. Schematic representation of touch-spinning device, where the polymer solution is extruded from the cartridge via applying air pressure. Once the rotational bar touches the polymer droplet, the fiber is pulled producing aligned fibers on the collector.

Fiber formation in this technique occurs due to the stretching of the liquid thread or bridge forming between the nozzle and rotating rod, as well as the solvent evaporation, resulting the solidification of the fiber. The main difference between these two mechanisms is the change in the force dynamics applied to the liquid thread at later steps of fiber formation. The most efficient mechanism in stretching the fibers is the direct contact of drawing the fibers with pulling the rod (the first mechanism) in the cold drawing stage, in comparison to the rotating electrode in electrospinning [71]. During spinning of fibers, the surface area of the liquid thread increases with its elongation, hence the solvent evaporates from the thread, and solidifies the fiber. Once the droplet hits the rotating rod, a pressure is generated, but it is greater than the breakthrough pressure, which causes the transition of the droplet from Cassie to fully wetted Wenzel state, leading to the wetting hysteresis. This does not have any effect on fiber diameter but plays an important role in avoiding the contamination of the rod with polymer deposits [69].

In touch-spinning, fiber stretching occurs in two directions: axial stretching and capillarity. Axial stretching owes to the stage rotation while the latter corresponds to draining the fluid from the fiber and back into the source droplet. Experiments have been performed to see if the different diameters of the rotating rods affects the fiber diameter, but no effect was demonstrated [68]. Fiber diameter is a function of an interplay of parameters, between the stretching of the polymer liquid from the surface supplying it and the tip of the rod [69]. Since mechanical force is the force drawing out the fibers, it determines both the fiber stretching, guiding the fibers onto the spool, where a better control over fiber alignment is achieved [70].

The rotational speed, viscosity of the polymer solution or melt, and the flow rate are the main factors affecting fiber diameter in this fabrication technique. As the rotational speed increases, fiber diameter decreases, owing to the pulling mechanism of the fibers, where solvent evaporation occurs faster. The faster/quicker the fibers are being pulled, the more they are being extended, thus lower fiber diameter. Polymer solution/melt concentration or viscosity also plays a role, such that an increase in viscosity leads to an increase in the axial viscous stress, hindering the stretching of fibers and increasing the fiber diameter. The manipulation of single nanofibers owes to the simplicity of the setup. The mesh size of touch-spun fibers can be controlled, due to the ability of drawing out fibers in several

mechanisms, such as orthogonal, unidirectional, and randomly oriented 2D or 3D meshes. Thus, the thickness and density can be controlled, allowing the combination of different fibers and materials within the fabrication process. This technique is scalable, easily implemented for laboratory and industrial manufacturing. It is very fast and practical, where no specific nor special equipment is required, neither the training of a personnel [68-70].

An additional advantage to touch-spinning in comparison to electrospinning includes the easy collection of fibers without impeding or obstructing their morphology. Although electrospinning can be done on a similar wire-frame collector, it is more commonly done onto a solid surface; removing the fibers from the collector is often difficult [69]. The main limitation to this fabrication technique is low productivity, where it is measured in a scale of centimeters per minutes (cm/min), yet it has been used in the production of scaffolds for tissue engineering. PCL meshes for filtration purposes were prepared via the simple winding of PCL fibers into meshes with specific sizes [72]. Unlike the limitation exhibited with electrospinning, where bioactive molecules as BSA cannot be incorporated into the mesh, a study conducted by Lee, S-J. et al., has achieved the incorporation of BSA within touch-spun PCL fibers that have promoted the alignment of neurite outgrowth of NSCs, signifying their potential use in treating conditions ranging from spinal cord injury to peripheral nerve lesions [69].

1.4 Conclusion

Nano- and microfibers obtained by different techniques have been used to obtain cell patterning and alignment for the last couple of decades and have shown good cell adhesion due to their ability to mimic the fibrous ECM. Different techniques have been developed and implemented to optimize and scale-up fiber production, as well as improve the control over exact fiber deposition and patterning (MEW and Touch spinning). The essential parameters governing MEW are thermal and electrical, meanwhile for touch-spinning, these properties are mechanical and depend strongly on the solvent system. Furthermore, the materials used are critical to the fiber processing and production depending on the mechanical and physico-chemical properties thereof.

In this dissertation, the focus is on developing and synthesizing PU-based copolymers which could be processed into fibers using several techniques (a combination of 3D printing and MEW, and touch spinning). Future applications of these fibrous scaffolds includes skeletal muscle tissue, specifically the tubular structures within this tissue.

2. Aims

The aim of this thesis was to develop polyurethane-based copolymers suitable for fiber production using Melt-electro writing and Touch-spinning techniques.

The set of polymers here presented offer the following advantages:

1. Biocompatibility and biodegradability.
2. Mechanical properties and processability.
3. Suitable environment for cells.

Hence, the aim of this work can be divided in three main objectives:

Objective 1: The fabrication of shape-changing bilayered scaffolds, which allow the growth of aligned skeletal muscle cells, using a combination of 3D printing and melt electrowriting inducing shape transformation. Aiming to achieve suitable mechanical properties which must be similar to the principal components of extracellular matrix (ECM).

Objective 2: The fabrication of highly aligned soft elastic fibrous scaffolds via touch spinning a family of polyester–polyurethane soft copolymers based on polycaprolactone with different molecular weights and chain extenders, demonstrating their potential for engineering muscle tissue. Moreover, the construction of highly oriented fiber scaffolds that can support the proliferation and alignment of muscle cells for muscle tissue engineering applications.

Objective 3: Designing and constructing highly aligned fibrous scaffolds that can mimic the structure of muscle tissues. The fabrication technique to be used is touch spinning and the material is a thermoplastic poly(1,4-butylene adipate)-based polyurethane elastomer, obtained via solvent-free polymerization.

3. Synopsis

This dissertation includes three published full papers, all of them as first author. The aim of this work was to develop new biodegradable and biocompatible polyurethane-based copolymers for muscle tissue engineering. The results presented in all three papers were obtained in the University of Bayreuth under the supervision of Prof. Dr. Leonid Ionov.

The papers are presented in the order of the objectives, mentioned in the previous section, section “2. Aims”. The first paper focuses on using a combination of fabrication techniques (MEW and 3D Printing) to produce scaffolds based on PCL-PU copolymers. The second paper explores a newly developed fabrication technique, touch spinning, using the polyurethanes from the first paper as well as modifying them in terms of molecular weights of their hard and soft segments. Finally, the last paper investigates the processing of poly(ester-urethane) elastomer, obtained in solvent-free conditions, and processing fibers using touch spinning, as in the previous paper.

3.1 Shape-Morphing Fibrous Hydrogel/Elastomer Bilayers

The first paper was published in *ACS Applied Bio Materials* under the title: **Shape-Morphing Fibrous Hydrogel/Elastomer Bilayers Fabricated by a Combination of 3D Printing and Melt Electrowriting for Muscle Tissue Regeneration.**

Here, a combination of 3D printing and Melt electrowriting techniques was used to fabricate a bilayer system. PCL-PU 1:2:1 copolymer fibers were drawn on top of a 3D printed HA-MA film, **Figure 8**. The soft, elastic, biocompatible, and biodegradable copolymer of PCL-PU [73, 74] was synthesized and used for the fabrication of the system. The second component of the shape-morphing structure is biocompatible and

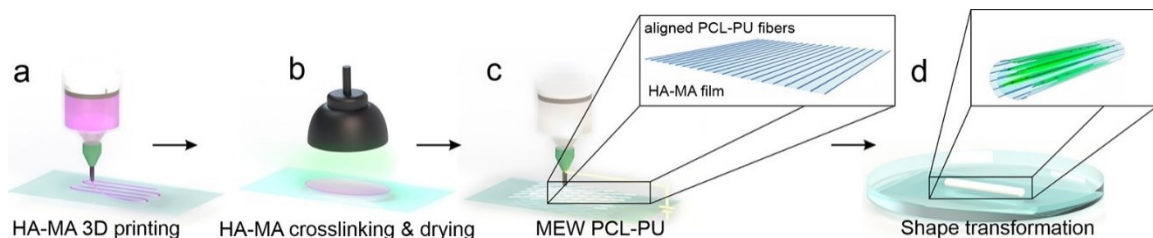


Figure 8. Scheme of the fabrication of shape-changing mats for the regeneration of muscle tissue by MEW of polycaprolactone-polyurethane (PCLPU) and 3D printing of HA-MA: (a) 3D printing of HA-MA; (b) cross-linking of printed HA-MA film; (c) deposition of uniaxially aligned fibers of PCL-PU using MEW; (d) seeding C2C12 myoblast on the bilayer, its shape transformation, and formation of a multilayer scroll tube suitable for cells encapsulation [2].

biodegradable methacrylated hyaluronic acid, which is one of the components of ECM [75, 76].

This system possessed improved topography, mechanical properties, and surface chemistry, in comparison with PCL [54] supporting a high degree of cell alignment and has the possibility of shape changing, forming tubular structures. The combination of techniques allowed best control in terms of size and thickness of the printed structures through programmed fabrication.

The sheets of cross-linked hyaluronic acid were able to undergo shape transformation and form tubular structures, due to the vertical gradient of cross-linking density obtained during cross-linking the polymer and triggered via its immersion in water [30]. Cell culture experiments demonstrated that myoblasts were occupying the spaces between the fibers, proliferating, and aligning along them. These scroll-like tubular structures can be further developed for obtaining vascularized tissues to transport nutrition and oxygen to the cells inside and for culturing a microtissues suitable for transplantation.

3.2 Soft Elastic Fibrous Scaffolds by Touch Spinning

The previous work showed promising results, therefore another fabrication technique as well as a combination of different polyurethane-based copolymers were investigated in the second article published in *ACS Applied Bio Materials* under the title: **Soft Elastic Fibrous Scaffolds for Muscle Tissue Engineering by Touch Spinning**. In this work, we reported the fabrication of porous touch-spun highly aligned and elastic scaffolds of polycaprolactone–polyurethane copolymers and demonstrated their promising character for the engineering of muscle tissue (**Figure 9**).

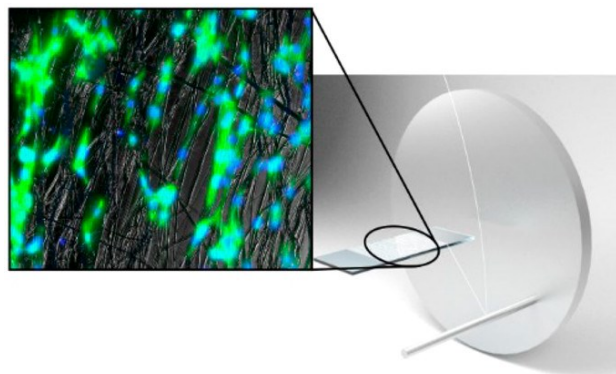


Figure 9. Schematic representation of touch-spun aligned fibers and real picture of cell alignment results [3].

To this aim, a family of polyester–polyurethane soft copolymers based on two different molecular weights of polycaprolactone (530 and 2000 g/mol) and three different kinds of chain extenders, such as 1,4-butanediol, and two molecular weights of PEG were synthesized. The combination of mechanical properties of the polymer demonstrated elastic deformation and elastic modulus in the range of 1 to 10 MPa depending on the composition. It was found that only 1 out of the 14 synthesized polymers possesses the suitable combination of properties for cell culturing. The combination of properties of the polymers and the method of fabrication of highly aligned fibrous structures demonstrated a potential for the application of this copolymer in muscle tissue engineering. Altogether, the importance of this approach is the fabrication of highly oriented fiber constructs that can support the proliferation and alignment of muscle cells.

3.3 Fibrous scaffolds for muscle tissue Engineering Based on Touch-Spun Poly(Ester-Urethane) Elastomer

The third article focuses on synthesizing a poly(ester-urethane) elastomer in solvent-free conditions and processing fibers via touch spinning with the aim to improve the results of the previous publications. This work is published in *Macromolecular Bioscience*, under the title: **Fibrous scaffolds for muscle tissue engineering based on touch-spun poly(ester-urethane)**.

Here, we report an approach for the fabrication of highly aligned microfibrinous scaffold of new thermoplastic polyurethane elastomer, whose soft segment is composed of poly(1,4 butylene adipate) and whose hard segment is formed by 1,4 butanediol and Methylene diphenyl diisocyanate (MDI) using the touch spinning technique and demonstrating its suitability for muscle tissue engineering (**Figure 10**).

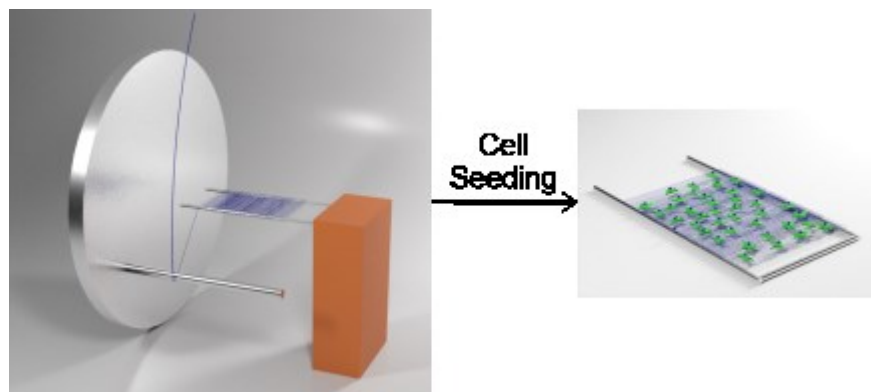


Figure 10. Schematic representation of processing a touch-spun scaffold and cell seeding on top.

The copolymer demonstrates an interesting combination of mechanical and thermal properties: a plastic and elastic characteristic of deformation, contraction at human body temperature, and had highly reliable elastomeric properties. The reported polymer demonstrates better mechanical properties, in comparison to similar polycaprolactone-based polyurethanes previously reported in articles 1 and 2, excellent biocompatibility that enables its use for fabrication of fibrous scaffolds allowing high cell alignment required for regeneration of such anisotropic tissues as muscle tissue.

4. Literature references

1. Tenenhaus M, Rennekampff H, Mulder G. Living cell products as wound healing biomaterials: Current and future modalities. *Wound Healing Biomaterials*. 2016:201-25.
2. Uribe-Gomez J, Posada-Murcia A, Shukla A, Ergin M, Constante G, Apsite I, et al. Shape-Morphing Fibrous Hydrogel/Elastomer Bilayers Fabricated by a Combination of 3D Printing and Melt Electrowriting for Muscle Tissue Regeneration. *ACS Appl Bio Mater*. 2021;4(2):1720-30.
3. Uribe-Gomez J, Posada-Murcia A, Shukla A, Alkhamis H, Salehi S, Ionov L. Soft Elastic Fibrous Scaffolds for Muscle Tissue Engineering by Touch Spinning. *ACS Appl Bio Mater*. 2021;4(7):5585-97.
4. Mukund K, Subramaniam S. Skeletal muscle: A review of molecular structure and function, in health and disease. *Wiley Interdisciplinary Reviews: Systems Biology and Medicine*. 2020;12(1):e1462.
5. Lieber RL. *Skeletal muscle structure, function, and plasticity*: Lippincott Williams & Wilkins; 2002.
6. Storm C, Pastore JJ, MacKintosh FC, Lubensky TC, Janmey PA. Nonlinear elasticity in biological gels. *Nature*. 2005;435(7039):191-4.
7. Levental I, Georges PC, Janmey PA. Soft biological materials and their impact on cell function. *Soft Matter*. 2007;3(3):299-306.
8. Solon J, Levental I, Sengupta K, Georges PC, Janmey PA. Fibroblast adaptation and stiffness matching to soft elastic substrates. *Biophysical journal*. 2007;93(12):4453-61.

9. Freed LE, Vunjak-Novakovic G, Biron RJ, Eagles DB, Lesnoy DC, Barlow SK, et al. Biodegradable polymer scaffolds for tissue engineering. *Bio/technology*. 1994;12(7):689-93.
10. Luo X. Biofabrication in microfluidics: a converging fabrication paradigm to exploit biology in microsystems. *J Bioeng Biomed Sci*. 2012;2.
11. Groll J, Boland T, Blunk T, Burdick JA, Cho D-W, Dalton PD, et al. Biofabrication: reappraising the definition of an evolving field. *Biofabrication*. 2016;8(1):013001.
12. Ionov L. 4D biofabrication: materials, methods, and applications. *Advanced healthcare materials*. 2018;7(17):1800412.
13. Moroni L, Boland T, Burdick JA, De Maria C, Derby B, Forgacs G, et al. Biofabrication: a guide to technology and terminology. *Trends in biotechnology*. 2018;36(4):384-402.
14. Guvendiren M, Molde J, Soares RM, Kohn J. Designing biomaterials for 3D printing. *ACS biomaterials science & engineering*. 2016;2(10):1679-93.
15. Chen F, Hochleitner G, Woodfield T, Groll J, Dalton PD, Amsden BG. Additive manufacturing of a photo-cross-linkable polymer via direct melt electrospinning writing for producing high strength structures. *Biomacromolecules*. 2016;17(1):208-14.
16. Visser J, Melchels FP, Jeon JE, Van Bussel EM, Kimpton LS, Byrne HM, et al. Reinforcement of hydrogels using three-dimensionally printed microfibrils. *Nature communications*. 2015;6(1):1-10.
17. Murphy SV, Atala A. 3D bioprinting of tissues and organs. *Nature biotechnology*. 2014;32(8):773-85.

18. Giannopoulos AA, Mitsouras D, Yoo S-J, Liu PP, Chatzizisis YS, Rybicki FJ. Applications of 3D printing in cardiovascular diseases. *Nature Reviews Cardiology*. 2016;13(12):701-18.
19. Richards D, Jia J, Yost M, Markwald R, Mei Y. 3D bioprinting for vascularized tissue fabrication. *Annals of biomedical engineering*. 2017;45(1):132-47.
20. Duan B. State-of-the-art review of 3D bioprinting for cardiovascular tissue engineering. *Annals of biomedical engineering*. 2017;45(1):195-209.
21. Li J, Zheng L, Cai H, Sun W, Shen M, Zhang G, et al. Polyethyleneimine-mediated synthesis of folic acid-targeted iron oxide nanoparticles for in vivo tumor MR imaging. *Biomaterials*. 2013;34(33):8382-92.
22. Zhang Y, Yu Y, Akkouch A, Dababneh A, Dolati F, Ozbolat IT. In vitro study of directly bioprinted perfusable vasculature conduits. *Biomaterials science*. 2015;3(1):134-43.
23. Gao Q, He Y, Fu J-z, Liu A, Ma L. Coaxial nozzle-assisted 3D bioprinting with built-in microchannels for nutrients delivery. *Biomaterials*. 2015;61:203-15.
24. Kolesky DB, Truby RL, Gladman AS, Busbee TA, Homan KA, Lewis JA. 3D bioprinting of vascularized, heterogeneous cell-laden tissue constructs. *Advanced materials*. 2014;26(19):3124-30.
25. Miller JS, Stevens KR, Yang MT, Baker BM, Nguyen D-HT, Cohen DM, et al. Rapid casting of patterned vascular networks for perfusable engineered three-dimensional tissues. *Nature materials*. 2012;11(9):768-74.
26. Kolesky DB, Homan KA, Skylar-Scott MA, Lewis JA. Three-dimensional bioprinting of thick vascularized tissues. *Proceedings of the national academy of sciences*. 2016;113(12):3179-84.

27. O'Bryan CS, Bhattacharjee T, Niemi SR, Balachandar S, Baldwin N, Ellison ST, et al. Three-dimensional printing with sacrificial materials for soft matter manufacturing. *MRS bulletin*. 2017;42(8):571-7.
28. Gladman AS, Matsumoto EA, Nuzzo RG, Mahadevan L, Lewis JA. Biomimetic 4D printing. *Nature materials*. 2016;15(4):413-8.
29. Raviv D, Zhao W, McKnelly C, Papadopoulou A, Kadambi A, Shi B, et al. Active printed materials for complex self-evolving deformations. *Scientific reports*. 2014;4(1):1-8.
30. Kirillova A, Maxson R, Stoychev G, Gomillion CT, Ionov L. 4D biofabrication using shape-morphing hydrogels. *Advanced Materials*. 2017;29(46):1703443.
31. Stroganov V, Pant J, Stoychev G, Janke A, Jehnichen D, Fery A, et al. 4D biofabrication: 3D cell patterning using shape-changing films. *Advanced Functional Materials*. 2018;28(11):1706248.
32. Zakharchenko S, Puretskiy N, Stoychev G, Stamm M, Ionov L. Temperature controlled encapsulation and release using partially biodegradable thermo-magneto-sensitive self-rolling tubes. *Soft Matter*. 2010;6(12):2633-6.
33. Stoychev G, Puretskiy N, Ionov L. Self-folding all-polymer thermoresponsive microcapsules. *Soft Matter*. 2011;7(7):3277-9.
34. Kwag HR, Serbo JV, Korangath P, Sukumar S, Romer LH, Gracias DH. A self-folding hydrogel in vitro model for ductal carcinoma. *Tissue Engineering Part C: Methods*. 2016;22(4):398-407.
35. Chung S, Ingle NP, Montero GA, Kim SH, King MW. Bioresorbable elastomeric vascular tissue engineering scaffolds via melt spinning and electrospinning. *Acta Biomaterialia*. 2010;6(6):1958-67.

36. Moroni L, Schotel R, Hamann D, de Wijn JR, van Blitterswijk CA. 3D fiber-deposited electrospun integrated scaffolds enhance cartilage tissue formation. *Advanced Functional Materials*. 2008;18(1):53-60.
37. Aram E, Mehdipour-Ataei S. A review on the micro-and nanoporous polymeric foams: Preparation and properties. 2016;65(7):358-75.
38. Norton CL. Method of and apparatus for producing fibrous or filamentary material. Google Patents; 1936.
39. Hrynevich A, Elçi BŞ, Haigh JN, McMaster R, Youssef A, Blum C, et al. Dimension-based design of melt electrowritten scaffolds. *Small*. 2018;14(22):1800232.
40. Lian H, Meng Z. Melt electrospinning vs. solution electrospinning: A comparative study of drug-loaded poly (ϵ -caprolactone) fibres. *Materials Science and Engineering: C*. 2017;74:117-23.
41. Brown TD, Dalton PD, Hutmacher DW. Direct writing by way of melt electrospinning. *Advanced Materials*. 2011;23(47):5651-7.
42. Jungst T, Muerza-Cascante ML, Brown TD, Standfest M, Hutmacher DW, Groll J, et al. Melt electrospinning onto cylinders: effects of rotational velocity and collector diameter on morphology of tubular structures. *Polymer International*. 2015;64(9):1086-95.
43. Castilho M, Feyen D, Flandes-Iparraguirre M, Hochleitner G, Groll J, Doevendans PA, et al. Melt electrospinning writing of poly-Hydroxymethylglycolide-co- ϵ -Caprolactone-based scaffolds for cardiac tissue engineering. *Advanced healthcare materials*. 2017;6(18):1700311.

44. Hochleitner G, Kessler M, Schmitz M, Boccaccini AR, Teßmar J, Groll J. Melt electrospinning writing of defined scaffolds using polylactide-poly (ethylene glycol) blends with 45S5 bioactive glass particles. *Materials Letters*. 2017;205:257-60.
45. Kade J, Tandon B, Weichhold J, Pisignano D, Persano L, Luxenhofer R, et al. Melt Electrowriting of Poly (vinylidene fluoride-co-trifluoroethylene). 2021.
46. Robinson TM, Hutmacher DW, Dalton PD. The next frontier in melt electrospinning: taming the jet. *Advanced Functional Materials*. 2019;29(44):1904664.
47. Tamayol A, Akbari M, Annabi N, Paul A, Khademhosseini A, Juncker D. Fiber-based tissue engineering: Progress, challenges, and opportunities. *Biotechnology advances*. 2013;31(5):669-87.
48. Bootsma K, Fitzgerald MM, Free B, Dimbath E, Conjerti J, Reese G, et al. 3D printing of an interpenetrating network hydrogel material with tunable viscoelastic properties. *Journal of the mechanical behavior of biomedical materials*. 2017;70:84-94.
49. Arslan H, Nojoomi A, Jeon J, Yum K. 3D printing of anisotropic hydrogels with bioinspired motion. *Advanced Science*. 2019;6(2):1800703.
50. Apsite I, Uribe JM, Posada AF, Rosenfeldt S, Salehi S, Ionov L. 4D biofabrication of skeletal muscle microtissues. *Biofabrication*. 2019;12(1):015016.
51. Farazin A, Akbari Aghdam H, Motififard M, Aghadavoudi F, Kordjamshidi A, Saber-Samandari S, et al. A polycaprolactone bio-nanocomposite bone substitute fabricated for femoral fracture approaches: Molecular dynamic and micromechanical Investigation. *Journal of Nanoanalysis*. 2019;6(3):172-84.
52. Delgado-Aguilar M, Puig R, Sazdovski I, Fullana-i-Palmer P. Polylactic acid/polycaprolactone blends: On the path to circular economy, substituting single-use commodity plastic products. *Materials*. 2020;13(11):2655.

53. Fuchs A, Youssef A, Seher A, Hochleitner G, Dalton P, Hartmann S, et al. Medical-grade polycaprolactone scaffolds made by melt electrospinning writing for oral bone regeneration—a pilot study in vitro. *BMC Oral Health*. 2019;19(1):1-11.
54. Constante G, Apsite I, Alkhamis H, Dulle M, Schwarzer M, Caspari A, et al. 4D biofabrication using a combination of 3D printing and melt-electrowriting of shape-morphing polymers. *ACS Applied Materials & Interfaces*. 2021;13(11):12767-76.
55. Ding H, Cao K, Zhang F, Boettcher W, Chang RC. A fundamental study of charge effects on melt electrowritten polymer fibers. *Materials & Design*. 2019;178:107857.
56. Zhmayev E, Cho D, Lak Joo Y. Electrohydrodynamic quenching in polymer melt electrospinning. *Physics of fluids*. 2011;23(7):073102.
57. Deitzel JM, BeckTan NC, Kleinmeyer JD, Rehrmann J, Tevault D. Generation of Polymer Nanofibers Through Electrospinning. Army Research Lab Aberdeen Proving Ground Md; 1999.
58. Goldfarb IJ, McGuchan R. Thermal Degradation of Polyesters: Part 1. Aliphatic Polymers. AIR FORCE MATERIALS LAB WRIGHT-PATTERSON AFB OH; 1968.
59. Kadomae Y, Maruyama Y, Sugimoto M, Taniguchi T, Koyama K. Relation between tacticity and fiber diameter in melt-electrospinning of polypropylene. *Fibers and Polymers*. 2009;10(3):275-9.
60. Zhang L-H, Duan X-P, Yan X, Yu M, Ning X, Zhao Y, et al. Recent advances in melt electrospinning. *RSC advances*. 2016;6(58):53400-14.
61. Li D, Xia Y. Electrospinning of nanofibers: reinventing the wheel? *Advanced materials*. 2004;16(14):1151-70.
62. Zaballa V, Friedrichs D. A Novel Tissue Welding Device Using Low-Voltage Far-Field Coaxial Electrospinning. *Journal of Medical Devices*. 2015;9(3).

63. Williamson MR, Black R, Kiely C. PCL–PU composite vascular scaffold production for vascular tissue engineering: attachment, proliferation and bioactivity of human vascular endothelial cells. *Biomaterials*. 2006;27(19):3608-16.
64. van de Weert M, Hennink WE, Jiskoot W. Protein instability in poly (lactic-co-glycolic acid) microparticles. *Pharmaceutical research*. 2000;17(10):1159-67.
65. Yang Y, Li X, Qi M, Zhou S, Weng J. Release pattern and structural integrity of lysozyme encapsulated in core-sheath structured poly(DL-lactide) ultrafine fibers prepared by emulsion electrospinning. *Eur J Pharm Biopharm*. 2008;69(1):106-16.
66. Casper CL, Yamaguchi N, Kiick KL, Rabolt JF. Functionalizing electrospun fibers with biologically relevant macromolecules. *Biomacromolecules*. 2005;6(4):1998-2007.
67. Li W, Shanti R, Tuan R. *Electrospinning Technology for Nanofibrous Scaffolds in Tissue Engineering*. Nanotechnologies for the Life Sciences. 2007.
68. Tokarev A, Asheghali D, Griffiths IM, Trotsenko O, Gruzd A, Lin X, et al. Touch-and Brush-Spinning of Nanofibers. *Advanced Materials*. 2015;27(41):6526-32.
69. Lee SJ, Asheghali D, Belvins B, Timsina R, Esworthy T, Zhou X, et al. Touch-Spun Nanofibers for Nerve Regeneration. 2020.
70. Gao H, Asheghali D, Yadavalli NS, Pham MT, Nguyen TD, Minko S, et al. Fabrication of core-sheath nanoyarn via touchspinning and its application in wearable piezoelectric nanogenerator. *The Journal of The Textile Institute*. 2020;111(6):906-15.
71. Asheghali D, Lee S-J, Furchner A, Gruzd A, Larson S, Tokarev A, et al. Enhanced neuronal differentiation of neural stem cells with mechanically enhanced touch-spun nanofibrous scaffolds. *Nanomedicine: Nanotechnology, Biology and Medicine*. 2020;24:102152.

72. Qin XH, Wang SY. Filtration properties of electrospinning nanofibers. *Journal of applied polymer science*. 2006;102(2):1285-90.
73. Wang W, Ping P, Yu H, Chen X, Jing X. Synthesis and characterization of a novel biodegradable, thermoplastic polyurethane elastomer. *Journal of Polymer Science Part A: Polymer Chemistry*. 2006;44(19):5505-12.
74. Mi H-Y, Jing X, Napiwocki BN, Hagerty BS, Chen G, Turng L-S. Biocompatible, degradable thermoplastic polyurethane based on polycaprolactone-block-polytetrahydrofuran-block-polycaprolactone copolymers for soft tissue engineering. *Journal of Materials Chemistry B*. 2017;5(22):4137-51.
75. Apsite I, Constante G, Dulle M, Vogt L, Caspari A, Boccaccini AR, et al. 4D Biofabrication of fibrous artificial nerve graft for neuron regeneration. *Biofabrication*. 2020;12(3):035027.
76. Sierra-Sánchez Á, Fernández-González A, Lizana-Moreno A, Espinosa-Ibáñez O, Martínez-Lopez A, Guerrero-Calvo J, et al. Hyaluronic acid biomaterial for human tissue-engineered skin substitutes: Preclinical comparative in vivo study of wound healing. *Journal of the European Academy of Dermatology and Venereology*. 2020;34(10):2414-27.

5. Publication list

1. **Uribe-Gomez, J.**, Posada-Murcia, A., Shukla, A., Alkhamis, H., Salehi, S., and Ionov, L. Soft Elastic Fibrous Scaffolds for Muscle Tissue Engineering by Touch Spinning, *ACS Applied Bio Materials.*, 2021, 4, 1720-1730
2. Posada Murcia, A., **Uribe Gómez, J. M.**, Sommer, J. U., Ionov, L. Two-Way Shape Memory Polymers: Evolution of Stress vs Evolution of Elongation, *Macromolecules.*, 2021, 54, 8255
3. **Uribe-Gomez, J.**, Posada-Murcia, A., Shukla, A., Ergin, M., Constante, G., Apsite, I., Dulle, M., Schwarzer, M., Caspari, A., Synytska, A., Salehi, S., Ionov, L. Shape-Morphing Fibrous Hydrogel/Elastomer Bilayers Fabricated by a Combination of 3D Printing and Melt Electrowriting for Muscle Tissue Regeneration, *ACS Applied Bio Materials*, 2021, 4, 1720-1730
4. Apsite, I., **Uribe, J. M.**, Posada, A. F., Rosenfeldt, S., Salehi, S., and Ionov, L. 4D biofabrication of skeletal muscle microtissues, *Biofabrication*, 2019, 12, 015016
5. **Uribe-Gomez, J.**, Schönfeld, D., Posada-Murcia, A., Roland, M. M., Caspari, A., Synytska, A., Salehi, S., Pretsch, T., Ionov, L. Fibrous scaffolds for muscle tissue engineering based on touch-spun poly(ester-urethane) elastomer. *Macromolecular Bioscience*, 2022, 2100427

6. Individual contribution to joined publications and manuscripts presented here

Publication 1: Shape-Morphing Fibrous Hydrogel/Elastomer Bilayers Fabricated by a Combination of 3D Printing and Melt Electrowriting for Muscle Tissue Regeneration. Juan Uribe-Gomez, Andrés Posada-Murcia, Amit Shukla, Mert Ergin, Gissela Constante, Indra Apsite, Dulle Martin, Madeleine Schwarzer, Anja Caspari, Alla Synytska, Sahar Salehi, and Leonid Ionov. ACS Applied Bio Materials. Published on: January 26, 2021. DOI: 10.1021/acsabm.0c01495

Author Contributions: **Juan Uribe-Gomez:** Concept of research, Polymer synthesis and characterization, Mechanical properties, 3D printing, Melt-electrowriting, Thermal characterization, Degradation test, Cell culture and writing the final manuscript. **Andrés Posada-Murcia:** Mechanical characterization, Scientific discussion and writing the final manuscript. **Amit Shukla:** SEM imaging and modify and optimize homemade devices. **Mert Ergin:** Melt-electro writing of PCL-PU and parameters optimization. **Gissela Constante:** Help with cell culture studies. **Indra Apsite:** Help with cell culture studies. **Dulle Martin:** SAXS and WAXS experiments. **Madeleine Schwarzer:** SAXS and WAXS experiments. **Anja Caspari:** Zeta potential studies. **Alla Synytska:** Zeta potential studies. **Sahar Salehi:** Help with cell culture studies, scientific discussion and writing the final manuscript. **Leonid Ionov:** Concept of research, Supervision of the project, Writing and completion of the final manuscript.

All authors have given approval to the final version of the manuscript.

Publication 2: Soft Elastic Fibrous Scaffolds for Muscle Tissue Engineering by Touch Spinning. Juan Uribe-Gomez, Andrés Posada-Murcia, Amit Shukla, Hanin Alkhamis, Sahar Salehi, and Leonid Ionov. ACS Applied Bio Materials. Published on: June 25, 2021. DOI: 10.1021/acsabm.1c00403

Author Contributions: **Juan Uribe-Gomez:** Concept of research, Polymer synthesis and characterization, Mechanical properties, Touch spinning of copolymers, Thermal characterization, Degradation test, Cell culture and writing the final manuscript. **Andrés**

Posada-Murcia: Mechanical characterization, Scientific discussion and writing the final manuscript. **Amit Shukla:** SEM imaging and modify and optimize homemade device. **Hanin Alhamis:** Touch spinning of PCL and parameters optimization. **Sahar Salehi:** Help with cell culture studies, Scientific discussion and writing the final manuscript. **Leonid Ionov:** Concept of research, Supervision of the project, Writing and completion of the final manuscript.

All authors have given approval to the final version of the manuscript.

Publication 3: **Uribe-Gomez, J.,** Schönfeld, D., Posada-Murcia, A., Roland, M. M., Caspari, A., Synytska, A., Salehi, S., Pretsch, T., Ionov, L. Fibrous scaffolds for muscle tissue engineering based on touch-spun poly(ester-urethane) elastomer. *Macromolecular Bioscience*, 2022, 2100427

Author Contributions: **Juan Uribe-Gomez:** Concept of research, Polymer characterization, Mechanical properties, Touch spinning, Thermal characterization, Degradation test, Cell culture and writing the final manuscript. **Dennis Schönfeld:** Synthesis, Polymer characterization, Thermal characterization and writing the final manuscript. **Andrés Posada-Murcia:** Mechanical characterization, Scientific discussion and writing the final manuscript. **Michel-Manuel Roland:** Touch spinning and degradation test. **Anja Caspari:** Zeta potential test. **Alla Synytska:** Zeta potential test. **Sahar Salehi:** Cytotoxicity test, Cell culture and writing the final manuscript. **Thorsten Pretsch:** Concept of research and writing the final manuscript. **Leonid Ionov:** Concept of research, Supervision of the project, Writing and completion of the final manuscript.

All authors have given approval to the final version of the manuscript.

7. Manuscripts

Manuscript 1

Shape-Morphing Fibrous Hydrogel/Elastomer Bilayers Fabricated by a Combination of 3D Printing and Melt Electrowriting for Muscle Tissue Regeneration

Juan Uribe-Gomez, Andrés Posada-Murcia, Amit Shukla, Mert Ergin, Gissela Constante, Indra Apsite, Dulle Martin, Madeleine Schwarzer, Anja Caspari, Alla Synytska, Sahar Salehi, and Leonid Ionov

ACS Applied Bio Materials

Published on: January 26, 2021

DOI: 10.1021/acsabm.0c01495

Shape-Morphing Fibrous Hydrogel/Elastomer Bilayers Fabricated by a Combination of 3D Printing and Melt Electrowriting for Muscle Tissue Regeneration

Juan Uribe-Gomez, Andrés Posada-Murcia, Amit Shukla, Mert Ergin, Gissela Constante, Indra Apsite, Dulle Martin, Madeleine Schwarzer, Anja Caspari, Alla Synytska, Sahar Salehi, and Leonid Ionov*



Cite This: *ACS Appl. Bio Mater.* 2021, 4, 1720–1730



Read Online

ACCESS |



Metrics & More

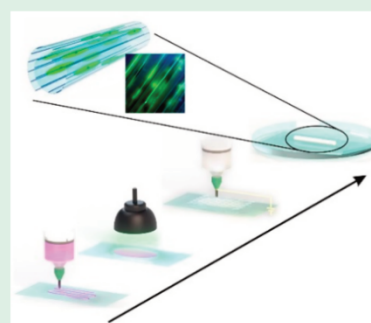


Article Recommendations



Supporting Information

ABSTRACT: This paper reports an approach for the fabrication of shape-changing bilayered scaffolds, which allow the growth of aligned skeletal muscle cells, using a combination of 3D printing of hyaluronic acid hydrogel, melt electrowriting of thermoplastic polycaprolactone-polyurethane elastomer, and shape transformation. The combination of the selected materials and fabrication methods allows a number of important advantages such as biocompatibility, biodegradability, and suitable mechanical properties (elasticity and softness of the fibers) similar to those of important components of extracellular matrix (ECM), which allow proper cell alignment and shape transformation. Myoblasts demonstrate excellent viability on the surface of the shape-changing bilayer, where they occupy space between fibers and align along them, allowing efficient cell patterning inside folded structures. The bilayer scaffold is able to undergo a controlled shape transformation and form multilayer scroll-like structures with cells encapsulated inside. Overall, the importance of this approach is the fabrication of tubular constructs with a patterned interior that can support the proliferation and alignment of muscle cells for muscle tissue regeneration.



KEYWORDS: melt electrowriting, biofabrication, shape-morphing, skeletal muscle, polyurethane copolymers

1. INTRODUCTION

In the past decades, an increasing interest in research in the field of skeletal muscle tissue engineering was observed as it enables new sources of tissues for transplantation without involving donors.^{1,2} Indeed, the problem of engineering skeletal muscle tissue is of great concern because the skeletal muscle tissue is not only responsible for locomotion but also makes up 40–45% of the total body mass.³ In this regard, one of the current goals in tissue engineering is the development of methods for the production of biomimetic and functional constructs. This can be an alternative to the current treatment of volumetric muscle loss (VML), such as prosthetic bracing and autogenic muscle flap transplantation.⁴ Although muscle tissue has a robust capability of regeneration when damage is minor, in VML injuries, which are characterized by tissue loss and soft tissue destruction, tissue regeneration is often incomplete. Reconstructive treatments are required, including transplantation, which is able to restore muscle strength and movement.^{5,6} In the absence of definitive treatment, this kind of injury mostly results in permanent disability and pain.⁷

Skeletal muscle is composed of numerous muscle fiber bundles, which are packed closely to induce guided contractions.⁸ This complex structure is generated by the differentiation of mononuclear myoblasts cells into long cellular multinuclear structures called myotubes, which

organize and assemble themselves to form oriented muscle fibers.⁹ Accordingly, it is evident that alignment of myoblast is essential for myogenesis and the engineering of anisotropic skeletal muscle tissue.¹⁰ Therefore, the development of new methods for the fabrication of matrices that favor the alignment of myoblasts and their three-dimensional (3D) organization, forming muscle bundles, is necessary to mimic the muscle tissue structure and its ECM in vitro.^{11,12}

In recent years, many techniques and approaches have been developed to generate oriented muscle fibers to induce myoblast alignment, such as microfabrication and micro-patterned surfaces,⁹ electrospinning,^{11,13} bioprinting,^{6,14} and melt electrowriting (MEW).¹⁵ Although electrospinning and bioprinting have been demonstrated to be promising for the alignment of cells, there is still room for improvement because of the imprecise deposition of fibers during electrospinning, and the absence of alignment cues for the encapsulated cells in

Received: November 17, 2020

Accepted: January 15, 2021

Published: January 26, 2021



the printed hydrogel that are needed to form the organized muscle tissue.^{13,16}

Therefore, melt electrowriting (MEW) comes to the fore, as it allows the deposition of fibers in a programmed way that is required for the fabrication of scaffolds with complex patterns and controlled topography.¹⁷ The MEW-fabricated fibers can potentially mimic the muscular architectures because of the microporous structures formed, provide high surface area, and act as support as well as guidance for myoblast cells.¹⁵ Many studies have been performed recently using the MEW technique to spin fibers from various thermoplastic materials with low melting points such polycaprolactone,¹⁷ poly hydroxymethylglycolide-*co-ε*-caprolactone,¹⁸ polylactide-poly-(ethylene glycol),¹⁹ and others. Although the MEW scaffolds can be used to print complex structures with varied patterns and high resolution, it cannot be used to print cell-laden structures alone,^{20,21} but in combination with 3D printing.^{22–25} The fabrication of complex multilayered 3D structures with aligned cells even using a combination of these methods is still challenging. This problem can be addressed using advanced technology such as 4D biofabrication. For example, we demonstrated the biofabrication of skeletal muscle microtissue using shape-changing double-layer electrospun mesh- polycaprolactone (PCL)/methacrylated alginate (AA-MA).¹⁵ Aligned PCL nanofibers were able to support alignment of myoblasts cells, whereas the electrospun mesh still lacked porosity and proper size and contained random fibers. Moreover, the bottom layer was made of electrospun random AA-MA fibers, which were not cell adhesive. The PCL that was used in this work was a stiff and plastic semicrystalline polymer.^{26–28} The PCL fibers cannot be deformed by cells even via buckling mechanism upon cell contraction because the fibers generate a very dense network with small mesh size.²⁹ The second component of the bilayer was alginate, which is biodegradable but not a component of ECM.³

Therefore, here we report the fabrication of an advanced system, which can potentially be used for skeletal muscle tissue engineering. The system possesses improved topography, mechanical properties, and surface chemistry, in addition to supporting a high degree of cell alignment. The advanced system is formed via 3D printing a bottom layer of methacrylate hyaluronic acid (HA-MA) and depositing MEW uniaxially aligned microfibers of the copolymer polycaprolactone-polyurethane (PCL-PU) on top of the HA-MA layer. Cells are then deposited on top of the bilayer. Hence, the bilayer was fabricated using a combination of methods of additive manufacturing allowing best control of size and thickness of the printed structures through programmed fabrication. The advantages of the current bilayer lie in the fabrication of topographically/chemically structured substrates (quasi 2D), the formation of the cell layer in an organized and oriented manner following the printed patterns, and finally, the possibility of shape changing and the formation of tubular structures. The proper selection of materials is also vital for providing a suitable environment for cells. The combination of these properties makes it less suitable for the fabrication of soft tissues, which undergo large and reversible deformations. In the current work, a soft, elastic, biocompatible, and biodegradable copolymer of PCL-PU^{30,31} is synthesized and used for the fabrication of soft shape-morphing structures that allow uniaxial cell alignment. The second component of the shape-morphing structure is biocompatible and biodegradable

hyaluronic acid, which is one of the components of ECM.^{32,33} Therefore, it is expected to be more suitable than alginate.^{34–37} Moreover, sheets of cross-linked hyaluronic acid are able to undergo shape transformation and form tubular structures. Shape transformation occurs because of the formation of a vertical gradient of cross-linking density obtained during cross-linking of the polymer and it is triggered by its immersion in water.³⁸ We demonstrate that the bilayer HA-MA-PCL-PU mat can fold and that it is suitable for the culture of C2C12 mouse myoblasts cells.

2. EXPERIMENTAL SECTION AND METHODS

2.1. Materials. Polycaprolactone diol (PCL-diol, Mn = 2000 g/mol, Sigma-Aldrich), Hexamethylene diisocyanate (HDI, Merck. HDI was dried using a 4 Å molecular sieve and then distilled under vacuum), 1,4-butanediol (BD, Sigma-Aldrich), dibutyltin dilaurate (DBTDL, Merck), hyaluronic acid sodium salt (HA, MW 1–2 Million Da, Carbosynth), eosin Y (EY, Sigma-Aldrich), triethanolamine (TEA, Sigma-Aldrich), 1-vinyl-2-pyrrolidone (VP, Sigma-Aldrich), dimethyl sulfoxide anhydrous (DMSO, Sigma-Aldrich), methacrylic anhydride (MA, Sigma-Aldrich), Ethanol (EtOH, Sigma-Aldrich), 2-propanol (IPA, abcr GmbH), sodium hydroxide (NaOH, Sigma-Aldrich), chloroform (Sigma-Aldrich), ethylenediaminetetraacetic acid (EDTA, Sigma-Aldrich), calcium chloride dehydrate (Sigma-Aldrich), Dulbecco's phosphate buffered saline (DPBS, Sigma-Aldrich), Dulbecco's modified Eagle medium (DMEM, Merck), penicillin-streptomycin (Pen/Strep, gibco), fetal bovine serum (FBS, Merck), GlutaMax (gibco), 4-(2-hydroxyethyl)-1-piperazineethanesulfonic acid (HEPES, Carl Roth), albumin fraction V (BSA, Roth), calcein AM (Thermo Fisher Scientific), ethidium EthD-1 (Thermo Fisher Scientific), Phalloidin Dylight 488 (Thermo Fisher Scientific), 4',6-diamidino-2-phenylindole (DAPI, Thermo Fisher Scientific), AlamarBlue HS cell viability reagent (Thermo Fisher Scientific), Triton X-100 (Sigma-Aldrich). The C2C12 myoblast (passage number less than 7) were purchased from ATCC (Manassas, VA).

2.2. Synthesis of PCL-PU. To synthesize PCL-PU polymers, we used the procedure described by Hao-Yang et al.³¹

2.3. Synthesis of Methacrylated Hyaluronic Acid (HA-MA). The methacrylation of hyaluronic acid was performed using the procedure described by Smeds et al.³⁹ 3% solution of hyaluronic acid was used for the synthesis. The details are given in ref 29.

2.4. FT-IR. Qualitative identification of functional groups of PCL-PU was done using FTIR spectroscopy (Bruker Tensor 27, USA) with spectral data spacing of 4 cm⁻¹ from 800 to 4000 cm⁻¹. The main bands in these spectra were stretching vibrations of NH groups in the 3500 to 3000 cm⁻¹ range. The characteristic stretching vibration of carbonyl group C=O ($\nu = 1727$ cm⁻¹) and C–N stretching ($\nu = 1535$ cm⁻¹) confirm the presence of urethane groups. The symmetric and asymmetric stretching vibrations of –CH₂ groups ($\nu = 2935$ and 2865 cm⁻¹), the stretching vibration of the C–O–C bond ($\nu = 1685$ cm⁻¹), and the stretching bands from the C–O bond of the ester group ($\nu = 1240$ and 1164 cm⁻¹) correspond to the PCL part of the copolymer.⁴⁰ (Figure S1)

2.5. NMR. Data were obtained using a Bruker Avance 500 spectrometer (Bruker BioSpin GmbH, Silberstreifen, Germany) (500.16 MHz for ¹H). ¹H NMR chemical shifts (δ) were reported in parts per million (ppm) relative to TMS, with the residual solvent peak used as an internal reference using ¹H NMR (500 MHz, DMSO-d₆, δ): 7.03 (s, 5H), 3.81 (s, 2H), 2.92 (s, 5H), 1.64–1.42 (m, 30H), 1.42–1.09 (m, 23H) corresponding to the polyurethane part and shifts 3.97 (t, $J = 6.5$ Hz, 13H) and 2.26 (t, $J = 7.3$ Hz, 14H) corresponding to polycaprolactone part (Figure S2).

2.6. 3D Printing. A custom-modified 3D printer (Prusa I3 Pro, Geetech, Shenzhen, China) was used to perform the 3D printing of hydrogels. Mechanical pressure was used for extrusion. Three different solutions of HA-MA (3, 5, and 7% W/V) were loaded into 3 mL syringes (Omnifix). Repetier-Host was used to design the

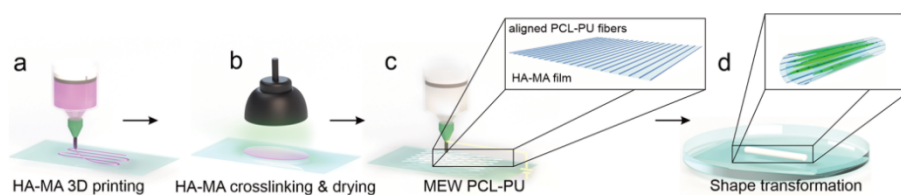


Figure 1. Scheme of the fabrication of shape-changing mats for the regeneration of muscle tissue by MEW of polycaprolactone-polyurethane (PCL-PU) and 3D printing of HA-MA: (a) 3D printing of HA-MA; (b) cross-linking of printed HA-MA film; (c) deposition of uniaxially aligned fibers of PCL-PU using MEW; (d) seeding C2C12 myoblast on the bilayer, its shape transformation, and formation of a multilayer scroll tube suitable for cells encapsulation.

dimensions of the films ($20 \times 5 \text{ mm}^2$) and command the 3D printer. HA-MA hydrogel solutions were printed onto glass slides ($76 \text{ mm} \times 26 \text{ mm}$) from 27G $0.4 \times 12 \text{ mm}$ blunt needles (Sterican). The distance between the tip of the needle and the glass slide was kept at $\leq 0.5 \text{ mm}$. One and two layers of each concentration were printed to increase the thickness of the hydrogel film and keep the 2D size of the films.

2.7. Melt Electrowriting (MEW). A custom-made melt electrowriting device was used to perform MEW in this study. The details are given in ref 29.

2.8. Scanning Electron Microscopy (SEM). Fiber morphology of PCL-PU was investigated using scanning electron microscopy SEM (Apreo, Thermo Fisher Scientific, USA) and field-emission scanning electron microscopy FE-SEM (FEI Teneo, FEI Co., Hillsboro, OR and Carl Zeiss Microscopy GmbH, Germany). The details are given in ref 32.

2.9. Dynamical Mechanical Analysis (DMA). The mechanical properties of PCL-PU films were characterized by dynamic mechanical analysis (DMA) tests in extension-deformation mode, samples with dimensions $7.0 \times 2.0 \times 0.12 \text{ mm}^3$ were prepared for this purpose. The DMA assays were performed at room temperature and $36 \text{ }^\circ\text{C}$ using a dynamic mechanical analyzer, MCR 702 MultiDrive (Anton Paar, Austria), equipped with solid rectangular fixtures (SRF5) and a temperature chamber (CTD 600 TDR). During the measurement, static (120 kPa) and dynamic forces (120 kPa) were applied, within a frequency range from 10 to 0.1 Hz to characterize the elastic properties of the materials.

2.10. Rheology. Rheological behavior of 3% HA-MA cross-linked and non-cross-linked solutions, as well as the rheological behavior of melted PCL-PU 110 and 121, were measured using MCR 702 (Anton Paar, Graz, Austria). Twenty-five millimeter diameter plate–plate geometry was used. The details are given in ref 32.

2.11. Thermogravimetric Analysis (TGA). Degradation of the PCL and PCL-PU fibers was studied using a temperature ramp applied by Mettler Toledo TGA 2 STAR System (USA) from 25 to $600 \text{ }^\circ\text{C}$ at a heating rate of $20 \text{ }^\circ\text{C}/\text{min}$ under a nitrogen atmosphere (Figure S3). The details are given in ref 32.

2.12. Differential Scanning Calorimetry (DSC). The thermal behavior of the PCL-diol and PCL-PU was studied using a DSC3 (Mettler Toledo, USA). The details are given in ref 32.

2.13. Small-Angle X-ray Scattering (SAXS). The scattering patterns were recorded using the SAXS system “Ganesha-Air” from (SAXSLAB/XENOC). The X-ray source of the laboratory-based system was a D2-MetalJet (Excillum) with a liquid metal anode operating at 70 kV and 3.57 mA with Ga- $K\alpha$ radiation (wavelength $\lambda = 0.1314 \text{ nm}$) providing small beam ($<100 \text{ }\mu\text{m}$). The details are given in ref 29 and 41.

2.14. Streaming Potential Measurements. Zeta potential was determined with SurPASS 3 (Anton Paar, Graz, A) by streaming potential measurements. The details are given in ref 29.

2.15. Cell Culture. C2C12 mouse muscle cells (passage <7) were cultured on aligned MEW fibers made of the copolymer PCL-PU 121, as well as the bilayer HA-MA–PCL-PU mat fixed on the on the cover glass. The details are given in ref 29.

2.16. Biological Characterization. Cell viability was determined after culturing in the bilayers as well as PCL-PU fibers was measured via a live/death assay. The details are given in refs 29 and 32.

2.17. Live/Dead Assay. The proliferation rate of the cells cultured on the bilayer and PCL-PU fibers was measured using the Alamar Blue assay after 1, 3, and 7 days of culture. The details are given in refs 29 and 32.

2.18. Actin Filament and Cell Nuclei Staining. To quantify the alignment of the muscle cells on bilayers and the PCL-PU fibers, we stained the actin filaments and nuclei using staining solution composed of blue fluorescent DAPI to target rich regions in adenine and thymine in DNA and green fluorescent Phalloidin Dylight 488 to selectively label F-actin in fixed cells in 10 mL of PBS. The details are given in ref 29 and 32.

2.19. Statistical Analyses. All data are presented as means \pm standard deviation (SD). Statistical analyses were performed using a Student’s *t* test and one-way analysis of variance (ANOVA) followed by Tukey’s multiple comparison test. A value of $p < 0.05$ was considered significant.

3. RESULTS AND DISCUSSION

We used a combination of 3D printing and MEW to prepare shape-changing bilayer mats of PCL-PU copolymer and methacrylic hyaluronic acid (HA-MA) to design new structures able to mimic the structure of muscle tissue and to investigate their interactions with cells. It is essential that the PCL-PU fibers are soft, elastic, and uniaxially aligned to guide the shape-transformation, provide support and guidance to the cells. HA-MA films contained Eosin Y and triethanolamine as photoinitiator and cross-linking agent, respectively (532 nm , green light). The first layers, the films, were fabricated via 3D printing hydrogel on glass slides. PCL-PU oriented fibers were deposited afterward using the MEW technique on top of the dried HA-MA films (Figure 1).

Synthesis of HA-MA was performed using the standard approach by reacting hyaluronic acid with methacrylic anhydride. The degree of methacrylation of HA-MA was determined as 94%, as described previously by Seidlits et al. (Figure S4).⁴² PCL-PU was synthesized by reacting PCL diol with hexamethylene diisocyanate and butanediol. The molar ratio between a diisocyanate and both diols was maintained at 1:1. The ratio between PCL diol:butanediol was varied in order to change the ratio between PCL and PU blocks in the range between 67.9 and 92.2% (Table 1).

We first investigated the thermal properties of PCL-PU using DSC. We observed two endothermic peaks: one at around $40\text{--}50 \text{ }^\circ\text{C}$ corresponding to the melting of PCL and another one at $120\text{--}160 \text{ }^\circ\text{C}$ corresponding to the melting of PU (Figure 2a and S5). The degree of crystallinity of the obtained PCL-PU copolymers is very low (Table 1) and was found not to correlate with the fraction of PU. Meanwhile, PCL-diol, which was used as reference exhibited a double

Table 1. Chemical Composition and Degree of Crystallinity of PCL-PU Copolymers^a

polymer PCL-PU	molar ratio (PCL:2000:HDI:BD)	mass fraction of PCL [%]	degree of crystallinity (DSC), [%]	elastic modulus [MPa], 36 °C	
				DMA	tensile
110	1:1:0	92.2	0.6	2	6.7
121	1:2:1	82.4	13.9	10	8.2
143	1:4:3	67.9	1.0	15	17.4 ^b

^aPCL = polycaprolactone; PU = polyurethane; HDI = hexamethylene diisocyanate; BD = butanediol; DSC = differential scanning calorimetry; DMA = dynamic mechanical analysis. ^bCalculated from the graph at room temperature.

melting transition at 43.8 and 49.5 °C with a total fusion enthalpy of 68.55 J g⁻¹ corresponding to a crystallinity of 50.4%. Meanwhile in the thermogram of the copolymers, it showed only a single melting endotherm observed at 34.0 °C. Thus, the introduction of PU blocks in the polymer strongly suppresses the crystallization of PCL.

Next, the mechanical properties of three PCL-PU copolymers were characterized using dynamic mechanical analysis (DMA) at room temperature and 37 °C (cell culture temperature) (Figure 2b). It was observed that the elastic modulus of the polymer is independent of frequency in the range 0.1–10 Hz and increases with the fraction of PU and it is in the range between 3 and 15 MPa. Increase in temperature results in a slight decrease in elastic modulus that can be associated with the softening of both PCL and PU blocks.

We performed cyclic measurements of stress–strain dependence in order to evaluate the shape recovery properties of polymers after stretching (Figure 2c). It was observed that PCL-PU 143 is brittle and breaks at 20% elongation. PCL-PU 110 and 121 were capable of withstanding stretching up to at least 200%. The elastic modulus of polymers obtained in tensile test experiments are 6.7 and 8.2 MPa for PCL-PU 110 and 121, respectively (Table 1). This value is very close to the elastic modulus of elastin, which is a protein responsible for the reversibility of ECM deformation. The polymer demonstrates partial recovery of its shape after stretching and the recovery degree increases with temperature. The reason for the increase in the recovery degree with an increase in temperature is the softening of PCL, which makes the behavior of the copolymer similar to that of rubbers. Because it was found that PCL-PU 143 is too brittle and the fibers formed by PCL 110 are too soft to be handled, we further focused on PCL 121, which has an

elastic modulus of ~8 MPa, can be stretched to 200%, and is capable of partial shape recovery after stretching.

Next, we investigated the rheological properties and printing of HA-MA. It was found that the storage modulus of the 3% HA-MA ink for 3D printing was about 0.8 Pa at 0.1 Hz and 122 Pa at 100 Hz. The storage modulus increased to ~5 Pa (0.1 Hz) and 1800 Pa (100 Hz) after exposing it to green light, indicating the cross-linking of the polymer. A decrease in the storage modulus with a decrease in frequency indicated the existence of temporary physical cross-links, which contribute to the rigidity of hydrogels at high frequencies (Figure 3 a).

The frequency sweep of the molten PCL-PU copolymers was also measured before MEW. The storage modulus for the molten PCL-PU 110 and PCL-PU 121 was found to be about 1.26 Pa at 0.1 Hz and 1460 Pa at 100 Hz and 1.96 Pa at 0.1 Hz and 1463 Pa at 100 Hz, respectively, showing nearly the same rheological behavior with relaxation time around one second in both cases (Figure 3b). The fibers were produced at 125 °C, 0.6 bar, and 4.0 kV at a 6 mm distance. Considering the data obtained with the DSC measurement, the heating temperature of PCL-PU for MEW was chosen between 90 and 125 °C. Different patterns such as parallel fibers, 45 and 90° mesh structures with uniform PCL-PU fibers were successfully obtained through MEW (Figure 3c, d).

The MEW PCL-PU fibers have wrinkled surface morphology (Figure 3e) that can originate from faster fiber surface solidification, in comparison to its core, and fiber contraction (relaxation) after its deposition. The structure of MEW fibers of PCL-PU 121 was studied using SAXS and WAXS (Figure 3f, g). Obtained results showed that PCL-PU 121 fibers are semicrystalline because of the presence of the characteristic peaks at $q = 15.1$ and 16.7 \AA^{-1} corresponding to the reflections of the PCL crystals toward 110 and 200 planes, which are overlapped with the interference of amorphous polyurethane (Figure 3h).⁴³ The degree of crystallinity is low, measured to be around 18.1%, which is close to that obtained by DSC (Table 1). We obtained the following values of order parameters from analysis of peak widths at different q : $S = 0.13$ ($q = 0.13\text{--}0.3 \text{ nm}^{-1}$); $S = 0.15$ ($q = 0.3\text{--}0.6 \text{ nm}^{-1}$); $S = 0.13$ ($q = 14.4\text{--}15.6 \text{ nm}^{-1}$) that indicates a very low degree of orientation of the polymer chains in the fibers (Figure 3i). No indication of the formation of the lamellar structure was revealed by the SAXS experiment. Thus, both DSC and XRD predominantly indicate the amorphous character of the polymer. Small crystallites play a role in physical cross-linking points ensuring the partial reversibility of deformation.

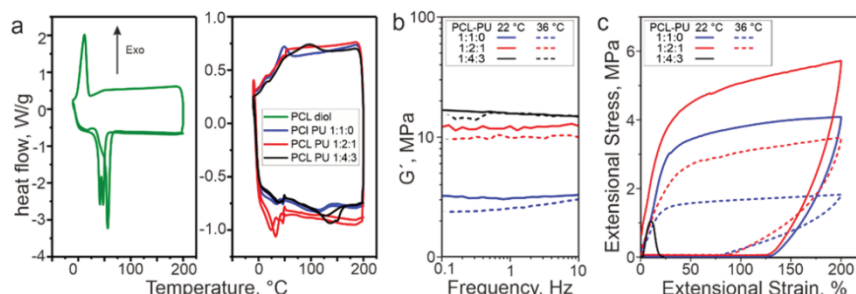


Figure 2. PCL-PU properties: (a) DSC of PCL-diols (left) and PCL-PU copolymers (right); (b) dynamical mechanical analysis (DMA) results of PCL-PU copolymers; (c) PCL-PU cyclic stress–strain curves.

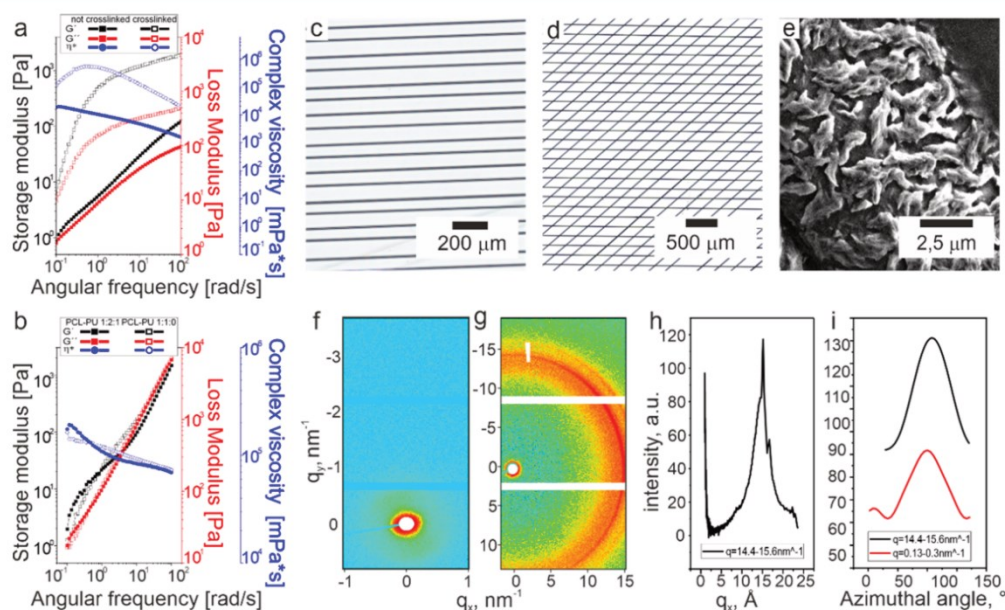


Figure 3. Behavior of HA-MA and PCL-PU fibers: (a) rheological properties of HA-MA solution and photo-cross-linked mat; (b) rheological behavior of PCL-PU in molten state at 125 °C for PCL-PU 121 and 165 °C for PCL-PU 110; (c) optical images of parallel fibers of MEW PCL-PU 121; (d) optical images of 45° mesh fibers; (e) SEM image of MEW PCL-PU fibers; (f) 2D scattering patterns in the low q region of PCL-PU 121 fibers; (g) 2D scattering patterns in the large q region of PCL-PU 121 fibers; (h) radial scattering intensity profiles obtained from WAXS; (i) azimuthal profile obtained from high and low q regions.

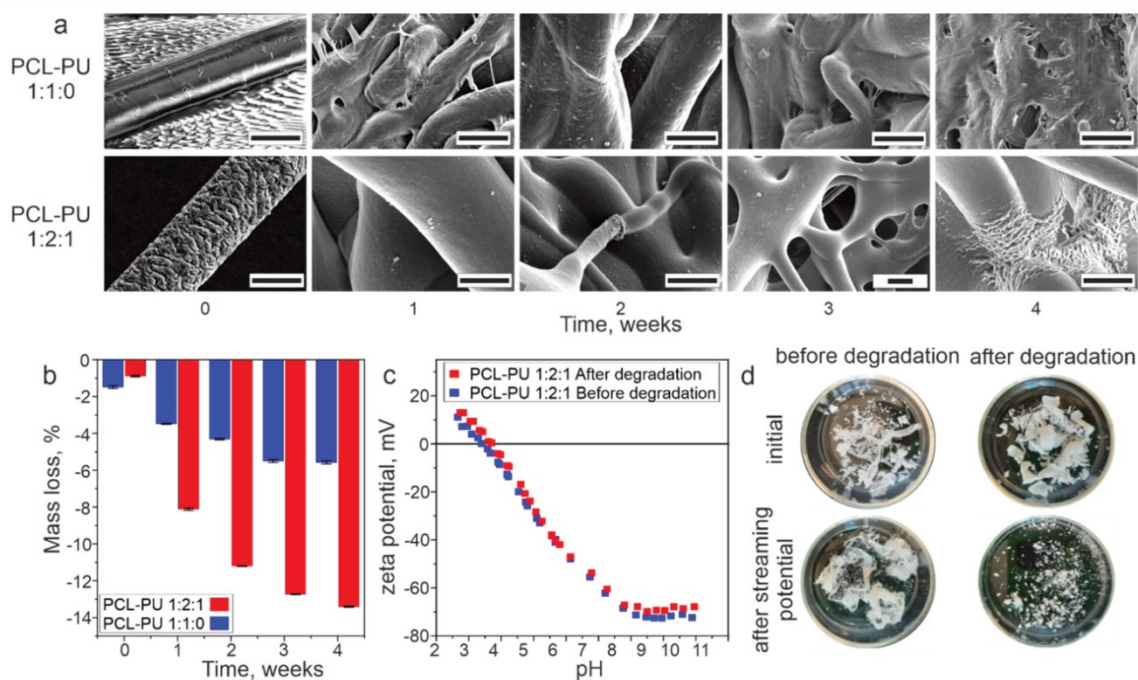


Figure 4. Degradation test of PCL-PU: (a) Morphology of PCL-PU MEW fibers after 1, 2, 3, and 4 weeks of degradation in PBS solution at 37 °C. Scale bars 10 μm ; (b) mass loss of PCL-PU MEW fibers during 4 weeks of degradation; (c) zeta potential of PCL-PU 1:2:1 fiber before and after degradation test; (d) images of fiber bundles before and after degradation test before and after exposure to liquid stream during zeta potential measurements.

PCL is the biodegradable block of the copolymer, which shall ensure the degradation of the polymers' chains and their splitting in shorter ones.^{31,44} Hence, we tested the real-time

degradation of MEW fibers of PCL-PU 110 and 121 in PBS. In this study, the hydrolytic degradation of PCL-PU fibers was performed by immersion in 3 \times PBS for up to 4 weeks at 37 °C.

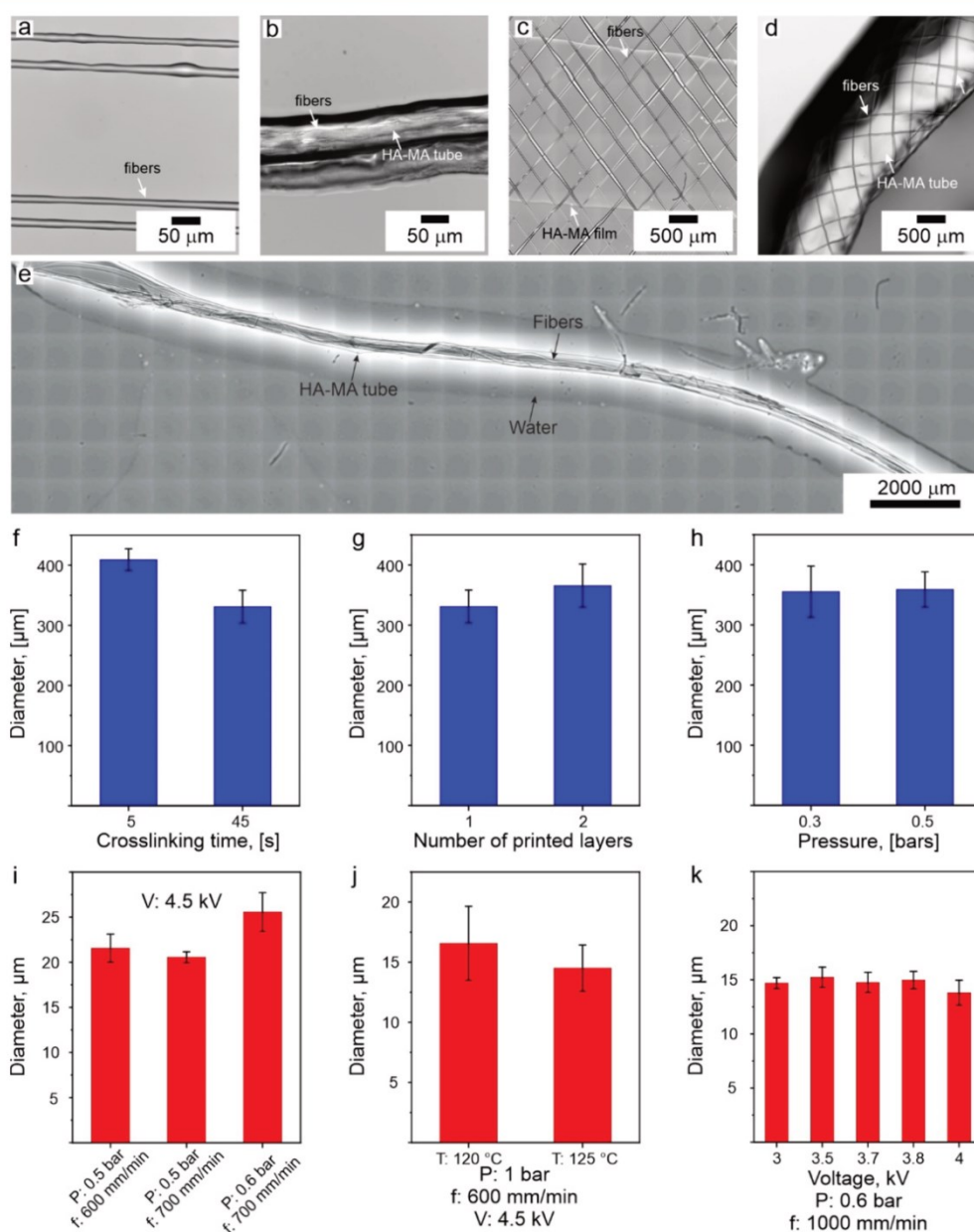


Figure 5. Optical images of HA-MA-PCL-PU bilayers and formed tubes: (a) MEW PCL-PU 121 aligned fibers on top of HA-MA film; (b) HA-MA tube with MEW PCL-PU 121 aligned fibers inside indicated by arrows; (c) MEW PCL-PU 121 90° mesh fibers on top of HA-MA film; (d) HA-MA tube formation with MEW PCL-PU 121 90° mesh fibers inside indicated by arrows; (e) large scale microscopy image of tube with fibers. Tube diameter vs 3D printing parameters: (f) effect of the cross-linking time; (g) number of printed layers; (h) pressure for a single layer. Fiber diameter vs MEW parameters: (i) effect of pressure and feed rate; (j) effect of temperature; (k) effect of voltage.

Degradation results show a higher degradation degree (about 7% in mass) for the copolymer containing BD as chain extender (Figure 4), which is explained by the presence of a higher amount of ester (urethane) hydrolyzable bonds. Comparing the results obtained in this study with the degradation test reported by Hao-Yang et al.³¹ for the PCL-PU 121 films, we can conclude that the higher surface area and porosity of the MEW fibers contribute to the degradation of the polymer. Taking into consideration that the degradation products are supposed to be absorbed and metabolized in vivo,

the PCL-PUs have the potential to be suitable for tissue engineering.

We have also performed an investigation of the change of zeta potential of the polymer upon its degradation. For this, we performed measurements on the same polymer before and after the degradation test. It was observed that the zeta potential decreases linearly with increase pH and becomes nearly independent of pH at pH >8. The isoelectric point (IEP) is around 3.4. This dependence of zeta potential on pH is due to the dissociation of carboxyl-terminal groups of

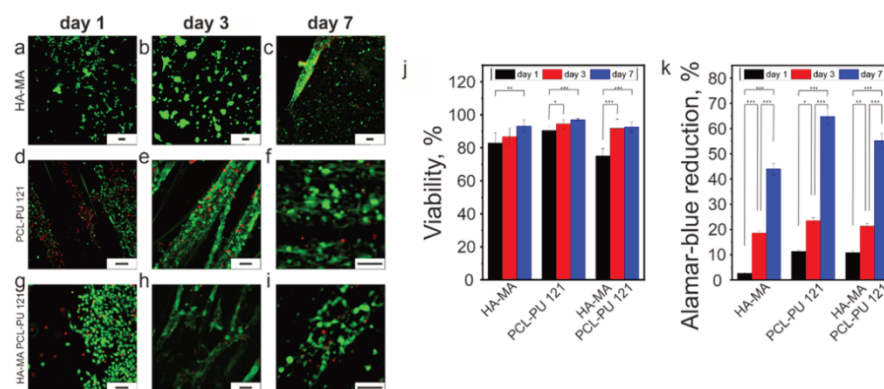


Figure 6. C2C12 myoblast cell culture: (a–i) viability of cells (Live/Dead assay) on (a–c) HA-MA films, (d–f) layer of PCL-PU 121 MEW fibers, and (g–i) bilayer (PCL-PU 121 MEW fibers on HA-MA scaffolds) after 1, 3, and 7 days of culture. Red, dead cells; green, live cells. Scale bars, 100 μm . (j) Quantification of cell viability after 1, 3, and 7 days of culture. (k) Cell metabolic activity after 1, 3, and 7 days of culture measured by Alamar Blue Assay. * $p \leq 0.05$; ** $p \leq 0.01$; *** $p \leq 0.001$; **** $p \leq 0.0001$.

polymer chains. First, we observed a slight increase in IEP from 3.4 to 3.6 and a decrease in zeta potential value at $\text{pH} > 8$. This change can be explained by a decrease in the surface density of the carboxyl group, which is due to the hydrolysis and elimination of caprolactone fragments; it is expected that ultimately, urethane fragments with linked diol shall stay undegraded. Second, it was visually observed that not-yet-degraded polymer fibers retain their shape upon exposure to liquid stream during zeta potential measurements. On the other hand, fibers after degradation break apart after zeta potential measurement due to liquid stream. Both these observations—change of IEP and zeta potential, as well as disintegration of fibers—clearly indicate the degradation of the polymer.

We studied the effect of fabrication conditions on the properties of mats (Figure 5). It was found that both the number of printed layers and the pressure applied during extrusion, which affect the thickness of the printed layer, do not significantly affect the diameter of the tube formed after folding (Figure 5e). Longer cross-linking decreases the tube diameter, as it affects the cross-linking degree and the swelling properties of polymers (Figure 5f–h). According to the Timoshenko equation,⁴⁵ the diameter must decrease with an increase in cross-linking density. The reason for the opposite effect is most probably incomplete cross-linking of the polymer at low irradiation time—the layer cross-linked over 5 s is thinner than that cross-linked over 45 s. On the basis of these observations, we selected the optimal conditions for the fabrication of the bilayers as single layer of HA-MA 3% (printed at 0.3 bar and cross-linked during 45 s by green light), and PCL-PU fibers melt electrospun on top (at 125 $^{\circ}\text{C}$, pressure 0.6 bar, and voltage 4.0 kV). Results obtained using different temperatures, feeding pressures, feed rates, and voltages are summarized in Figure 5i–k. Briefly, an increase in 5 $^{\circ}\text{C}$ temperature results in a decrease in fiber diameter ~ 2 μm . The diameter of the fibers shows a direct relation with the pressure and inversed respect to the feed rate producing bigger fibers at higher pressures and slower motions. The fiber diameter is almost independent of the voltage, but it affects the alignment. The distance between the fibers was fixed at 100 μm because this spacing, as it was demonstrate earlier,⁴⁶ is able to provide good cell alignment. MEW provides a high speed of fiber deposition, requiring a large amplitude of the x - and y -

table movement. Therefore, the size of the structure formed by PCL-PU fibers was larger than the printed HA-MA layer. We observed that the cross-linked HA-MA layer ruptures the PCL-PU fibers upon swelling and rolling, resulting in the formation of tubes with the ornament of PCL-PU fibers on their inner surface. It was found that the presence of the fibers and the pattern they form does not affect the folding direction and diameter of formed tubes.

Finally, we performed cell culture studies on the shape-changing bilayers of HA-MA and uniaxially aligned elastomeric fibers. The experiments were performed on flat fixed scaffolds to avoid the folding because it is not possible to image the cells properly in rolled structures. The bilayer scaffold was fixed by applying a ring; the removal of the rings results in the rolling of scaffolds with adsorbed cells on it. Cells were cultured on HA-MA, PCL-PU 121 MEW aligned fibers, and bilayer mats treated with FNC (protein-based mixture) to promote cell adhesion, showed a high viability above 80% independent of the material. As it was shown in Figure 6, myoblasts adhered on HA-MA films showed inhomogeneous cell distribution and rather formed clusters. Moreover, after 7 days of culture, those clusters did not show any alignment and remained with a round morphology (Figure 6a–c). Meanwhile, cells cultured on PCL-PU fibers preferred to grow in the gaps between the fibers and avoided growing directly on the fibers (Figure 6d–f). Interestingly, cells cultured on HA-MA–PCL-PU bilayers showed a different behavior and adhered to the fibers as well as formed bridges between them, whereas they had an HA-MA film underneath (Figure 6g–i). We did not observe cell growth on top of the fibers, which could be explained because of the similarity of the fiber diameter to the cell size. The cell viability at day one on the bilayers was significantly lower than the viability on HA-MA, but after day 3 and 7 of culture, the viability on the bilayers increases showing no significant differences respect to the HA-MA films or PCL-PU fibers (Figure S6a). It can be explained by the properties of the materials that form the bilayer, a hydrophilic HA-MA film with hydrophobic PCL-PU fibers on top. It also explains the cell distribution in the gaps of the fibers. In all cases, an increase in the viability and metabolic activity with time was observed (Figure 6j). It was observed that cell proliferation over 7 days of culture on PCL-PU fiber is significantly higher than that on HA-MA films. The cell metabolic activity was measured by

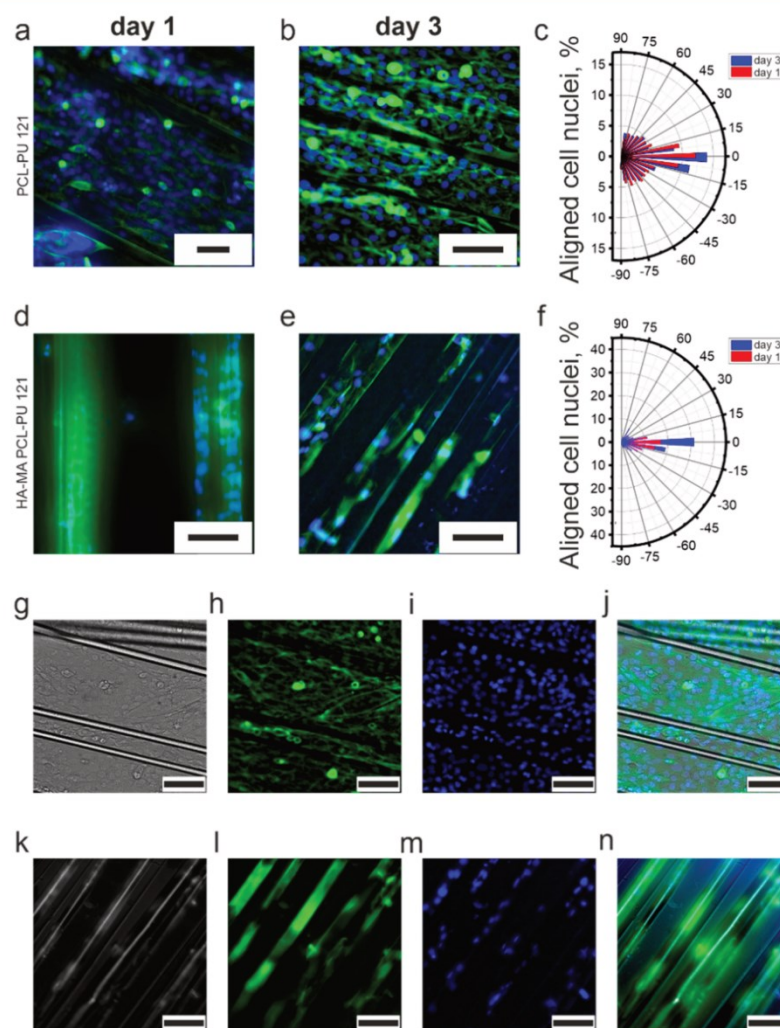


Figure 7. Alignment of C2C12 myoblast cell on PCL-PU 121 MEW fibers and bilayer PCL-PU 121 MEW fibers on HA-MA scaffolds coated with FNC after 1 and 3 days of culture: (a, b) fluorescence images of cells on PCL-PU 121 MEW fibers on days 1 and 3; (c) quantification analysis of cell nuclei alignment on PCL-PU 121 MEW fibers; (d, e) fluorescence images of cells on PCL-PU 121 MEW fibers on HA-MA scaffolds on days 1 and 3; (f) quantification analysis of cells nuclei alignment on PCL-PU 121 MEW on HA-MA scaffolds; (g–j) single-channel and merge fluorescence image presentation of cells on PCL-PU 121 MEW fibers at day 3 after culture; (k–n) single-channel and merge fluorescence image presentation of cells on bilayer PCL-PU 121 MEW fibers on HA-MA scaffolds at day 3 after culture. Scale bars, 100 μm .

Alamar Blue assay and showed that on the bilayer it was intermediate in comparison to those on either one of the HA-MA films and PCL-PU MEW fibers. It is worth mentioning that the lower metabolic activity of cells on HA-MA films as well as the preferred arrangement of cells in the gaps between PCL-PU fibers does not affect the suitability of the bilayer for biofabrication (Figure 6k), as cells demonstrate both good viability and metabolic activity.

Cell alignment on PCL-PU 121 fibers and HA-MA PCL-PU bilayers was analyzed after actin filament and cell nuclei staining. Cell alignment on the HA-MA layer was not studied, as live/dead experiments already demonstrate that cells are disordered and there is no guidance reference to quantify the alignment, as in the case of random fibers. Staining experiments confirmed the preference of cells in the gaps between PCL-PU fibers. After 3 days of culture, cell alignment between -10° and 10° was measured to be about 33.9%. We

found that this alignment was improved after 3 days of culture because of the spaces between the fibers and the high cell proliferation. Furthermore, we observed that on the bilayers, the presence of an HA-MA layer in the mat supported higher adhesion of cells and increased the attachment to the fibers. This resulted in a higher alignment degree of about 57.5%. Nevertheless, even when the cells grew in the gaps between the fibers in the absence of HA-MA, they aligned themselves in the direction of fibers (Figure 7). Thus, the developed approach allows the encapsulation of uniaxially aligned cells inside the formed polymer tube.

4. CONCLUSION

In this work, we report an approach for the manufacturing of shape-changing scaffold using a combination of 3D printing of hyaluronic acid hydrogel, melt electrowriting of thermoplastic polycaprolactone-polyurethane elastomer, and

shape transformation of the bilayer for the growth of muscle cells. The combination of the selected fabrication methods and materials allows several important advantages. In particular, both polymers are biocompatible and biodegradable. The use of nearly amorphous, elastic, and soft polycaprolactone-polyurethane copolymer instead of widely used pure plastic polycaprolactone is more suitable, as the formed structures are expected to undergo large and reversible actuation upon cell contraction. The use of 3D printing of hydrogel allows the programmed manufacturing of structures with the desired shape. Whereas melt electrowriting allows longitudinal deposition of copolymer fibers, this uniaxial alignment of fibers is essential for cell alignment. We found that myoblasts occupy space between the fibers and align along them. Finally, the bilayer scaffold is able to change their shape and form multilayer scroll-like structures. These scroll-like tubular structures can be further developed for obtaining vascularized tissues to transport nutrition and oxygen to the cells inside and for culturing a microtissues suitable for transplantation.

■ ASSOCIATED CONTENT

Supporting Information

The Supporting Information is available free of charge at <https://pubs.acs.org/doi/10.1021/acsabm.0c01495>.

Infrared spectra of PCL-PU 121; NMR spectra of PCL-PU 121; thermogravimetric analysis of PCL-PU 121; NMR spectra of HA-MA; differential scanning calorimetry in time scale of PCL-diol 2000 kDa, PCL-PU 110, PCL-PU 121, and PCL-PU 143; C2C12 myoblast cell culture presented with detailed significant differences after quantification of cell viability after 1, 3, and 7 days of culture and cell metabolic activity after 1, 3, and 7 days of culture measured by Alamar Blue Assay (PDF)

■ AUTHOR INFORMATION

Corresponding Author

Leonid Ionov – Faculty of Engineering Sciences and Bavarian Polymer Institute, University of Bayreuth, Bayreuth 95447, Germany; orcid.org/0000-0002-0770-6140; Email: leonid.ionov@uni-bayreuth.de

Authors

Juan Uribe-Gomez – Faculty of Engineering Sciences, University of Bayreuth, Bayreuth 95447, Germany

Andrés Posada-Murcia – Faculty of Engineering Sciences, University of Bayreuth, Bayreuth 95447, Germany

Amit Shukla – Faculty of Engineering Sciences, University of Bayreuth, Bayreuth 95447, Germany

Mert Ergin – Faculty of Engineering Sciences, University of Bayreuth, Bayreuth 95447, Germany

Gissela Constante – Faculty of Engineering Sciences, University of Bayreuth, Bayreuth 95447, Germany

Indra Apsite – Faculty of Engineering Sciences, University of Bayreuth, Bayreuth 95447, Germany

Dulle Martin – Forschungszentrum Jülich GmbH Jülich Centre for Neutron Science (JCNS-1) and Institute for Complex Systems (ICS-1), Jülich 52428, Germany

Madeleine Schwarzer – Leibniz Institute of Polymer Research Dresden e. V., Dresden 01069, Germany; orcid.org/0000-0001-6204-1025

Anja Caspari – Leibniz Institute of Polymer Research Dresden e. V., Dresden 01069, Germany

Alla Synytska – Leibniz Institute of Polymer Research Dresden e. V., Dresden 01069, Germany; Faculty of Mathematics and Science, Institute of Physical Chemistry and Polymer Physics, Dresden University of Technology, Dresden 01062, Germany; orcid.org/0000-0002-0643-7524

Sahar Salehi – Department of Biomaterials, University of Bayreuth, 95447 Bayreuth, Germany

Complete contact information is available at:

<https://pubs.acs.org/doi/10.1021/acsabm.0c01495>

Author Contributions

The manuscript was written through contributions of all authors. All authors have given approval to the final version of the manuscript.

Notes

The authors declare no competing financial interest.

■ ACKNOWLEDGMENTS

This work was supported by DFG (IO 68/14-1, IO 68/1-2, IO 68/17-1, SY 125/6-3, SA 3575/1-1; Project N 326998133 – SFB/TRR225 (subproject B03)). We would further like to thank Prof. Scheibel for providing us facilities like DSC, TGA, and SEM equipment to conduct this research and Arch. Ignacio Uribe for the render, Laura Pedraza, and Diana Rodríguez for paper revisions.

■ ABBREVIATIONS

ECM, extracellular matrix; VML, volumetric muscle loss; MEW, melt electrowriting; PCL, polycaprolactone; PU, polyurethane; AA-MA, methacrylated alginate; HA-MA, methacrylate hyaluronic acid; PCL-PU, polycaprolactone-polyurethane; HDI, hexamethylene diisocyanate; BD, butanediol; DBTDL, dibutyltin dilaurate; TEA, triethanolamine; VP, 1-vinyl-2-pyrrolidinone; DMSO, dimethyl sulfoxide; MA, methacrylic anhydride; EtOH, ethanol; IPA, 2-Propanol; EDTA, ethylenediaminetetraacetic acid; DPBS, Dulbecco's phosphate buffered saline; DMEM, Dulbecco's modified Eagle medium; Pen/strep, penicillin-streptomycin; FBS, fetal bovine serum; HEPES, 4-(2-hydroxyethyl)-1-piperazineethanesulfonic acid; BSA, albumin fraction V; EthD-1, ethidium; DAPI, 4',6-diamidino-2-phenylindole; FT-IR, Fourier transform infrared spectroscopy; NMR, nuclear magnetic resonance; SEM, scanning electron microscopy; TGA, thermogravimetric analysis; SAXS, small-angle X-ray scattering; DSC, differential scanning calorimetry; DMA, dynamic mechanical analysis

■ REFERENCES

- (1) Chen, F. M.; Liu, X. Advancing biomaterials of human origin for tissue engineering. *Prog. Polym. Sci.* **2016**, *53*, 86–168.
- (2) Porzionato, A.; Stocco, E.; Barbon, S.; Grandi, F.; Macchi, V.; De Caro, R. Tissue-engineered grafts from human decellularized extracellular matrices: a systematic review and future perspectives. *Int. J. Mol. Sci.* **2018**, *19* (12), 4117.
- (3) Kwee, B. J.; Mooney, D. J. Biomaterials for skeletal muscle tissue engineering. *Curr. Opin. Biotechnol.* **2017**, *47*, 16–22.
- (4) Berthiaume, F.; Maguire, T. J.; Yarmush, M. L. Tissue engineering and regenerative medicine: history, progress, and challenges. *Annu. Rev. Chem. Biomol. Eng.* **2011**, *2*, 403–430.
- (5) Zhang, D.; Yan, K.; Zhou, J.; Xu, T.; Xu, M.; Lin, J.; Bai, J.; Ge, G.; Hu, D.; Si, W.; et al. Myogenic differentiation of human amniotic mesenchymal cells and its tissue repair capacity on volumetric muscle loss. *J. Tissue Eng.* **2019**, *10*, 204173141988710.

- (6) Russell, C. S.; Mostafavi, A.; Quint, J. P.; Panayi, A. C.; Baldino, K.; Williams, T. J.; Daubendiek, J. G.; Hugo Sanchez, V.; Bonick, Z.; Trujillo-Miranda, M.; et al. In Situ Printing of Adhesive Hydrogel Scaffolds for the Treatment of Skeletal Muscle Injuries. *ACS Applied Bio. Materials* **2020**, *3* (3), 1568–1579.
- (7) Nuutila, K.; Sakthivel, D.; Kruse, C.; Tran, P.; Giatsidis, G.; Sinha, I. Gene expression profiling of skeletal muscle after volumetric muscle loss. *Wound. Repair. Regen.* **2017**, *25* (3), 408–413.
- (8) Ostrovidov, S.; Shi, X.; Sadeghian, R. B.; Salehi, S.; Fujie, T.; Bae, H.; Ramalingam, M.; Khademhosseini, A. Stem cell differentiation toward the myogenic lineage for muscle tissue regeneration: a focus on muscular dystrophy. *stem. cell. rev. rep.* **2015**, *11* (6), 866–884.
- (9) Ebrahimi, M.; Ostrovidov, S.; Salehi, S.; Kim, S. B.; Bae, H.; Khademhosseini, A. Enhanced skeletal muscle formation on microfluidic spun gelatin methacryloyl (GelMA) fibres using surface patterning and agrin treatment. *J. Tissue Eng. Regener. Med.* **2018**, *12* (11), 2151–2163.
- (10) Yang, G. H.; Lee, J.; Kim, G. The fabrication of uniaxially aligned micro-textured polycaprolactone struts and application for skeletal muscle tissue regeneration. *Biofabrication* **2019**, *11* (2), 025005.
- (11) Ostrovidov, S.; Ebrahimi, M.; Bae, H.; Nguyen, H. K.; Salehi, S.; Kim, S. B.; Kumatani, A.; Matsue, T.; Shi, X.; Nakajima, K.; et al. Gelatin–polyaniline composite nanofibers enhanced excitation–contraction coupling system maturation in myotubes. *ACS Appl. Mater. Interfaces* **2017**, *9* (49), 42444–42458.
- (12) Mueller, C.; Trujillo-Miranda, M.; Maier, M.; Heath, D. E.; O'Connor, A. J.; Salehi, S. Effects of External Stimulators on Engineered Skeletal Muscle Tissue Maturation. *Adv. Mater. Interfaces* **2021**, *8*, 2001167.
- (13) Apsite, I.; Uribe, J. M.; Posada, A. F.; Rosenfeldt, S.; Salehi, S.; Ionov, L. 4D biofabrication of skeletal muscle microtissues. *Biofabrication* **2020**, *12* (1), 015016.
- (14) Kim, J. H.; Seol, Y. J.; Ko, I. K.; Kang, H. W.; Lee, Y. K.; Yoo, J. J.; Atala, A.; Lee, S. J. 3D bioprinted human skeletal muscle constructs for muscle function restoration. *Sci. Rep.* **2018**, *8* (1), 1–15.
- (15) Zhang, Y.; Zhang, Z.; Wang, Y.; Su, Y.; Chen, M. 3D myotube guidance on hierarchically organized anisotropic and conductive fibers for skeletal muscle tissue engineering. *Mater. Sci. Eng., C* **2020**, *116*, 111070.
- (16) Ostrovidov, S.; Salehi, S.; Costantini, M.; Suthiwanich, K.; Ebrahimi, M.; Sadeghian, R. B.; Fujie, T.; Shi, X.; Cannata, S.; Gargioli, C.; et al. 3D bioprinting in skeletal muscle tissue engineering. *Small* **2019**, *15* (24), 1805530.
- (17) Brown, T. D.; Dalton, P. D.; Huttmacher, D. W. Direct writing by way of melt electrospinning. *Adv. Mater.* **2011**, *23* (47), S651–S657.
- (18) Castilho, M.; Feyen, D.; Flandes-Ipparraguirre, M.; Hochleitner, G.; Groll, J.; Doevendans, P. A.; Vermonden, T.; Ito, K.; Sluijter, J. P.; Malda, J. Melt electrospinning writing of poly-Hydroxymethylglycolide-co-ε-Caprolactone-based scaffolds for cardiac tissue engineering. *Adv. Healthcare Mater.* **2017**, *6* (18), 1700311.
- (19) Hochleitner, G.; Kessler, M.; Schmitz, M.; Boccaccini, A. R.; Teßmar, J.; Groll, J. Melt electrospinning writing of defined scaffolds using polylactide-poly (ethylene glycol) blends with 4SSS bioactive glass particles. *Mater. Lett.* **2017**, *205*, 257–260.
- (20) Tamayol, A.; Akbari, M.; Annabi, N.; Paul, A.; Khademhosseini, A.; Juncker, D. Fiber-based tissue engineering: Progress, challenges, and opportunities. *Biotechnol. Adv.* **2013**, *31* (5), 669–687.
- (21) Robinson, T. M.; Huttmacher, D. W.; Dalton, P. D. The Next Frontier in Melt Electrospinning: Taming the Jet. *Adv. Funct. Mater.* **2019**, *29* (44), 1904664.
- (22) Bootsma, K.; Fitzgerald, M. M.; Free, B.; Dimbath, E.; Conjerti, J.; Reese, G.; Konkolewicz, D.; Berberich, J. A.; Sparks, J. L. 3D printing of an interpenetrating network hydrogel material with tunable viscoelastic properties. *J. Mech. Behav. Biomed.* **2017**, *70*, 84–94.
- (23) Costantini, M.; Testa, S.; Mozetic, P.; Barbetta, A.; Fuoco, C.; Fornetti, E.; Tamiro, F.; Bernardini, S.; Jaroszewicz, J.; Swięszkowski, W.; Trombetta, M.; Castagnoli, L.; Seliktar, D.; Garstecki, P.; Cesareni, G.; Cannata, S.; Rainer, A.; Gargioli, C. Microfluidic-enhanced 3D bioprinting of aligned myoblast-laden hydrogels leads to functionally organized myofibers in vitro and in vivo. *Biomaterials* **2017**, *131*, 98–110.
- (24) Arslan, H.; Nojoomi, A.; Jeon, J.; Yum, K. 3D printing of anisotropic hydrogels with bioinspired motion. *Adv. Sci.* **2019**, *6* (2), 1800703.
- (25) De Ruijter, M.; Ribeiro, A.; Dokter, I.; Castilho, M.; Malda, J. Simultaneous micropatterning of fibrous meshes and bioinks for the fabrication of living tissue constructs. *Advanced healthcare materials. Adv. Healthcare Mater.* **2019**, *8* (7), 1800418.
- (26) Farazin, A.; Aghdam, H. A.; Motififard, M.; Aghadavoudi, F.; Kordjamschidi, A.; Saber-Samandari, S.; Khandan, A. A polycaprolactone bio-nanocomposite bone substitute fabricated for femoral fracture approaches: Molecular dynamic and micro-mechanical Investigation. *J. Nanoanaly.* **2019**, *6* (3), 172–184.
- (27) Fuchs, A.; Youssef, A.; Seher, A.; Hochleitner, G.; Dalton, P. D.; Hartmann, S.; Brands, R. C.; Müller-Richter, U. D. A.; Linz, C. Medical-grade polycaprolactone scaffolds made by melt electrospinning writing for oral bone regeneration—a pilot study in vitro. *BMC Oral Health* **2019**, *19* (1), 28.
- (28) Delgado-Aguilar, M.; Puig, R.; Sazdovskii, I.; Fullana-i-Palmer, P. Polylactic Acid/Polycaprolactone Blends: On the Path to Circular Economy, Substituting Single-Use Commodity Plastic Products. *Materials* **2020**, *13* (11), 2655.
- (29) Constante, G.; Apsite, I.; Alkhamis, H.; Dulle, M.; Schwarzer, M.; Caspari, A.; Synytska, A.; Salehi, S.; Ionov, L., 4D Biofabrication Using a Combination of 3D Printing and Melt-Electrowriting of Shape-Morphing Polymers. *ACS Appl. Mater. Interfaces* **2021**, in press, DOI: 10.1021/acsami.0c18608.
- (30) Wang, W.; Ping, P.; Yu, H.; Chen, X.; Jing, X. Synthesis and characterization of a novel biodegradable, thermoplastic polyurethane elastomer. *J. Polym. Sci., Part A: Polym. Chem.* **2006**, *44* (19), S505–S512.
- (31) Mi, H.-Y.; Jing, X.; Napiwocki, B. N.; Hagerty, B. S.; Chen, G.; Turng, L.-S. Biocompatible, degradable thermoplastic polyurethane based on polycaprolactone-block-polytetrahydrofuran-block-polycaprolactone copolymers for soft tissue engineering. *J. Mater. Chem. B* **2017**, *5* (22), 4137–4151.
- (32) Apsite, I.; Constante, G.; Dulle, M.; Vogt, L.; Caspari, A.; Boccaccini, A. R.; Synytska, A.; Salehi, S.; Ionov, L. 4D Biofabrication of fibrous artificial nerve graft for neuron regeneration. *Biofabrication* **2020**, *12* (3), 035027.
- (33) Sierra-Sánchez, Á.; Fernández-González, A.; Lizana-Moreno, A.; Espinosa-Ibáñez, O.; Martínez-Lopez, A.; Guerrero-Calvo, J.; Fernández-Porcel, N.; Ruiz-García, A.; Ordóñez-Luque, A.; Carriel, A.; Arias-Santiago, S. Hyaluronic acid biomaterial for human tissue-engineered skin substitutes: Preclinical comparative in vivo study of wound healing. *J. Eur. Acad. Dermatol. Venereol.* **2020**, *34* (10), 2414–2427.
- (34) Jeffery, A. F.; Churchward, M. A.; Mushahwar, V. K.; Todd, K. G.; Elias, A. L. Hyaluronic acid-based 3D culture model for in vitro testing of electrode biocompatibility. *Biomacromolecules* **2014**, *15* (6), 2157–2165.
- (35) Reichelt, S.; Becher, J.; Weisser, J.; Prager, A.; Decker, U.; Möller, S.; Berg, A.; Schnabelrauch, M. Biocompatible polysaccharide-based cryogels. *Mater. Sci. Eng., C* **2014**, *35*, 164–170.
- (36) Chandrasekharan, A.; Seong, K. Y.; Yim, S. G.; Kim, S.; Seo, S.; Yoon, J.; Yang, S. Y. In situ photocrosslinkable hyaluronic acid-based surgical glue with tunable mechanical properties and high adhesive strength. *J. Polym. Sci., Part A: Polym. Chem.* **2019**, *57* (4), S22–S30.
- (37) Zhang, Q.; Wei, X.; Ji, Y.; Yin, L.; Dong, Z.; Chen, F.; Zhong, M.; Shen, J.; Liu, Z.; Chang, L. Adjustable and Ultrafast Light-Cured Hyaluronic Acid Hydrogel: Promoting Biocompatibility and Cell Growth. *J. Mater. Chem. B* **2020**, *8*, S441–S450.
- (38) Kirillova, A.; Maxson, R.; Stoychev, G.; Gomillion, C. T.; Ionov, L. 4D Biofabrication Using Shape-Morphing Hydrogels. *Adv. Mater.* **2017**, *29* (46), 1703443.

- (39) Smeds, K. A.; Grinstaff, M. W. Photocrosslinkable polysaccharides for in situ hydrogel formation. *J. Biomed. Mater. Res.* **2001**, *54*, 115.
- (40) Zhang, L.; Huang, M.; Yu, R.; Huang, J.; Dong, X.; Zhang, R.; Zhu, J. Bio-based shape memory polyurethanes (Bio-SMPUs) with short side chains in the soft segment. *J. Mater. Chem. A* **2014**, *2* (29), 11490–11498.
- (41) Sims, M. T.; Abbott, L. C.; Richardson, R. M.; Goodby, J. W.; Moore, J. N. Considerations in the determination of orientational order parameters from X-ray scattering experiments. *Liq. Cryst.* **2019**, *46* (1), 11–24.
- (42) Seidlits, S. K.; Khaing, Z. Z.; Petersen, R. R.; Nickels, J. D.; Vanscoy, J. E.; Shear, J. B.; Schmidt, C. E. The effects of hyaluronic acid hydrogels with tunable mechanical properties on neural progenitor cell differentiation. *Biomaterials* **2010**, *31* (14), 3930–3940.
- (43) Oh, G.; Rho, J.; Lee, D. Y.; Lee, M. H.; Kim, Y. Z. Synthesis and characterization of electrospun PU/PCL hybrid scaffolds. *Macromol. Res.* **2018**, *26* (1), 48–53.
- (44) Blakney, A. K.; Simonovsky, F. I.; Suydam, I. T.; Ratner, B. D.; Woodrow, K. A. Rapidly biodegrading PLGA-polyurethane fibers for sustained release of physicochemically diverse drugs. *ACS Biomater. Sci. Eng.* **2016**, *2* (9), 1595–1607.
- (45) Timoshenko, S. Analysis of bi-metal thermostats. *J. Opt. Soc. Am.* **1925**, *11* (3), 233–255.
- (46) Ostrovidov, S.; Hosseini, V.; Ahadian, S.; Fujie, T.; Parthiban, S. P.; Ramalingam, M.; Bae, H.; Kaji, H.; Khademhosseini, A. Skeletal muscle tissue engineering: methods to form skeletal myotubes and their applications. *Tissue Eng., Part B* **2014**, *20* (5), 403–436.

Supporting Information

Shape-morphing fibrous hydrogel/elastomer bilayers fabricated by a combination of 3D printing and melt electrowriting for muscle tissue regeneration

Juan Uribe-Gomez[§], Andrés Posada-Murcia[§], Amit Shukla[§], Mert Ergin[§], Gissela Constante[§],
Indra Apsite[§], Dulle Martin[†], Madeleine Schwarzer[‡], Anja Caspari[‡], Alla Synytska^{‡||}, Sahar
Salehi[⊥] and Leonid Ionov^{§*}.

[§] Faculty of Engineering Sciences and Bavarian Polymer Institute, University of Bayreuth,
Ludwig Thoma Str. 36A, 95447 Bayreuth, Germany.

[†] Forschungszentrum Jülich GmbH Jülich Centre for Neutron Science (JCNS-1) and Institute for
Complex Systems (ICS-1), Wilhelm-Johnen-Straße, 52428 Jülich, Germany

[‡] Leibniz Institute of Polymer Research Dresden e. V., Hohe Straße 6, 01069 Dresden, Germany.

^{||} Dresden University of Technology, Faculty of Mathematics and Science, Institute of Physical
Chemistry and Polymer Physics, 01062 Dresden, Germany.

[⊥] Department of Biomaterials, University of Bayreuth, Prof.-Rüdiger-Bormann Str. 1, 95447
Bayreuth, Germany

*E-mail: leonid.ionov@uni-bayreuth.de

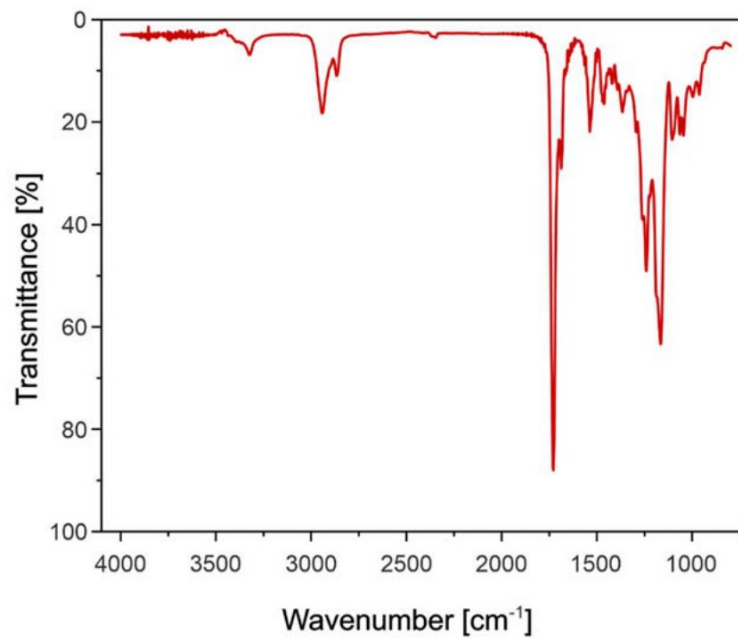


Figure S1. Infrared spectra of PCL-PU 121.

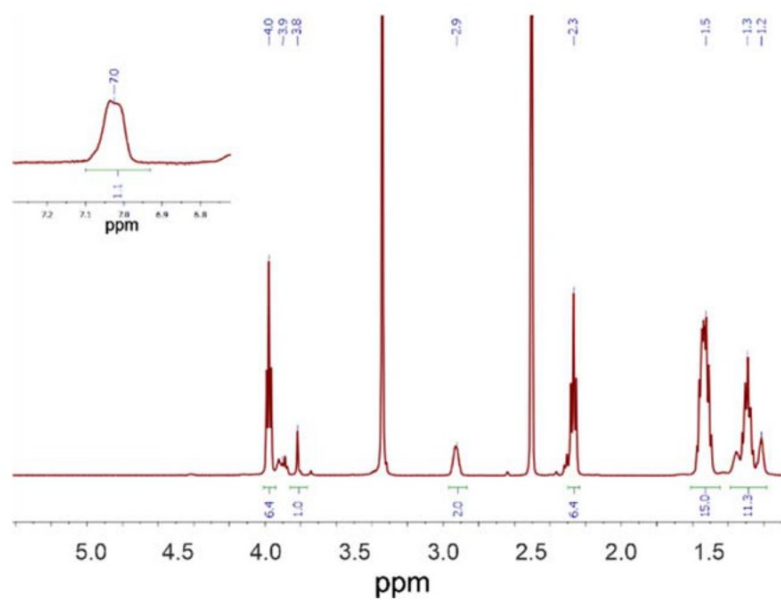


Figure S2. NMR spectra of PCL-PU 121.

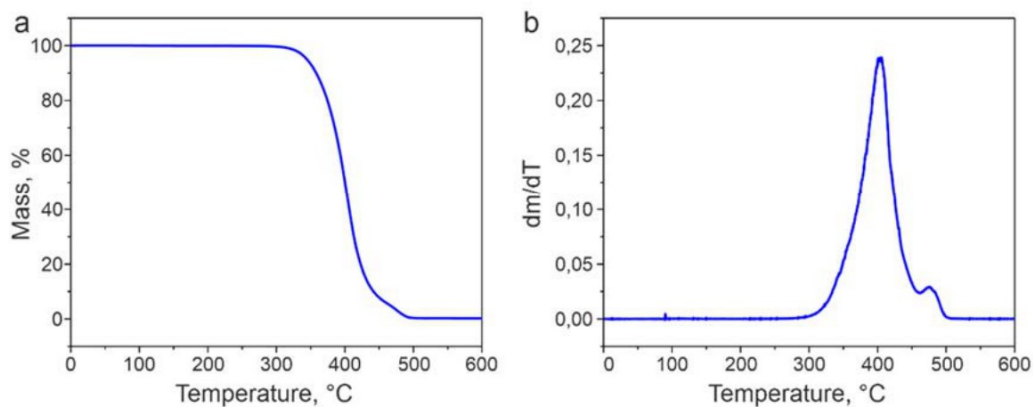


Figure S3. Thermogravimetric analysis of PCL-PU 121: a) weight fraction; b) dm/dT.

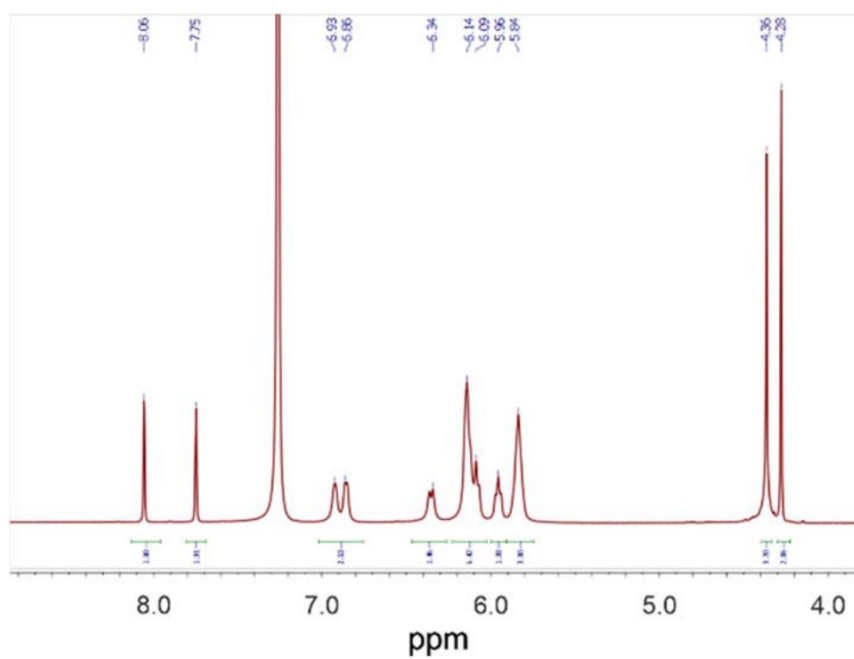


Figure S4. NMR spectra of HA-MA.

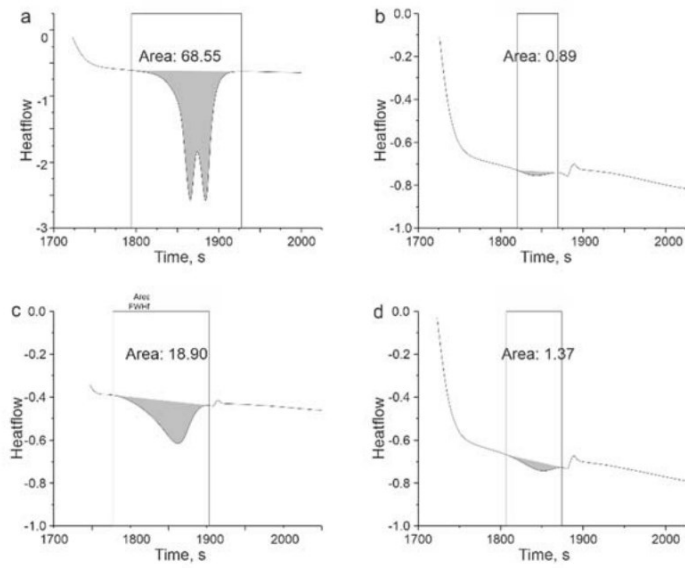


Figure S5. Differential scanning calorimetry in time scale with areas for crystallinity calculations: a) PCL-diol 2000 kDa; b) PCL-PU 110; c) PCL-PU 121; d) PCL-PU 143.

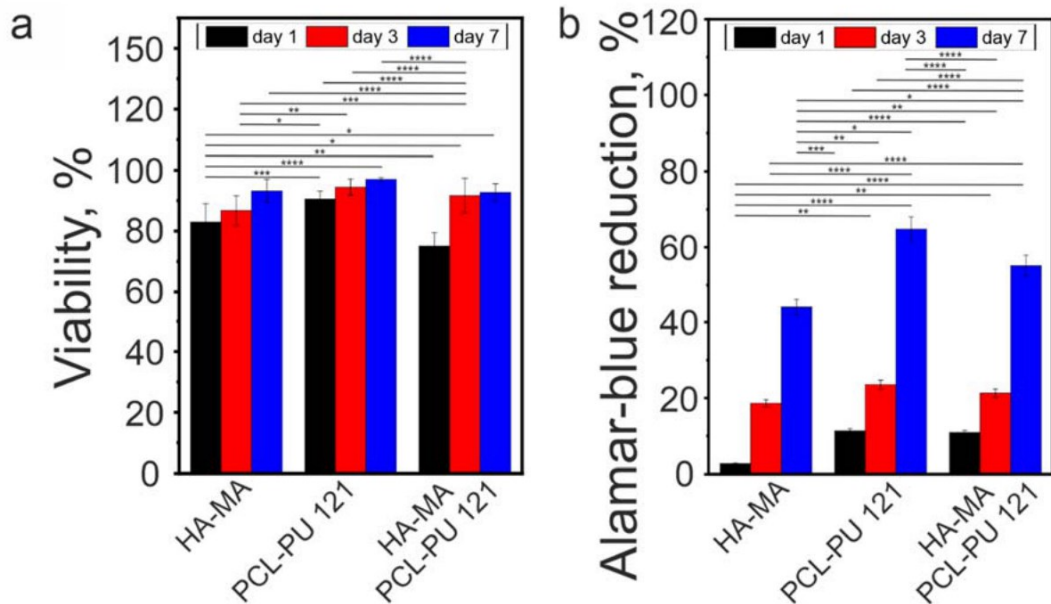


Figure S6. C2C12 myoblast cell culture presented with detailed significant differences after a) quantification of cell viability after 1, 3, and 7 days of culture; b) cell metabolic activity after 1, 3, and 7 days of culture measured by Alamar Blue Assay * $p \leq 0.05$; ** $p \leq 0.01$; *** $p \leq 0.001$; **** $p \leq 0.0001$.

Corrections Manuscript 1

Shape-Morphing Fibrous Hydrogel/Elastomer Bilayers Fabricated by a Combination of 3D Printing and Melt Electrowriting for Muscle Tissue Regeneration

Page 43: NMR data were obtained using a Bruker Avance 500 spectrometer (Bruker BioSpin GmbH, Silberstreifen, Germany) (500.16 MHz for ^1H). ^1H NMR chemical shifts (δ) were reported in parts per million (ppm) relative to TMS, with the residual solvent peak used as an internal reference using ^1H NMR (500MHz, DMSO-d_6 δ): 7.03 (s, 5H), 3.81 (s, 2H), 2.92 (s, 5H), 1.64 – 1.42 (m, 30H), 1.42 – 1.09 (m, 23H). corresponding to the polyurethane part and shifts 3.97 (t, $J = 6.5$ Hz, 13H) and 2.26 (t, $J = 7.3$ Hz, 14H) corresponding to polycaprolactone part. And shifts at 1.64 – 1.42 (m, 30H) and 1.42 – 1.09 (m, 23H). overlapping PCL and Polyurethane parts (Figure S2).

Page 44: Results and discussion: instead of: "HA-MA films contained Eosin Y and triethanolamine as photo-initiator and crosslinking agent" read: "HA-MA films contained Eosin Y and triethanolamine as photo-initiator system"

Page 54: Correction of the figure S2

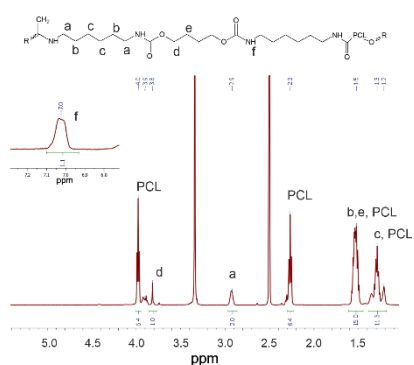


Figure S2. NMR spectra of PCL-PU 1:2:1 in DMSO

Page 55 Correction of the figure S4.

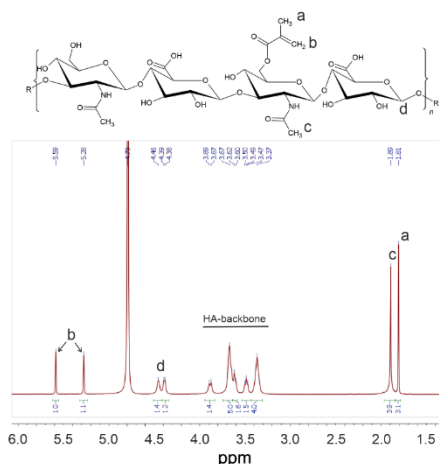


Figure S4. NMR spectra of HA-MA in D_2O

Manuscript 2

Soft Elastic Fibrous Scaffolds for Muscle Tissue Engineering by Touch Spinning

*Juan Uribe-Gomez, Andrés Posada-Murcia, Amit Shukla, Hanin Alkhamis, Sahar Salehi,
and Leonid Ionov*

ACS Applied Bio Materials

Published on: June 25, 2021

DOI: 10.1021/acsabm.1c00403

Soft Elastic Fibrous Scaffolds for Muscle Tissue Engineering by Touch Spinning

Juan Uribe-Gomez, Andrés Posada-Murcia, Amit Shukla, Hanin Alkhamis, Sahar Salehi, and Leonid Ionov*



Cite This: *ACS Appl. Bio Mater.* 2021, 4, 5585–5597



Read Online

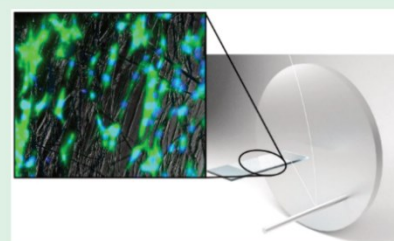
ACCESS |

Metrics & More

Article Recommendations

Supporting Information

ABSTRACT: This paper reports an approach for the fabrication of highly aligned soft elastic fibrous scaffolds using touch spinning of thermoplastic polycaprolactone–polyurethane elastomers and demonstrates their potential for the engineering of muscle tissue. A family of polyester–polyurethane soft copolymers based on polycaprolactone with different molecular weights and three different chain extenders such as 1,4-butanediol and polyethylene glycols with different molecular weight was synthesized. By varying the molar ratio and molecular weights between the segments of the copolymer, different physicochemical and mechanical properties were obtained. The polymers possess elastic modulus in the range of a few megapascals and good reversibility of deformation after stretching. The combination of the selected materials



and fabrication methods allows several essential advantages such as biocompatibility, biodegradability, suitable mechanical properties (elasticity and softness of the fibers), high recovery ratio, and high resilience mimicking properties of the extracellular matrix of muscle tissue. Myoblasts demonstrate high viability in contact with aligned fibrous scaffolds, where they align along the fibers, allowing efficient cell patterning on top of the structures. Altogether, the importance of this approach is the fabrication of highly oriented fiber constructs that can support the proliferation and alignment of muscle cells for muscle tissue engineering applications.

KEYWORDS: Touch-spinning, biofabrication, skeletal muscle, polyurethane copolymers, microfibers

INTRODUCTION

In recent years, research in the field of skeletal muscle tissue engineering has attracted increasing interest, as it opens up new sources for donor-free tissue transplantation.^{1,2} Despite advances in this area, the design and fabrication of engineered skeletal muscle tissues, which form more than 650 different muscles and comprise 40–45% of the total mass of the human body,^{3,4} continue to be challenging. Muscles have a specific structure that is very important for their function.⁵ They are formed by uniaxially aligned muscle fibers, which are single muscle cells. Therefore, to enhance the fusion of the muscle cells during the myogenesis and formation of the multinuclear contractile myofibers, it is essential to provide the uniaxial orientation of cells in engineered muscle tissues. To this end, many techniques (for reviews on micro/nanofabrication, see Ramalingam and Khademhosseini,⁶ Khademhosseini and Peppas,⁷ Zorlutuna et al.,⁸ and Ostrovidov et al.⁹), such as soft lithography,¹⁰ hot embossing,¹¹ electrospinning,^{11,12} photolithography and solvent casting,¹³ passive or active stretching,¹⁴ and the use of electrical fields,^{15,16} have been applied to create an environment that induces cell alignment. All these approaches can be divided into two main groups.¹⁷

The first strategy consists of fabrication of hydrogels with a relatively low initial cell density (several million per milliliter that correspond to several vol %) and exposing them to oscillating/constant mechanical deformation or pulsing electric

stimulation.^{18–22} In this case, the cells in the entire sample are exposed to stimuli and tend to orient themselves. The problem is that cell density is much lower than their density in muscle tissues, and cells/myotubes form multiple individual clusters surrounded by a hydrogel. To reach a high cell density in an engineered tissue, long maturation under-stimulation is required. The second strategy is based on the use of chemically/topographically patterned substrates.^{23–25} In this case, cells can form a continuous layer and tend to align themselves following the pattern; however, they are only able to form a relatively thin aligned cell sheet. This problem can potentially be solved by stacking multiple cell sheets with the uniaxial alignment of cells on top of each other.

The use of fibrous materials made by electrospinning is one of the most promising strategies in this regard. The fabrication of substrates with aligned fibers is possible using two parallel bars, which is a fairly slow processor, as well as using a very rapidly rotating drum.^{22,26,27} One limitation of electrospinning with a rotating drum is poor control of the morphology of fibrous mats

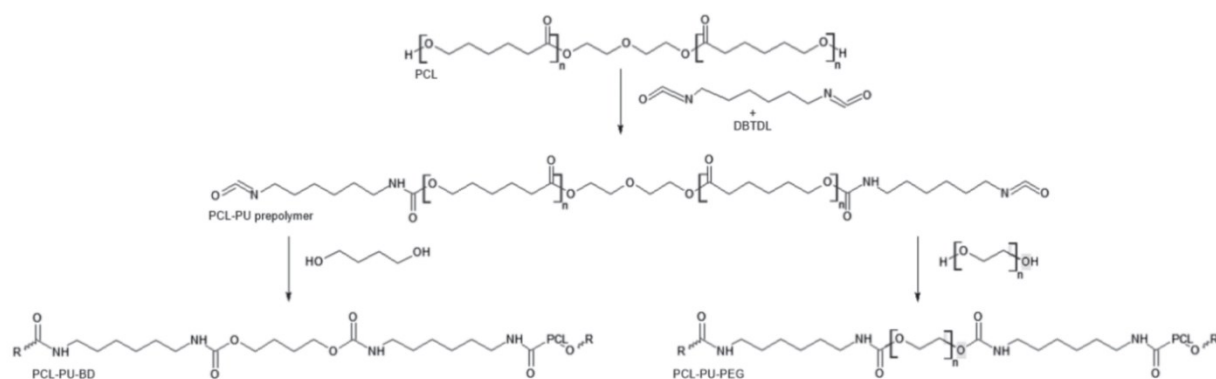
Received: April 2, 2021

Accepted: June 8, 2021

Published: June 25, 2021



Scheme 1. . Synthesis Flowchart of PCL-HDI-BDs and PCL-HDI-PEGs



and the deposition of fibers which tend to be unevenly deposited due to the large distance between syringe and collector. Melt electrowriting is an alternative to electrospinning and can also be used for the fabrication of scaffolds.^{28–31} In contrast to conventional electrospinning, it allows precise and programmed deposition of fibers.³² Yet, it is a very slow process—the typical fabrication rate is 50 mm/s and is simply limited by the maximal movement rate of the linear actuator.^{24,31,33,34} As a result, polymer melts are exposed to high temperatures for several hours in a dispenser that can change their properties due to degradation or further polymerization. Another nanofiber spinning technique proposed by Minko^{35–37} is touch spinning (TS) based on touching polymer solution or melt by a rapidly rotating rod, which draws a fiber upon its movement. The main advantages of TS over electrospinning are that the distance between a cannula, from which the polymer solution is extruded, and fiber spinning element is small, allowing more precise deposition of fibers and that it does not require a high voltage source, which makes it much safer processing technique. TS allows a very fast deposition of fibers that are provided by a rapidly rotating motor in contrast with Melt Electro-Writing (MEW). While this method for fiber fabrication is very promising, TS has not been proved to be suitable for muscle tissue engineering applications.

Various polymers have been used for the fabrication of fibrous structures for muscle tissue engineering using electrospinning and melt electrowriting such as polycaprolactone (PCL),³⁸ poly(L-lactic acid),³⁹ poly(lactide-co-glycolide),⁴⁰ polypropylene,⁴¹ collagen, combinations of PCL with carbon nanotubes,⁴² polyaniline,^{43,44} etc. Thermoplastic/plastic polymers such as polycaprolactone, polylactide have an elastic modulus in the range of hundreds of megapascals, and they are much stiffer than cells. Another disadvantage of these polymers is that they demonstrate a yield point (transition to irreversible plastic deformation) at small elongation, meaning that once the fibers of these polymers are stretched to ~20% (strain typically used for mechanical stretching of muscle cells), they are not able to retain their initial shape—the deformation is irreversible and fibers simply buckle and straighten during mechanical stimulation. This irreversibility of deformation does not allow efficient stimulation of cells at a large amplitude of deformation. This problem, however, could be solved by using thermoplastic elastomers, which can be processed from melt or solution, are softer than semicrystalline thermoplastic polymers, and demonstrate reversibility of deformation.

This paper advances the field of biofabrication and materials processing by reporting the fabrication of elastic, soft, and aligned fibrous scaffolds for muscle tissue engineering using touch spinning of biodegradable, biocompatible elastic block copolymers. These copolymers, which consist of biodegradable aliphatic polyester block linked to each other by polyurethane block, are much softer ($E \approx 1\text{--}10$ MPa) than common polyesters and demonstrate considerable reversibility of deformation.

■ EXPERIMENTAL SECTION

Materials. Polycaprolactone diol (PCL-diol, $M_n = 2000$ g/mol (PCL2000) and 530 g/mol (PCL500), Sigma-Aldrich), hexamethylene diisocyanate (HDI, Merck, dried using a 4 Å molecular sieve and distilled under vacuum), 1,4-butanediol (BD, Sigma-Aldrich), dibutyltin dilaurate (DBTDL, Merck), polyethylene glycol (PEG, $M_n = 3000$ g/mol (PEG3000) and 400 g/mol (PEG400), Sigma-Aldrich), dimethyl sulfoxide anhydrous (DMSO, Sigma-Aldrich), (EtOH, Sigma-Aldrich), *N,N*-dimethylformamide (DMF, Sigma-Aldrich), toluene (Sigma-Aldrich), hexane (Sigma-Aldrich), 2-propanol (IPA, abcr GmbH), chloroform (Sigma-Aldrich), ethylenediaminetetraacetic acid (EDTA, Sigma-Aldrich), calcium chloride dehydrate (Sigma-Aldrich), Dulbecco's phosphate buffered saline (DPBS, Sigma-Aldrich), Dulbecco's Modified Eagle Medium (DMEM, Merck), penicillin–streptomycin (Pen/Strep, gibco), fetal bovine serum (FBS, Merck), glutaMax (gibco), 4-(2-hydroxyethyl)-1-piperazineethanesulfonic acid (HEPES, Carl Roth), calcein-AM (Thermo Fisher Scientific), Ethidium EthD-1 (Thermo Fisher Scientific), phalloidin Dylight™ 488 (Thermo Fisher Scientific), 4',6-diamidino-2-phenylindole (DAPI, Thermo Fisher Scientific), alamarBlue HS Cell Viability Reagent (Thermo Fisher Scientific), FNC solution (fibronectin, collagen, albumin mixture, Athena Enzyme Systems), and Triton X-100 (Sigma-Aldrich) were used as received. The C2C12 myoblast (passage number less than 7) was purchased from ATCC (Manassas, VA).

Synthesis of PCL–PUs. Polycaprolactone–Polyurethane copolymers were synthesized by a two-step polymerization process according to the procedure described by Hao-Yang et al.⁴⁵ First, a prepolymer (Scheme 1) was synthesized. For this purpose, PCL-diol and HDI were mixed in anhydrous DMSO under nitrogen flow at 70 °C followed by the dropwise addition of the DBTDL catalyst (0.05 wt % with respect to the monomer). The reaction was carried out for 3 h to yield an isocyanate-terminated viscous prepolymer (Scheme 1). The chain extender BD or PEG was dissolved in anhydrous DMSO and added dropwise to the prepolymers. The reaction was kept under a nitrogen atmosphere at 70 °C for 3 h to obtain the PCL–PUs copolymer. After the reaction, the synthesized PCL–PUs were precipitated in excess of DI water and quenched in IPA for 3 days. Finally, the PCL–PUs were dried in a vacuum oven at 60 °C for 3 days and stored in a desiccator until further use. The yields of the obtained PCL–PUs were in the

range of 78% to 89%. The molar ratios between the soft segment, the hard segment, and the chain extender were 1:1:0, 1:2:1, and 1:4:3. Synthesized PCL-PU were named according to molecular weights of the soft segment, the chain extender, and the molar ratios (Table 1). For

Table 1. PCL-PU Copolymer Names and Compositions

name	soft segment	hard segment	chain extender	molar ratio
PCL2000-HDI 1:1	PCL 2000 g/mol	HDI	N/A	1:1:0
PCL2000-HDI-BD 1:2:1	PCL 2000 g/mol	HDI	BD	1:2:1
PCL2000-HDI-BD 1:4:3	PCL 2000 g/mol	HDI	BD	1:4:3
PCL500-HDI 1:1	PCL 530 g/mol	HDI	N/A	1:1:0
PCL500-HDI-BD 1:2:1	PCL 530 g/mol	HDI	BD	1:2:1
PCL500-HDI-BD 1:4:3	PCL 530 g/mol	HDI	BD	1:4:3
PCL2000-HDI-PEG400 1:2:1	PCL 2000 g/mol	HDI	PEG 400 g/mol	1:2:1
PCL2000-HDI-PEG3000 1:4:3	PCL 2000 g/mol	HDI	PEG 3000 g/mol	1:4:3
PCL500-HDI-PEG400 1:2:1	PCL 530 g/mol	HDI	PEG 400 g/mol	1:2:1
PCL500-HDI-PEG3000 1:4:3	PCL 530 g/mol	HDI	PEG 3000 g/mol	1:4:3

example, PCL2000-HDI-BD 1:2:1 indicates that PCL 2000 g/mol was the soft segment, and butanediol (BD) was the chain extender in molar ratio 1:2:1; PCL500-HDI-PEG400 1:2:1 indicates that PCL Mn 530 g/mol was the soft segment, PEG 400 g/mol was the chain extender, and the molar ratio was 1:2:1. Polymers with no chain extender have 1:1 in their designation.

NMR. The nuclear magnetic resonance spectra of soluble synthesized PCL-PU were obtained using a Bruker Avance 500 spectrometer (Bruker BioSpin GmbH, Silberstreifen, Germany) (500.16 MHz for ^1H). ^1H NMR chemical shifts (δ) were reported in parts per million (ppm) relative to tetramethylsilane (TMS), with the residual solvent peak used as an internal reference using DMSO- d_6 (500 MHz, DMSO- d_6 , δ): 7.03 (s), 3.81 (s), 2.92 (s), 1.64–1.42 (m), 1.42–1.09 (m) corresponding to the polyurethane part, shifts 3.97 (t, $J = 6.5$ Hz); 2.26 (t, $J = 7.3$ Hz) corresponding to polycaprolactone part and 3.51 (s) corresponding to the PEG protons.

FT-IR. Fourier transform infrared spectra were measured in transmittance mode using a Bruker Tensor 27 (USA) spectrometer, with spectral data spacing of 4 cm^{-1} from 800 to 4000 cm^{-1} . The main bands in these spectra were stretching vibrations of NH groups in the 3500 to 3000 cm^{-1} range. The characteristic stretching vibration of carbonyl group C=O ($\nu = 1727\text{ cm}^{-1}$) and C–N stretching ($\nu = 1535\text{ cm}^{-1}$) confirm the presence of urethane groups. The symmetric and asymmetric stretching vibrations of $-\text{CH}_2$ groups ($\nu = 2935$ and 2865 cm^{-1}) more intense in PEG copolymers, the stretching vibration of the C–O–C bond ($\nu = 1685\text{ cm}^{-1}$) and the stretching bands from the C–O bond of the ester group ($\nu = 1240$ and 1164 cm^{-1}) correspond to the PCL part of the copolymer overlapped with the bending of $-\text{CH}_2$ groups of PEG.⁴⁶

GPC. Molecular weights (number-average molecular weight (Mn); weight-average molecular weight (Mw)) and polydispersity indices (PDI) were measured by gel permeation chromatography using an instrument with 2 PSS-GRAM gel columns (particle size = $10\ \mu\text{m}$) with porosity ranging from 100 to $3000\ \text{\AA}$ (PSS, Mainz, Germany) together with a refractive index detector (Agilent Technologies). DMF (HPLC grade) with lithium bromide (5 g/L) was used as a solvent (for dissolving polymer and as eluting solvent) with a flow rate of 0.5 mL/min, toluene (HPLC grade) was used as an internal standard. The calibration was done with narrowly distributed polystyrene (PS, homopolymers, PSS calibration kit). An injection volume of $20\ \mu\text{L}$ was

used for all the measurements. The samples were dissolved in DMF and filtered through a $0.22\ \mu\text{m}$ PTFE filter before analysis.

DSC. The thermal behavior of the PCL-diol and PCL-PU were investigated using differential scanning calorimetry (DSC3, Mettler Toledo, USA). DSC measurements were performed by loading 5–7 mg of the polymers in a closed aluminum crucible. Three different scans were performed. In the first one, the polymers were scanned in three steps: (1) heating from 25 to $200\text{ }^\circ\text{C}$ and holding at $200\text{ }^\circ\text{C}$ for 5 min to eliminate any thermal history, (2) cooling to $25\text{ }^\circ\text{C}$, and (3) heating to $200\text{ }^\circ\text{C}$ again with temperature rate of $10\text{ }^\circ\text{C}/\text{min}$. The second one was as follows: (1) heating from 0 to $200\text{ }^\circ\text{C}$ and holding at $200\text{ }^\circ\text{C}$ for 5 min to eliminate any thermal history, (2) cooling to $0\text{ }^\circ\text{C}$, and (3) heating to $200\text{ }^\circ\text{C}$ again with a temperature rate of $10\text{ }^\circ\text{C}/\text{min}$. The third one was as follows: (1) heating from -70 to $200\text{ }^\circ\text{C}$ and holding at $200\text{ }^\circ\text{C}$ for 5 min to eliminate any thermal history, (2) cooling to $-70\text{ }^\circ\text{C}$, and (3) heating to $200\text{ }^\circ\text{C}$ again with a temperature rate of $10\text{ }^\circ\text{C}/\text{min}$.

TGA. Thermogravimetric analysis (TGA 2 STAR System, Mettler Toledo (USA)) was performed from 25 to $600\text{ }^\circ\text{C}$ at a heating rate of $20\text{ }^\circ\text{C}/\text{min}$ under air atmosphere.

Mechanical Testing. Thin films of PCL-PU were cast onto glass slides from 25 wt % solutions of synthesized PCL-PU in chloroform at room temperature. After the films were air-dried at room temperature for 24 h, they were manually removed and placed into a vacuum desiccator for 3 days to ensure complete evaporation of the solvent. Rectangular strips ($\sim 10 \times 4 \times 0.4\text{ mm}^3$) were prepared for mechanical tests. Tensile tests were performed on a Dynamic Mechanical Analyzer (DMA, MCR 702 MultiDrive Anton Paar, Austria) equipped with Solid Rectangular Fixtures (SRFS) and a temperature chamber (CTD 600 TDR). During the measurement, static (120 kPa) and dynamic forces (120 kPa) were applied, within a frequency range from 10 to 0.1 Hz, to characterize the elastic properties of the materials in extension-deformation mode. The measurements were made at 20 and $37\text{ }^\circ\text{C}$.

Cyclic tensile tests of films were performed using the same configuration of DMA to investigate the sustainability of the PCL-PU copolymers. The samples were loaded and prestretched until a force around 0 N is achieved, and then stretched at 1 min^{-1} to 50% and 200% strain and released at 1 min^{-1} until the initial length for 10 consecutive cycles; the samples were tested at 20 and $37\text{ }^\circ\text{C}$. From the recorded tensile strain–stress data, the percentage recovery ratio (R_r) of each cycle was calculated using eq 1,

$$\%R_r = \left(1 - \frac{\varepsilon}{\varepsilon_0}\right) \times 100 \quad (1)$$

where ε is the residual strain after the unloading steps, ε_0 is stretching amplitude, which in our case is 0.5 (50%). The property of materials to absorb energy after elastic deformation is named resilience (R_e) and was calculated using eq 2⁴⁵

$$\%R_e = \left(\frac{W_{\text{unload}}}{W_{\text{load}}}\right) \times 100 \quad (2)$$

where W_{unload} represents the area under the stress–strain curve in the release step, and W_{load} represents the area under the stress–strain curve in the stretch step.

Touch Spinning. Touch spinning was performed in a custom-made touch spinning device similar to one published by Minko.³⁶ The PCL-PU were dissolved in chloroform at room temperature under magnetic stirring for 3 h. The solution concentrations were optimized to yield continuous bead-free fibers with the smallest possible diameters. The concentrations were 20% w/v for PCL500-HDI-BD 1:2:1, 25% w/v for PCL2000-HDI-BD 1:2:1, and 17% w/v for PCL500-HDI-PEG3000 1:2:1. The prepared solutions were loaded into a plastic dispenser with an 18-gauge PTFE blunt-end needle (I.D. 0.838 mm). Touch spinning was performed with a rotating rod attached to a wheel/disc and stable bridged collector, distances of 1.0 mm and 5.0 cm; correspondingly, the separation between the parallel bars in the collector was 2.5 cm. Rotational speed was fixed at maximum speed (3000 rpm), and feeding air pressure was varied between 0.1 and 0.15 bar.

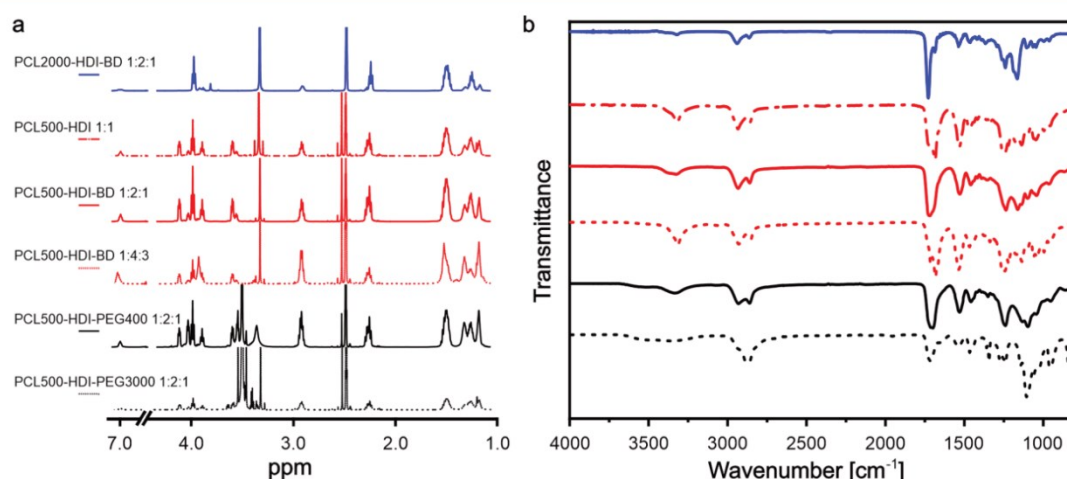


Figure 1. (a) NMR and (b) FTIR spectra of the selected synthesized PCL–PU copolymers.

SEM. Scanning electron microscopy (SEM, Apreo, Thermo Fisher Scientific, USA) and field emission scanning electron microscopy FE-SEM (FEI Teneo, FEI Co., Hillsboro, OR and Carl Zeiss Microscopy GmbH, Germany) were used to characterize the morphological properties of PCL–PUs fibers. Fully dried samples were coated with ~ 10 nm gold or 1.3 nm platinum to ensure electrical conductivity.

Cell Culture. C2C12 mouse myoblast cells (with passage number less than 7) were cultured on aligned fibers made of the copolymers PCL530-HDI-BD 1:2:1, PCL2000-HDI-BD 1:2:1, and PCL530-HDI-PEG3000 1:2:1 with a size of 4.0 cm^2 . Before cell seeding, fibrous scaffolds were fixed in crowns (Scaffdex CellCrown inserts) with an effective internal area of 0.2 cm^2 and sterilized by washing with ethanol 70% v/v for 30 min and exposing to UV light for 1 h under the clean bench. To enhance the cell adhesion, the scaffolds were coated with sterilized FNC solution for 1 h. Fibers without coating were tested as a control. Following the coating, a cell suspension with a density of 10^6 cell mL^{-1} was seeded on top and incubated for 1 h to achieve the initial attachment of the cells. The growth medium for C2C12 cells containing DMEM, FBS serum 10% v/v, Pen/Strep 1%, Glutamin 4.0 mM, and HEPES 20 mM was added to the samples and was refreshed every second day.

Live/Dead Assay, Proliferation Rate, and Alignment. The cell viability was analyzed using a live/dead assay at different time points, 1, 3, and 7 days after the culture in the growth medium. A staining solution containing green-fluorescent Calcein AM in DPBS to target the esterase activity within the cytoplasm of living cells and the red fluorescence ethidium homodimer-1 (EthD-1) was used to indicate dead cells. The samples were covered with the staining solution and incubated for 30 min at room temperature before imaging. After each time point, samples were visualized under the Nikon Eclipse Ti2 fluorescence microscope attached to a DS-Qi2 digital Nikon camera and Nis-D Elements v 4.550 software was used for image analysis. The viability of the cells was calculated by counting the number of live and dead cells in ten different images from three different samples.

The proliferation rate of the cells cultured on the PCL–PUs fibers was measured using Alamar Blue assay after 1, 3, and 7 days of culture. According to the manufacturer's protocol, 10% of reagent was added to the samples with the medium at each time point and incubated at 37°C for 90 min and stirring gently every 30 min to avoid gradients. The reacted media from each sample was removed and kept on ice in the dark; $100 \mu\text{L}$ of that was transferred to a 96 well plate followed by measuring its absorbance using a plate reader (Berthold Tech TriStar2S, Germany) at 535 nm of excitation and 590 nm of emission wavelength. The negative control was prepared by mixing 10% Alamar blue in medium, and the positive control was prepared by mixing 10% reduced Alamar Blue in sterile Milli-Q water. Three repeats were

considered for each composition, and the proliferation of the samples was measured after 1, 3, and 7 days in culture.

To quantify the alignment of the muscle cells on the PCL–PUs fibers after 1, 3, and 7 days in culture, the actin filaments and nuclei were stained using a staining solution of DAPI and Phalloidin DyLight 488 in PBS to target rich regions in adenine and thymine in DNA and to selectively label F-actin in fixed cells, respectively. First, the cell-cultured samples were fixed with formaldehyde (3.7%) solution for 15 min at room temperature. After washing with PBS, the cells were permeabilized with Triton (0.1%) solution for 5 min and washed with PBS. Next, the samples were covered and incubated with staining solution for 30 min at room temperature following by imaging using a fluorescence microscope. To determine cell alignment, morphological changes of nuclei were analyzed using ImageJ and orientation plug-in in ten images from three different samples per day in culture. Nuclei orientation angles $-10^\circ < x < 10^\circ$ with respect to the fibers were considered as aligned.

Statistical Analyses. All results were treated using the software origin version 9.7 and are presented as mean \pm standard deviation (SD). All the values were averaged at least in triplicate, and statistical analyses were performed using a Student's *t* test and one-way analysis of variance (ANOVA). Tukey's test was used to evaluate specific differences in values. A value of $p < 0.05$ was considered significant.

RESULTS AND DISCUSSION

Fourteen different PCL–PU copolymers with different lengths of PCL block (2000 g/mol and 530 g/mol), chain extenders (BD, PEG diol 400 g/mol, PEG diol 3000 g/mol), and composition (molar ratio PCL:diisocyanate:chain extender = 1:1:0 (designated as 1:1), 1:2:1, and 1:4:3) were synthesized as described in the Experimental Section. The molecular weight of obtained polymers is around $48\,000 \text{ g mol}^{-1}$ with PDI values less than 2.5 (Figure S1 and Table S1). Six selected copolymers were characterized by ^1H NMR and FTIR to verify their molecular structures. The ^1H NMR spectra (Figure 1a) show multiple peaks at the same chemical shift because all the copolymers have the same chemical structure of the soft segment. In general, the peaks in the high field between 1.0 and 2.0 ppm were assigned to the methylene groups of the PCL, HDI, and/or BD. The peak at 2.3 ppm corresponds to PCL diol $\text{CH}_2\text{--CO}$ groups. Characteristic HDI peak corresponds to NH--CH_2 at 2.9 ppm. The distinct peaks at 3.6 and 4.1 correspond to ether and ester bonds that link two PCL moieties to form the PCL-diol (the integrals are proportional to the molecular weight). The resonance signal

at 3.9 also corresponds to PCL diol CO–O–CH₂–CH₂ groups.^{45,47,48} Characteristic PEG ¹H NMR signals are located at 3.5 ppm corresponding to the backbone of the polymer.⁴⁹ The ¹H NMR shows no significant differences in the signals between synthesized PCL–PUs with different molecular weights of PCL; however, they differ in the integrals. The same is observed with polymers with different PEG chain extenders. The NMR data were used to estimate the composition of copolymers (Table 2), which was found to be in very good agreement with the composition expected from the ratio between the amount of monomers used for polymerization.

Table 2. Composition of Synthesized Polymers According to NMR and Amount of Monomers Used for Polymerization

sample	mass fraction [%] NMR		mass fraction [%] calculated	
	soft segment	hard segment	soft segment	hard segment
PCL2000-HDI-BD 1:2:1	77.1	22.2	82.4	17.6
PCL500-HDI 1:1	65.3	34.7	75.9	24.1
PCL500-HDI-BD 1:2:1	61.1	38.9	55.4	44.6
PCL500-HDI-BD 1:4:3	35.0	65.0	36.0	64.0
PCL500-HDI-PEG3000	28.3	71.7	13.7	77.6
PCL500-HDI-PEG400	55.3	44.7	41.9	58.1

A set of representative FTIR spectra of the synthesized PCL–PUs are shown in Figure 1b. The band at 3528 cm⁻¹, which corresponds to the OH stretching characteristic of the PCL diols, is not present in any spectra. Instead of that, all the spectra of the PCL–PUs show a characteristic band at 3316 cm⁻¹ corresponding to NH stretching, confirming the reaction. The C=O stretching region shows a band between 1690 and 1720 cm⁻¹ instead of the band at 1721 cm⁻¹ of the PCL-diol carbonyl group.⁵⁰ Another two characteristic bands observed at 1681 and 1537 cm⁻¹ corresponding to N–C stretching and amide II, respectively, indicating the urethane linkage in the PCL–PUs, which is strong evidence for the successful synthesis of PUs.^{45,50} Thus, both IR and NMR confirm the successful synthesis of copolymers.

The TGA (Figure 2a) was carried out to investigate the thermal degradation of the polymers and their composition. Pure PCL and PEG monomers were used as reference samples (Figure 2b). It was found decomposition of PEG and PCL occurs in close temperature ranges. This does not allow easy interpretation of TGA results. On the other hand, we observed that while pure monomers demonstrate single-step decomposition, copolymers demonstrate clear two or even three steps. There is a general trend that amplitude of low-temperature decomposition step (step 1, Table 3) decreases with the decrease of mass fraction of PCL and chain extender, meaning that high-temperature steps (steps 2 and 3, Table 3) can be attributed to the urethane part of copolymers.

The chemical composition of polymers has a profound effect on their thermal behavior, which was studied by DSC (Figure 3). Since the behavior of polymers is substantially influenced by their history, we carried out three kinds of DSC experiments: prepared polymers and fibers were heated starting from –70, 0, and 20 °C, and then cooled to the starting temperature. These

starting temperatures are selected due to the specific thermal properties of PCL and PEG monomers used for the synthesis of polymers. PCL500 and PEG400 crystallize at a temperature well below 0 °C and melt around 0 °C, meaning that these blocks must remain liquid if copolymers are processed at room temperature that is generally supported by experimental observations (Table 4). We found that the degree of crystallinity of PCL in block copolymers obtained from the first melting peak is lower than that of pure PCL with the same molecular weight, which is most probably due to higher molecular weight and hindrance of crystallization by PU segments. The degree of crystallinity of PCL2000 decreases with the increase of the fraction of the PU block. It is interesting that PCL500 has crystallization below 0 °C and is not semicrystalline in the block copolymer without the chain extender PCL500-HDI-BD. The addition of a chain extender (PCL500-HDI-BD 1:2:1) allows crystallization of PCL500 that is expressed in the appearance of the melting peak and is most probably related to the increase of molecular weight of PCL blocks by chain extenders that allow its slow crystallization—this polymer also demonstrates cold crystallization at around 0 °C and melting peak at around 40 °C when heated starting from –70 °C. It is very interesting that we do not observe the crystallization peak of the polymer upon cooling that can be explained by the slowness of crystallization. Further increase of the fraction of polyurethane (PCL500-HDI-BD 1:4:3) disturbs crystallization of PCL500, and the polymer becomes amorphous if not exposed to –70 °C.

Interpretation of DSC results of copolymers with PEG chain extender is complicated because both PCL and PEG blocks are able to crystallize and their thermal behavior in the block copolymer is different from that of pure blocks. In order to elucidate the origin of melting/crystallization peaks, we added a small amount of water to swell PEG block and prevent its crystallization. It was found that wet polymers exhibit neither crystallization (Figure S4) nor melting behavior, meaning that DSC peaks belong to PEG. A control DSC experiment of wet PCL500-HDI-BD 1:2:1 and PCL2000-HDI-BD 1:2:1 shows that crystallization of PCL blocks in copolymers alone is not affected by the presence of water (Figure S4).

We performed slow (1 °C/min) DSC heating/cooling of PCL2000-HDI-BD with a different ratio. These polymers exhibit no crystallization at a temperature above 0 °C (Figure S3) at a cooling rate of 10 °C/min. On the other hand, the slow cooling enables crystallization of PCL2000-HDI 1:1 at 20 °C and PCL2000-HDI-BD 1:2:1 at 5 °C. It was found that the PCL2000-HDI-BD 1:4:3 cannot crystallize even at slow cooling. Thus, while almost all PCL–PU copolymers do not crystallize on rapid cooling, some of them are able to crystallize on slow cooling. This allows us to assume that, while as prepared fibers can often be amorphous and, as a result, elastic, their storage at room temperature can lead to partial crystallization of the PCL block that can significantly change their mechanical properties by introducing partially plastic behavior.

The synthesized polymers were planned to be used for the fabrication of fibers. We have therefore evaluated the processability of the synthesized polymers—we have tested their solubility in polar and nonpolar organic solvents as well as their melting/flow behavior. It has been found that lengthening the PU block reduces the solubility of polymers—either becoming insoluble or only soluble in hot solvents. The replacement of BD chain extender with PEG as well as the length increase of PCL and PEG blocks has the same effect—solubility of polymer decreases. Insoluble and nonmelting

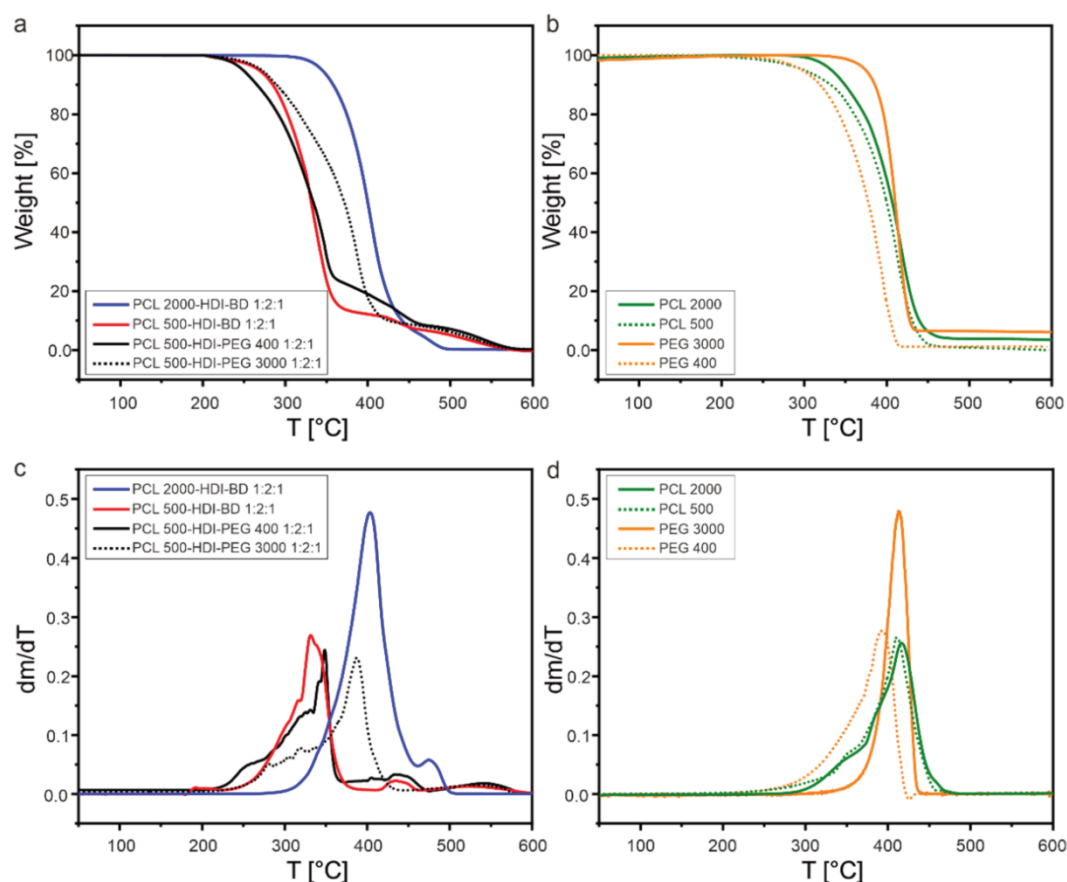


Figure 2. Thermogravimetric analysis: (a) mass loss of the selected synthesized PCL–PUs; (b) mass loss of the precursors; (c) dm/dT of the chosen synthesized PCL–PUs; (d) dm/dT of the precursors.

Table 3. Comparison of TGA Results and Composition of Copolymers

copolymers	mass fraction from synthesis		mass fraction from TGA		
	% PCL	% chain extender	Step 1	Step 2	Step 3
PCL2000-HDI-BD 1:2:1	82.4	3.7	92.5	7.5	
PCL500-HDI-BD 1:2:1	55.4	9.4	87.2	6.0	6.8
PCL500-HDI-PEG3000 1:2:1	13.7	77.6	88.7	11.2	
PCL500-HDI-PEG400 1:2:1	41.9	31.6	76.2	15.8	8.0

polymers (bold font in Table 5) were discarded for the purposes of this research. Thus, only 7 polymers out of 14 demonstrated potential suitability for the fabrication of scaffolds.

We investigated the mechanical properties of the synthesized polymers using DMA and cyclic tensile testing. It was found that the storage modulus of all polymers is nearly independent of frequency in the range from 0.1 to 10 Hz and decreases nearly linearly with the decrease of PCL mass fraction in the block copolymer for copolymers with PCL500 and PCL2000 blocks (Figure 4a–c). An increase of temperature to 37 °C results in a slight decrease of the modulus; the reduction is more pronounced in the case of copolymers with PCL500 blocks, as DMA revealed. Copolymers with PEG chain extenders are

particularly sensitive to the increase of temperature and the presence of humidity—the elastic modulus of dry PCL500-HDI-PEG3000 1:2:1 is around 30 MPa. An increase of temperature to 37 °C decreases the modulus to ca. 2 MPa, and humidity at 20 °C drops the modulus to ca. 1 MPa, which can be attributed to the melting/swelling of PEG blocks. The copolymer PCL500-HDI-PEG400 1:2:1 is so soft ($E' = 0.5$ MPa at 20 °C) that measurement of its modulus at 37 °C and in a wet state was technically impossible (Figure 4d).^{51,52} It was found that the environment (humidity of the air) has no effect on the mechanical properties of PCL500-HDI-PEG3000 1:2:1 and PCL200-HDI-BD 1:2:1 polymers (Figure S6).

We performed cyclic mechanical loading/unloading studies to evaluate the reversibility of the deformation of the polymers, which are able to form fibers. The polymers were cyclically stretched to up to 50% (Figure 4e) and 200% (Figure S5), while stress was recorded. It was found that in the first stretching cycle, the stress–strain dependence is nearly linear at small deformation. From second and further cycles at 20 °C, the stress–strain dependencies have a clear J-like shape due to incomplete reversible deformation—polymer is able to partially recover the initial shape after the release of applied force. After the first cycle, the material underwent a partial plastic deformation. Afterward, cycling between 30% and 50% with respect to the initial length results in nearly complete reversibility of deformation. Polymers with the BD chain

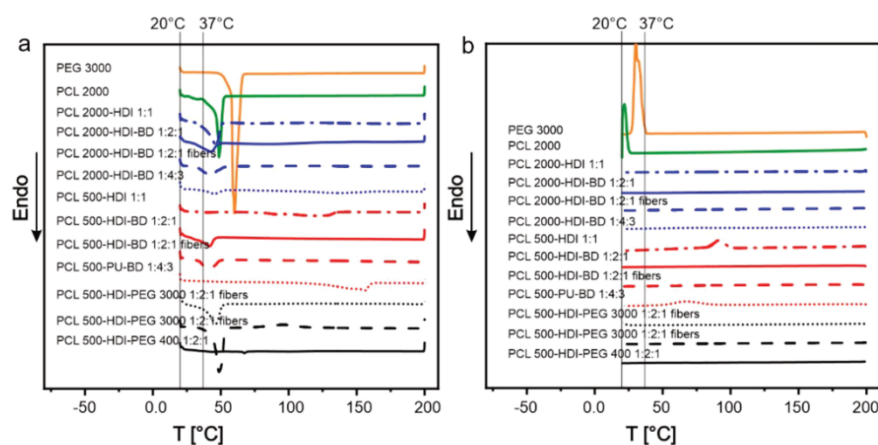


Figure 3. PCL–PUs thermal properties: (a) DSC first heating from 20 to 200 °C; (b) DSC first cooling from 200 to 20 °C. Room temperature (20 °C) and temperature of cell culture experiments (37 °C) and marked with narrow lines.

Table 4. DSC Data for PEG, PCL, PCL2000-PU, PCL500-PU, and PCL500-PU-PEGs

sample	mass fraction of PCL [%]	starting temp. [°C]	thermal properties				crystallinity [%] ^a		
			T_m [°C]	ΔH_m [J/g]	T_c [°C]	ΔH_c [J/g]	of PCL block	of block copolymer	
PEG 3000		-70 °C	69.9	135.8	46.7	122.3			
		20 °C	59.9	180.8	30.4	153.2			
PEG 400		-70 °C	8.8	15.7	-20.4	13.7			
		20 °C	-	-	-	-			
PCL 2000	100	-70 °C	43.5–37.9	68.1	17.9	67.1	50.1	50.1	
		20 °C	48.7	69.3	21.8	63.1	51.4	51.4	
PCL 500	100	-70 °C	-26.7–7.7	7.0	-25.9	5.4	5.1	5.1	
		20 °C	-	-	-	-	0	0	
PCL2000-HDI-BD	1:1	92.2	-70 °C	41.5	43.4	11.7	36.9	31.9	29.4
		20 °C	46.2	50.7	20.1	34.0	37.5	34.6	
	1:2:1	82.4	-70 °C	36.9	35.3	-2.6	20.1	26.0	21.4
		20 °C	42.7	23.7	-	-	17.6	14.5	
	1:4:3	67.9	-70 °C	30.8	14.5	-16.1	6.8	15.6	10.6
		20 °C	45.6	9.1	-	-	6.7	4.6	
PCL500-HDI-BD	1:1	75.9	-70 °C	-	-	-	0	0	
		20 °C	-	-	-	-	0	0	
	1:2:1	55.4	-70 °C	37.1	19.4	4.3 ^b	18.9 ^b	14.3	7.9
		20 °C	41.9	20.2	-	-	14.9	8.3	
	1:4:3	36.0	-70 °C	41.5	25.9	-	-	19.2	10.6
		20 °C	13.9	29.5	-	-	21.7	7.8	
PCL500-HDI-PEG3000	1:2:1	13.7	-70 °C	45.7	46.0	9.8	35.4	0 ^c	0 ^c
		20 °C	46.2	47.1	20.21	52.1	0 ^c	0 ^c	
		20 °C	48.7	78.9	-	-	0 ^c	0 ^c	
PCL500-HDI-PEG400	1:2:1	41.9	-70 °C	18.1	2.1	0.0	2.4	0 ^c	0 ^c
		20 °C	43.2	1.9	-	-	0 ^c	0 ^c	

^aDegree of crystallinity = ΔH_m sample / ΔH_m 100% crystalline polymer. ΔH_m of 100% crystalline PEG is 206.2 J/g, and ΔH_m of 100% crystalline PCL is 135 J/g. ^bFrom cold crystallization peak. ^cPolymer does not show crystallization/melting peaks in the temperature range 0–60 °C in a wet state, meaning that crystallization in a dry state is due to PEG block.

extender demonstrate a recovery ratio of around 40%; polymers with the PEG3000 chain extender demonstrate a recovery ratio of about 60%. An increase in temperature results in a decrease in slope (Table 6). Furthermore, the recovery ratio is nearly independent of the maximal strain to which the polymer was exposed: 50% or 200% (Figure S5). The polymers are able to recover 40–60% of their length with respect to the length in a

stretched state. The recovery ratio of copolymers with PCL500 blocks increases to ca. 80–90% upon heating to 37 °C that is due to the considerable softening of polymers. On the other hand, the recovery ratio of copolymers with long PCL blocks (PCL 2000) remains unchanged upon heating to 37 °C when the PCL2000 block starts to melt.

Table 5. Solubility and Melting Behavior of Synthesized PCL–PU Copolymers

sample	molar ratio	solubility ^a					melting/flow ^b
		DMF	DMSO	CHCl ₃	toluene	hexane	
PCL500-HDI	1:1	Yes	Yes	Yes	Yes	No	Yes
PCL500-HDI-BD	1:2:1	Yes	Yes	Yes	No	No	Yes
	1:4:3	Hot	Hot	No	No	No	Yes
PCL500-HDI-PEG400	1:2:1	Yes	Yes	Yes	No	No	Yes
	1:4:3	Hot	Hot	No	No	No	No
PCL500-HDI-PEG3000	1:2:1	Yes	Hot	Yes	No	No	Yes
	1:4:3	No	Hot	No	No	No	No
PCL2000-HDI	1:1	Yes	Yes	Yes	Yes	No	Yes
PCL2000-HDI-BD	1:2:1	Hot	Hot	Yes	No	No	Yes
	1:4:3	Hot	Hot	Hot	Yes	No	Yes
PCL2000-HDI-PEG400	1:2:1	Hot	No	No	No	No	No
	1:4:3	No	No	No	No	No	No
PCL2000-HDI-PEG3000	1:2:1	No	No	No	No	No	Yes
	1:4:3	No	No	No	No	No	No

^aSolubility was measured in 10% solutions; partially dissolved or non-fully dissolved polymers were considered insoluble. ^bSmall amount of each polymer was heated to determine if the polymer flows or burns.

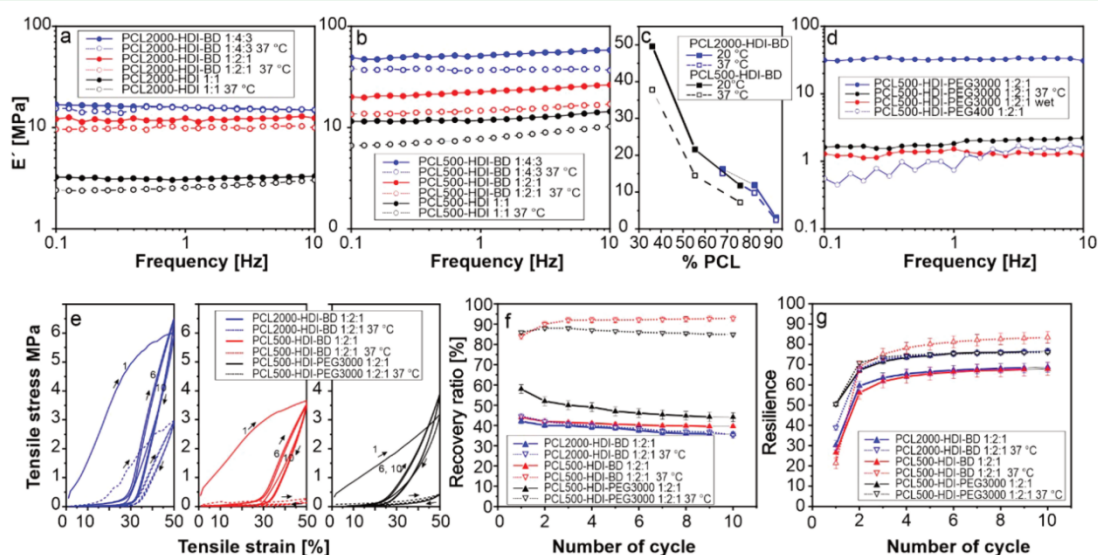


Figure 4. Mechanical properties of copolymers: (a–c) DMA; (d) tensile stress versus tensile strain; (e) representative cyclic tensile test curves (1, 6, and 11 cycles are shown), (f) film recovery ratio, and (g) resilience in ten cycles of loading and unloading.

Table 6. Summary of Mechanical Properties of Synthesized Polymers

polymer	E' (MPa)					E' (DMA)		
	cycle 1 50%		cycle 3 50%		cycle 1 200%	cycle 3 200%		
	20 °C	37 °C	20 °C	37 °C	20 °C	20 °C	37 °C	
PCL500-HDI 1:1					was not measured		12.3	8.0
PCL500-HDI-BD 1:2:1	9.2	1.3	0.6	0.2	8.3	1.1	22.7	14.9
PCL2000-HDI 1:1					was not measured		3.2	2.6
PCL2000-HDI-BD 1:2:1	18.4	9.2	0.8	0.3	17.8	1.2	12.1	9.9
PCL500-HDI-PEG3000 1:2:1	5.5	0.6	0.6	0.3	5.7	0.2	32.5	1.9

The elastic modulus obtained using DMA is comparable to or slightly higher than that extracted from tensile tests that can be attributed to the difference between the methods. The DMA provides modulus obtained at very small deformations. On the other hand, the value of modulus from tensile tests was extracted from elongation up to ~20% when the polymer starts to undergo

plastic deformation. This range of elongation is relevant for mechanical stimulation applied to muscle cells. On the other hand, one sees that stress–strain curves have three distinct regions: stress rapidly increases at very small deformation (1–2%), and then the slope decreases and remains nearly constant up to $\epsilon \approx 30\%$; further, an increase of strain results in a further

decrease of the slope of the stress–strain curve. The observed complex mechanical behavior of copolymers can be attributed to their complex molecular architecture: the copolymers consist of slowly crystallizing PCL block and polyurethane linker, which are able to form hydrogen bonds with each other. The elastic behavior of copolymers can be attributed to physical cross-linking provided by hydrogen bonds between urethane groups. The particular reversibility can be attributed to the creep of partially crystallized PCL and to the splitting of hydrogen bonds under mechanical stress and the formation of new ones. Resilience,⁵³ which is a fraction of work stored in deformation energy, increases during the cycling of polymers and also increases with an increase of temperature. The reason for the increase of resilience during cycling is most probably a structure of polymer—they consist of plastic and elastic components, which deform irreversibly and reversibly, respectively, that is provided by their block-like architecture. We explain softening of polymers, an increase in recovery ratios, and resilience by softening of PCL blocks.

We also studied the mechanical properties of touch-spun PCL2000-HDI-BD 1:2:1 fibers and reference pure PCL fibers (85 kDa) (Figure 5). It was found the elastic modulus of PCL

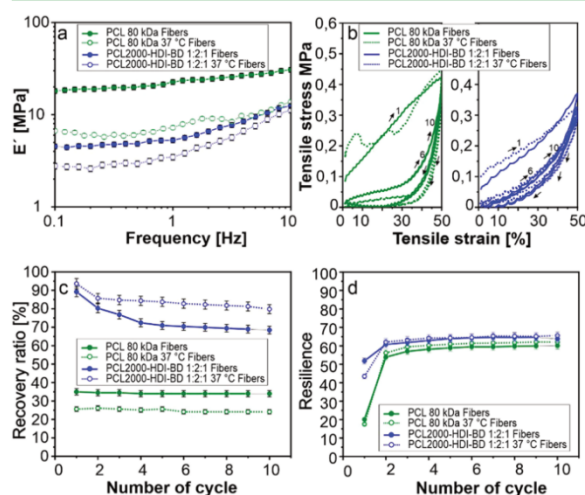


Figure 5. Mechanical properties of PCL (80 kDa) and PCL–PU copolymer fibers: (a) DMA; (b) representative cyclic tensile test curves (1, 6, and 11 cycles are shown); (c) recovery ratio; (d) resilience in ten cycles of loading and unloading.

fibers is in the range of 8–20 MPa depending on temperature; the elastic modulus of the copolymers is approximately 3–4 times lower (Figure 5a). These values can be imprecise due to uncertainties in measurements of cross-sectional areas of fibrous samples, which was the reason films were studied first. The most important difference between PCL–PU copolymer and PCL is the different character of stress–strain curves obtained in the cycling stretching experiment (Figure 5b). Stretched PCL is simply unable to recover its shape after stretching to 50%, because it is a thermoplastic polymer—its recovery ratio is around 25% at 37 °C, much lower than the recovery ratio of the copolymer, which is around 85% that is even higher than that for polymer film (Figure 4). Both polymers have similar resilience. This experiment clearly shows the advantage of PCL–PU copolymers over commonly used thermoplastic polymers such as PCL—they can be reversibly stretched.

Properties characterized stress–strain curve, resilience, recovery ratio, breaking strain, etc., and the combinations between them are essential to mimic the mechanical properties of soft tissues. For example, the mammalian tendon is highly resilient (resilience >90%) but relatively inextensible (breaking strain of ~13%), whereas elastin is resilient (90%) and extensible (a breaking strain of ~150%) but lacks toughness.^{53,54} Moreover, many tissues have a J-like shaped stress–strain curve that is provided by coiled collagen fibers. These three PCL-based elastomers possess an essential combination of properties such as high flexibility, high recoverability, and low stiffness, achieving suitable mechanical properties enabling their potential use, for instance, in muscle tissue engineering.

In this study, aligned fibrous scaffolds were prepared from three PCL–PUs polymers, which can be processed in solution and possess suitable mechanical properties. By optimizing the touch-spinning parameters, uniform blob-free fibers were obtained for three kinds of PCL–PUs with 1:2:1 composition and BD and PEG3000 chain extenders (Figure 6a–c). The other four processable copolymers (Table 4) without chain extender (1:1 ratio) and with 1:4:3 compositions were not able to form fibers. The fiber diameter and fiber orientation were evaluated by testing ten samples of each copolymer. It was found that PCL500-HDI-PEG3000 1:2:1 formed uniform fibers with narrow diameter distribution and alignment. Simultaneously, the PCL2000-HDI-BD 1:2:1 showed a wider fiber diameter distribution and alignment, and the PCL500-HDI-BD 1:2:1 showed broader diameter distributions due to the bridges (Figure 6) formed between the fibers during the processing indicated by arrows.

Finally, we performed cell culture studies on the fibrous PCL–PUs scaffold. For this, cell viability, proliferation, and alignment were quantified. The first experiments (Figure S7 and S8) revealed that the scaffolds made by PCL500 based copolymers are not suitable for cell culture, as PCL500-HDI-BD 1:2:1 and PCL500-HDI-PEG3000 1:2:1 fibers disintegrated and got very soft in PBS at 37 °C and could not be handled (Figure S7). This means that just one polymer PCL2000-HDI-BD 1:2:1 out of all 14 synthesized copolymers is suitable for cell culture due to the combination of processability, the ability to form stable fibers, and the mechanical stability. As we demonstrated in previous work,²⁴ this copolymer is biodegradable.

In order to improve cell adhesion to the PCL2000-HDI-BD 1:2:1 scaffold, it was treated with FNC (fibronectin mixture) (Figure S8). It can be seen that after 1 day of culture, only a few cells adhered to fibers, while the coating improved the early attachment of the cells; moreover, cells adhered and distributed homogeneously on top of the fibrous layers (Figure 7a–d). Moreover, cells begin to align along the fibers. Interestingly, in contrast to our previous work,²⁴ where muscle cells cultured on 10- μ m-thick PCL fibers fabricated by melt electrospinning preferred to grow in the gaps between the fibers; here, the same cells tend to grow on top of fibers. We attribute the differences in the cell behavior to different fiber spaces—the distance between the fibers prepared by melt electrospinning is comparable to the size of the cells and cells fit in the gap between them; the distance between fibers prepared in this work by touch spinning is much smaller and cells are able to sit on top of them.²⁴ It was found that cell viability increases with time and reaches 88% after 7 days, which is higher than that reported in our previous studies on fibers obtained by melt electrospinning.²⁴ Cell proliferation also increases with time (Figure 7e).

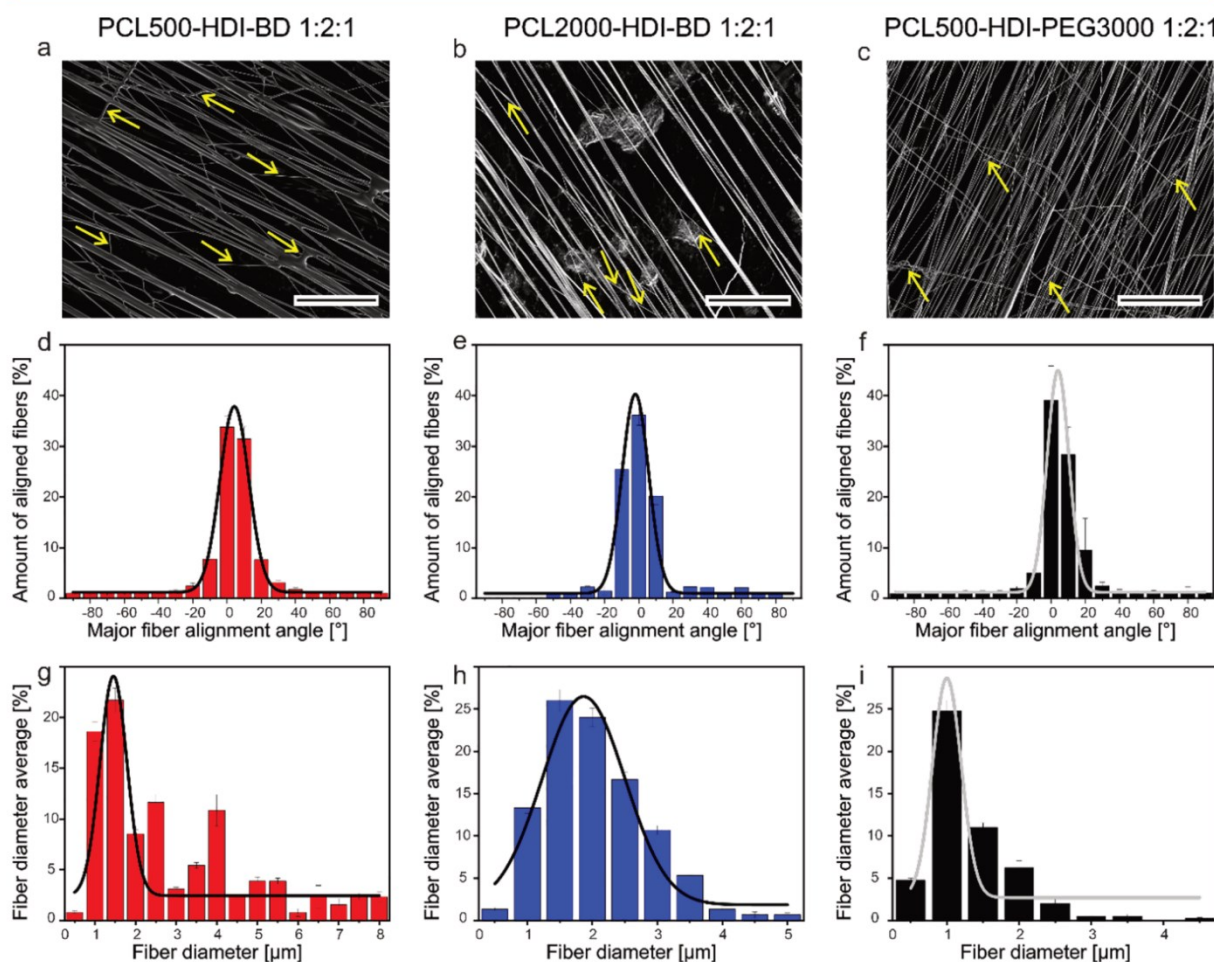


Figure 6. (a–c) SEM images of touch-spun fibers, scale bars 100 μm . (d–f) Fiber alignment of the touch-spun fibers. (g–i) Average fiber diameter of the touch-spun fibers.

The fibers were deformed during sample transfer (Figure 7a–d) that, however, does not affect their interactions with cells. Although disordering of fibers can be seen as an undesirable effect, we consider this observation to be an indication of one very important advantage of touch spun fibers—they are not strongly linked to each other and form very dense mesh as usually observed when fibers are prepared by electrospinning. As a result, cells might have more space and can penetrate the space between cells to form a 3D structure.

Cell alignment on the PCL2000-HDI-BD 1:2:1 fiber scaffold was evaluated after staining the actin filament and cell nuclei. Staining experiments confirmed the preference of cells to grow on top of the fibers (Figure 7f–i, Figure S10). It was determined that the degree of cell alignment improves during cell incubation (Figure 7j): nearly 20% of cells are aligned on day 1, 28% of cells are aligned on day 3, and already 43% of cells are aligned after 7 days showing statistical significance ($p \leq 0.001$) between all time points. It must be noted that the cells were considered to be aligned if the angle formed with the main direction of orientation of fibers was in the range between -10° and 10° . Notably, cell alignment is worse than that of fibers (Figure 7). This difference can be explained by the small distance between fibers so that cells can bridge them and change orientation. We found that cell

alignment improved after 7 days of culture, because cells prefer to grow along the fibers in the space between them instead of forming bridges between the fibers (Figure 7j). Thus, the developed approach allows the cell proliferation and uniaxial alignment of cells along the touch-spun fibers.

CONCLUSION

In this work, we report the fabrication of porous elastic highly aligned scaffolds using touch-spinning of polycaprolactone–polyurethane copolymers and demonstrate their promising character for the engineering of muscle tissue. For this, a family of polyester–polyurethane soft copolymers based on two different molecular weights of polycaprolactone (530 g/mol and 2000 g/mol) and three different kinds of chain extenders such as 1,4-butanediol and two molecular weights of PEG were synthesized. Polymers demonstrate an interesting combination of plastic and elastic character of deformation: the recovery ratio is ca. 40–60% after 1 cycle of extension, which is independent of the degree of an extension, and remains nearly constant during further stretching cycles—polymer demonstrates elastic deformation and possesses elastic modulus in the range of 1–10 MPa that depends on the composition. Thus, the copolymers are much softer than commonly used polyesters such as PLA and

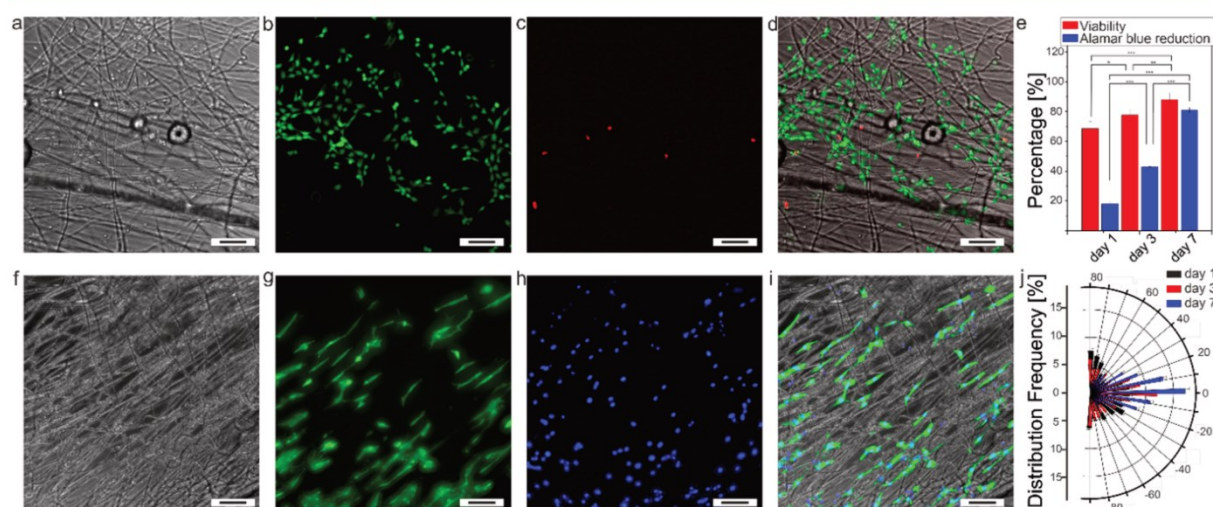


Figure 7. C2C12 myoblast cell culture: (a–d) viability of cells (Live/Dead assay) on PCL2000-HDI-BD 1:2:1 touch-spun scaffolds (red – dead cells; green – live cells at day 7 of culture); (e) quantification of cell viability and cell metabolic activity after 1, 3, and 7 days of culture measured by Alamar Blue Assay. * $p \leq 0.05$; ** $p \leq 0.01$; *** $p \leq 0.001$; (f–i) cell nuclei alignment on PCL2000-HDI-BD 1:2:1 touch-spun scaffolds at day 7 of culture; quantification analysis of cell nuclei alignment. Scale bars 50 μm .

PCL, which possess elastic modulus in the range of hundreds of MPa. It was found that out of 14 synthesized polymers, only 1 possesses a combination of properties making it suitable for cell culturing: processability (solubility in organic solvents); the ability to preserve the fiber morphology in cell culture media at 37 °C; and good cell adhesion, proliferation, and alignment. This combination of properties of polymers and method of fabrication of fibrous structures can be early proof of the promising application of this copolymer for muscle tissue engineering.

■ ASSOCIATED CONTENT

Supporting Information

The Supporting Information is available free of charge at <https://pubs.acs.org/doi/10.1021/acsabm.1c00403>.

GPC profile of selected copolymers; Mw, Mn, and PDI results from GPC measurements; derivative thermogravimetry Gaussian fitting results of selected copolymers; DSC Thermal properties of PCL–PUs copolymers; DSC Thermal properties of wet, selected PCL–PUs copolymers; Tensile stress versus tensile strain curves of polymers that form fibers; Effect of water immersion of a film of PCL500-HDI-PEG3000 1:2:1; C2C12 myoblasts cell culture, the viability of cells (Live/Dead assay) on PCL500-HDI-BD 1:2:1 and PCL500-HDI-PEG3000 1:2:1 touch-spun fibers; C2C12 myoblasts cell culture, the viability of cells (Live/Dead assay) on PCL2000-HDI-BD 1:2:1 touch-spun scaffolds coated and non-coated with FNC (PDF)

■ AUTHOR INFORMATION

Corresponding Author

Leonid Ionov – Faculty of Engineering Sciences and Bavarian Polymer Institute, University of Bayreuth, 95447 Bayreuth, Germany; orcid.org/0000-0002-0770-6140; Email: leonid.ionov@uni-bayreuth.de

Authors

Juan Uribe-Gomez – Faculty of Engineering Sciences and Bavarian Polymer Institute, University of Bayreuth, 95447 Bayreuth, Germany

Andrés Posada-Murcia – Faculty of Engineering Sciences and Bavarian Polymer Institute, University of Bayreuth, 95447 Bayreuth, Germany

Amit Shukla – Faculty of Engineering Sciences and Bavarian Polymer Institute, University of Bayreuth, 95447 Bayreuth, Germany

Hanin Alkhamis – Faculty of Engineering Sciences and Bavarian Polymer Institute, University of Bayreuth, 95447 Bayreuth, Germany

Sahar Salehi – Department of Biomaterials, University of Bayreuth, 95447 Bayreuth, Germany

Complete contact information is available at:

<https://pubs.acs.org/doi/10.1021/acsabm.1c00403>

Author Contributions

The manuscript was written through the contributions of all authors. All authors have given approval to the final version of the manuscript.

Notes

The authors declare no competing financial interest.

■ ACKNOWLEDGMENTS

This work was supported by DFG (IO 68/14-1, IO 68/17-1, SA 3575/1-1). We would further like to thank Prof. Scheibel for providing us access to TGA and SEM, and Arch. Ignacio Uribe for helping with the image rendering.

■ ABBREVIATIONS

ECM, extracellular matrix; PCL, polycaprolactone; PU, polyurethane; PCL–PU, polycaprolactone–polyurethane; HDI, hexamethylene diisocyanate; BD, butanediol; DBTDL, dibutyltin dilaurate; PEG, polyethylene glycol; DMSO, dimethyl sulfoxide; EtOH, ethanol; IPA, 2-propanol; EDTA, ethylenediaminetetraacetic acid; DPBS, Dulbecco's phosphate buf-

ferred saline; DMEM, Dulbecco's Modified Eagle Medium; pen/strep, penicillin–streptomycin; FBS, Fetal Bovine Serum; HEPES, 4-(2-hydroxyethyl)-1-piperazineethanesulfonic acid); BSA, Albumin Fraction V; EthD-1, ethidium; DAPI, 4',6-diamidino-2-phenylindole; FT-IR, Fourier-transform infrared spectroscopy; NMR, nuclear magnetic resonance; SEM, scanning electron microscopy; TGA, thermogravimetric analysis; SAXS, small-angle X-ray scattering; DSC, differential scanning calorimetry; DMA, dynamic mechanical analysis

REFERENCES

- (1) Chen, F. M.; Liu, X. Advancing biomaterials of human origin for tissue engineering. *Prog. Polym. Sci.* **2016**, *53*, 86–168.
- (2) Porzionato, A.; Stocco, E.; Barbon, S.; Grandi, F.; Macchi, V.; De Caro, R. Tissue-engineered grafts from human decellularized extracellular matrices: a systematic review and future perspectives. *Int. J. Mol. Sci.* **2018**, *19* (12), 4117.
- (3) Rivas, D.; Fielding, R. Skeletal muscle. *Encyclopedia of Human Nutrition* **2013**, 193–199.
- (4) Kwee, B. J.; Mooney, D. J. Biomaterials for skeletal muscle tissue engineering. *Curr. Opin. Biotechnol.* **2017**, *47*, 16–22.
- (5) Nguyen, J. H.; Chung, J. D.; Lynch, G. S.; Ryall, J. G. The microenvironment is a critical regulator of muscle stem cell activation and proliferation. *Front. Cell Dev. Biol.* **2019**, *7*, 254.
- (6) Ramalingam, M.; Khademhosseini, A. Micropatterned biomaterials for cell and tissue engineering. *Tissue engineering principles and practices* **2012**, 1–18.
- (7) Khademhosseini, A.; Peppas, N. A. Micro- and nanoengineering of biomaterials for healthcare applications. *Adv. Healthcare Mater.* **2013**, *2*, 10–12.
- (8) Zorlutuna, P.; Annabi, N.; Camci-Unal, G.; Nikkiah, M.; Cha, J. M.; Nichol, J. W.; Manbachi, A.; Bae, H.; Chen, S.; Khademhosseini, A. Microfabricated biomaterials for engineering 3D tissues. *Adv. Mater.* **2012**, *24* (14), 1782–1804.
- (9) Ostrovidov, S.; Seidi, A.; Ahadian, S.; Ramalingam, M.; Khademhosseini, A. Micro- and Nanoengineering Approaches to Developing Gradient Biomaterials Suitable for Interface Tissue Engineering. *Micro and nanotechnologies in engineering stem cells and tissues* **2013**, 52–79.
- (10) Wang, P. Y.; Yu, H. T.; Tsai, W. B. Modulation of alignment and differentiation of skeletal myoblasts by submicron ridges/grooves surface structure. *Biotechnol. Bioeng.* **2010**, *106* (2), 285–294.
- (11) Shen, J. Y.; Chan-Park, M. B. E.; Feng, Z. Q.; Chan, V.; Feng, Z. W. UV-embossed microchannel in biocompatible polymeric film: application to control of cell shape and orientation of muscle cells. *J. Biomed. Mater. Res., Part B* **2006**, *77* (2), 423–430.
- (12) Aviss, K.; Gough, J.; Downes, S. Aligned electrospun polymer fibres for skeletal muscle regeneration. *Eur. Cell. Mater.* **2010**, *19* (1), 193–204.
- (13) Altomare, L.; Gadegaard, N.; Visai, L.; Tanzi, M. C.; Fare, S. Biodegradable microgrooved polymeric surfaces obtained by photolithography for skeletal muscle cell orientation and myotube development. *Acta Biomater.* **2010**, *6* (6), 1948–1957.
- (14) Pennisi, C. P.; Olesen, C. G.; de Zee, M.; Rasmussen, J.; Zachar, V. Uniaxial cyclic strain drives assembly and differentiation of skeletal myocytes. *Tissue Eng., Part A* **2011**, *17* (19–20), 2543–2550.
- (15) Ahadian, S.; Ramón-Azcón, J.; Ostrovidov, S.; Camci-Unal, G.; Hosseini, V.; Kaji, H.; Ino, K.; Shiku, H.; Khademhosseini, A.; Matsue, T. Interdigitated array of Pt electrodes for electrical stimulation and engineering of aligned muscle tissue. *Lab Chip* **2012**, *12* (18), 3491–3503.
- (16) Ramón-Azcón, J.; Ahadian, S.; Obregón, R.; Camci-Unal, G.; Ostrovidov, S.; Hosseini, V.; Kaji, H.; Ino, K.; Shiku, H.; Khademhosseini, A. Gelatin methacrylate as a promising hydrogel for 3D microscale organization and proliferation of dielectrophoretically patterned cells. *Lab Chip* **2012**, *12* (16), 2959–2969.
- (17) Ostrovidov, S.; Hosseini, V.; Ahadian, S.; Fujie, T.; Parthiban, S. P.; Ramalingam, M.; Bae, H.; Kaji, H.; Khademhosseini, A. Skeletal muscle tissue engineering: methods to form skeletal myotubes and their applications. *Tissue Eng., Part B* **2014**, *20* (5), 403–436.
- (18) Liu, H.; Carvalhais, L. C.; Schenk, P. M.; Dennis, P. G. Effects of jasmonic acid signalling on the wheat microbiome differ between body sites. *Sci. Rep.* **2017**, *7* (1), 1–8.
- (19) Davis, B. N.; Yen, R.; Prasad, V.; Truskey, G. A. Oxygen consumption in human, tissue-engineered myobundles during basal and electrical stimulation conditions. *APL bioengineering* **2019**, *3* (2), 026103.
- (20) Mueller, C.; Trujillo-Miranda, M.; Maier, M.; Heath, D. E.; O'Connor, A. J.; Salehi, S. Effects of External Stimulators on Engineered Skeletal Muscle Tissue Maturation. *Adv. Mater. Interfaces* **2021**, *8* (1), 2001167.
- (21) Ostrovidov, S.; Salehi, S.; Costantini, M.; Suthiwanich, K.; Ebrahimi, M.; Sadeghian, R. B.; Fujie, T.; Shi, X.; Cannata, S.; Gargioli, C.; Tamayol, A.; Dokmeci, M. R.; Orive, G.; Swieszkowski, W.; Khademhosseini, A. 3D Bioprinting in Skeletal Muscle Tissue Engineering. *Small* **2019**, *15* (24), 1805530.
- (22) Apsite, I.; Uribe, J. M.; Posada, A. F.; Rosenfeldt, S.; Salehi, S.; Ionov, L. 4D biofabrication of skeletal muscle microtissues. *Biofabrication* **2020**, *12* (1), 015016.
- (23) Mohamed, M. A.; Fallahi, A.; El-Sokkary, A. M.; Salehi, S.; Akl, M. A.; Jafari, A.; Tamayol, A.; Fenniri, H.; Khademhosseini, A.; Andreadis, S. T. Stimuli-responsive hydrogels for manipulation of cell microenvironment: From chemistry to biofabrication technology. *Prog. Polym. Sci.* **2019**, *98*, 101147.
- (24) Uribe-Gomez, J.; Posada-Murcia, A.; Shukla, A.; Ergin, M.; Constante, G.; Apsite, I.; Martin, D.; Schwarzer, M.; Caspari, A.; Synytska, A.; Salehi, S.; Ionov, L. Shape-Morphing Fibrous Hydrogel/Elastomer Bilayers Fabricated by a Combination of 3D Printing and Melt Electrowriting for Muscle Tissue Regeneration. *ACS Appl. Biol. Mater.* **2021**, *4* (2), 1720–1730.
- (25) Ostrovidov, S.; Ebrahimi, M.; Bae, H.; Nguyen, H. K.; Salehi, S.; Kim, S. B.; Kumatani, A.; Matsue, T.; Shi, X.; Nakajima, K. Gelatin–polyaniline composite nanofibers enhanced excitation–contraction coupling system maturation in myotubes. *ACS Appl. Mater. Interfaces* **2017**, *9* (49), 42444–42458.
- (26) Katta, P.; Alessandro, M.; Ramsier, R.; Chase, G. Continuous electrospinning of aligned polymer nanofibers onto a wire drum collector. *Nano Lett.* **2004**, *4* (11), 2215–2218.
- (27) Dalton, P. D.; Klee, D.; Möller, M. Electrospinning with dual collection rings. *Polymer* **2005**, *46* (3), 611–614.
- (28) Brown, T. D.; Dalton, P. D.; Hutmacher, D. W. Direct Writing By Way of Melt Electrospinning. *Adv. Mater.* **2011**, *23* (47), S651–S657.
- (29) Groll, J.; Boland, T.; Blunk, T.; Burdick, J. A.; Cho, D.-W.; Dalton, P. D.; Derby, B.; Forgacs, G.; Li, Q.; Mironov, V. A.; Moroni, L.; Nakamura, M.; Shu, W.; Takeuchi, S.; Vozzi, G.; Woodfield, T. B. F.; Xu, T.; Yoo, J. J.; Malda, J. Biofabrication: reappraising the definition of an evolving field. *Biofabrication* **2016**, *8* (1), 013001.
- (30) Dalton, P. D. Melt electrospinning with additive manufacturing principles. *Curr. Opin. Biomed. Eng.* **2017**, *2*, 49–57.
- (31) Robinson, T. M.; Hutmacher, D. W.; Dalton, P. D. The Next Frontier in Melt Electrospinning: Taming the Jet. *Adv. Funct. Mater.* **2019**, *29* (44), 1904664.
- (32) Constante, G.; Apsite, I.; Alkhamis, H.; Dulle, M.; Schwarzer, M.; Caspari, A.; Synytska, A.; Salehi, S.; Ionov, L. 4D Biofabrication Using a Combination of 3D Printing and Melt-Electrowriting of Shape-Morphing Polymers. *ACS Appl. Mater. Interfaces* **2021**, *13* (11), 12767–12776.
- (33) Brown, T. D.; Dalton, P. D.; Hutmacher, D. W. Direct writing by way of melt electrospinning. *Adv. Mater.* **2011**, *23* (47), S651–S657.
- (34) Wunner, F. M.; Bas, O.; Saidu, N. T.; Dalton, P. D.; Pardo, E. M. D.-J.; Hutmacher, D. W. Melt electrospinning writing of three-dimensional poly (ϵ -caprolactone) scaffolds with controllable morphologies for tissue engineering applications. *J. Visualized Exp.* **2017**, *130*, e56289.
- (35) Asheghali, D.; Lee, S.-J.; Furchner, A.; Gruz, A.; Larson, S.; Tokarev, A.; Stake, S.; Zhou, X.; Hinrichs, K.; Zhang, L. G. Enhanced neuronal differentiation of neural stem cells with mechanically

- enhanced touch-spun nanofibrous scaffolds. *Nanomedicine* **2020**, *24*, 102152.
- (36) Tokarev, A.; Asheghali, D.; Griffiths, I. M.; Trotsenko, O.; Gruz, A.; Lin, X.; Stone, H. A.; Minko, S. Touch-and Brush-Spinning of Nanofibers. *Adv. Mater.* **2015**, *27* (41), 6526–6532.
- (37) Lee, S.-J.; Asheghali, D.; Blevins, B.; Timsina, R.; Esworthy, T.; Zhou, X.; Cui, H.; Hann, S. Y.; Qiu, X.; Tokarev, A. Touch-Spun Nanofibers for Nerve Regeneration. *ACS Appl. Mater. Interfaces* **2020**, *12* (2), 2067–2075.
- (38) Apsite, I.; Uribe, J. M.; Posada, A. F.; Rosenfeldt, S.; Salehi, S.; Ionov, L. 4D biofabrication of skeletal muscle microtissues. *Biofabrication* **2020**, *12* (1), 015016.
- (39) Cronin, E. M.; Thurmond, F. A.; Bassel-Duby, R.; Williams, R. S.; Wright, W. E.; Nelson, K. D.; Garner, H. R. Protein-coated poly (L-lactic acid) fibers provide a substrate for differentiation of human skeletal muscle cells. *J. Biomed. Mater. Res.* **2004**, *69* (3), 373–381.
- (40) Narayanan, N.; Jiang, C.; Wang, C.; Uzunalli, G.; Whittern, N.; Chen, D.; Jones, O. G.; Kuang, S.; Deng, M. Harnessing fiber diameter-dependent effects of myoblasts toward biomimetic scaffold-based skeletal muscle regeneration. *Front. Bioeng. Biotechnol.* **2020**, *8*, 203.
- (41) Neumann, T.; Hauschka, S. D.; Sanders, J. E. Tissue engineering of skeletal muscle using polymer fiber arrays. *Tissue Eng.* **2003**, *9* (5), 995–1003.
- (42) McKeon-Fischer, K.; Flagg, D.; Freeman, J. Coaxial electrospun poly (ϵ -caprolactone), multiwalled carbon nanotubes, and polyacrylic acid/polyvinyl alcohol scaffold for skeletal muscle tissue engineering. *J. Biomed. Mater. Res., Part A* **2011**, *99* (3), 493–499.
- (43) Ku, S. H.; Lee, S. H.; Park, C. B. Synergic effects of nanofiber alignment and electroactivity on myoblast differentiation. *Biomaterials* **2012**, *33* (26), 6098–6104.
- (44) Chen, M.-C.; Sun, Y.-C.; Chen, Y.-H. Electrically conductive nanofibers with highly oriented structures and their potential application in skeletal muscle tissue engineering. *Acta Biomater.* **2013**, *9* (3), 5562–5572.
- (45) Mi, H.-Y.; et al. Biocompatible, degradable thermoplastic polyurethane based on polycaprolactone-block-polytetrahydrofuran-block-polycaprolactone copolymers for soft tissue engineering. *J. Mater. Chem. B* **2017**, *5* (22), 4137–4151.
- (46) Zhang, L.; Huang, M.; Yu, R.; Huang, J.; Dong, X.; Zhang, R.; Zhu, J. Bio-based shape memory polyurethanes (Bio-SMPUs) with short side chains in the soft segment. *J. Mater. Chem. A* **2014**, *2* (29), 11490–11498.
- (47) Nair, P. A.; Ramesh, P. Electrospun biodegradable calcium containing poly (ester-urethane) urea: Synthesis, fabrication, in vitro degradation, and biocompatibility evaluation. *J. Biomed. Mater. Res., Part A* **2013**, *101* (7), 1876–1887.
- (48) Chan-Chan, L. H.; Solis-Correa, R.; Vargas-Coronado, R. F.; Cervantes-Uc, J. M.; Cauch-Rodríguez, J.; Quintana, P.; Bartolo-Pérez, P. Degradation studies on segmented polyurethanes prepared with HMDI, PCL and different chain extenders. *Acta Biomater.* **2010**, *6* (6), 2035–2044.
- (49) Dust, J. M.; Fang, Z. H.; Harris, J. M. Proton NMR characterization of poly (ethylene glycols) and derivatives. *Macromolecules* **1990**, *23* (16), 3742–3746.
- (50) Behera, P. K.; Mondal, P.; Singha, N. K. Polyurethane with an ionic liquid crosslinker: a new class of super shape memory-like polymers. *Polym. Chem.* **2018**, *9* (31), 4205–4217.
- (51) Huh, D. S.; Cooper, S. L. Dynamic mechanical properties of polyurethane block polymers. *Polym. Eng. Sci.* **1971**, *11* (5), 369–376.
- (52) Martin, D. J.; Meijs, G. F.; Renwick, G. M.; Mccarthy, S. J.; Gunatillake, P. A. The effect of average soft segment length on morphology and properties of a series of polyurethane elastomers. I. Characterization of the series. *J. Appl. Polym. Sci.* **1996**, *62* (9), 1377–1386.
- (53) Gosline, J.; Lillie, M.; Carrington, E.; Guerette, P.; Ortlepp, C.; Savage, K. Elastic proteins: biological roles and mechanical properties. *Philos. Trans. R. Soc., B* **2002**, *357*, 121–132.
- (54) Lv, S.; Dudek, D. M.; Cao, Y.; Balamurali, M.; Gosline, J.; Li, H. Designed biomaterials to mimic the mechanical properties of muscles. *Nature* **2010**, *465* (7294), 69–73.

Supporting Information

Soft elastic fibrous scaffolds for muscle tissue engineering by touch spinning

Juan Uribe-Gomez[§], Andrés Posada-Murcia[§], Amit Shukla[§], Hanin Alkhamis[§], Sahar Salehi[†]

and Leonid Ionov^{§}.*

§ Faculty of Engineering Sciences and Bavarian Polymer Institute University of Bayreuth

Ludwig Thoma Str. 36A, 95447, Bayreuth, Germany.

† Department of Biomaterials, University of Bayreuth Prof.-Rüdiger-Bormann Str. 1, 95447

Bayreuth, Germany

*E-mail: leonid.ionov@uni-bayreuth.de

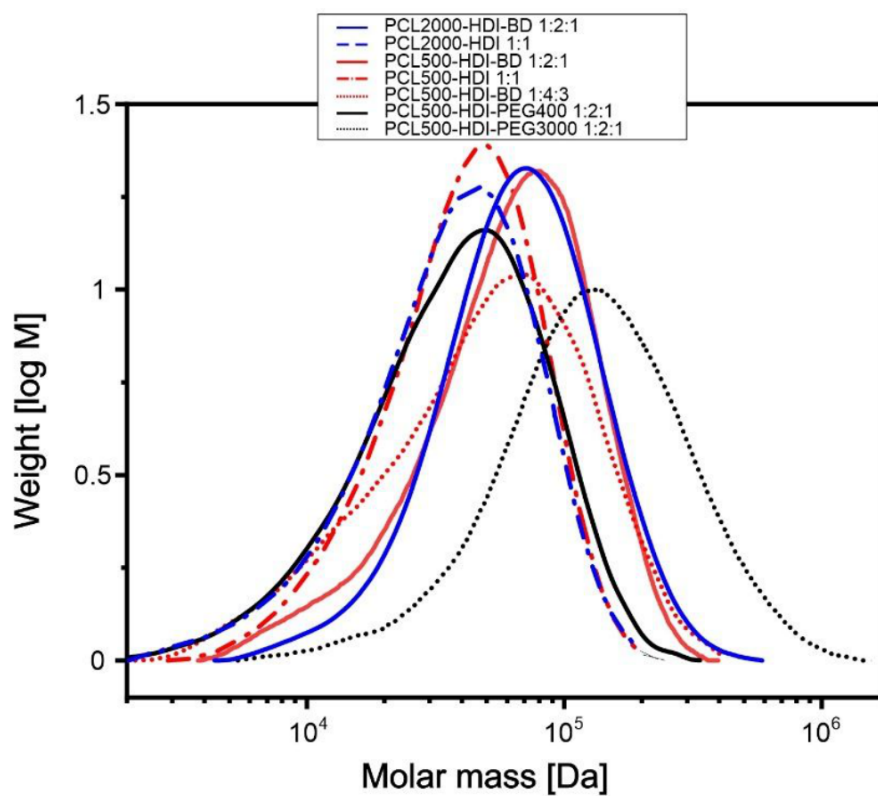


Figure S1. GPC profile of selected copolymers.

Table S1. Mw, Mn, and PDI results from GPC measurements using DMF as the solvent. The unit of molecular weight is g mol^{-1} .

Polymer	Mn ($\times 10^3$)	Mw ($\times 10^3$)	PDI
PCL2000-HDI-BD 1:2:1*	38.0*	67.0*	1.8*
PCL2000-HDI-BD 1:2:1	49.8	82.9	1.7
PCL500-HDI 1:1	30.1	48.5	1.6
PCL500-HDI-BD 1:2:1	42.0	75.6	1.8

PCL500-HDI-BD 1:4:3	29.9	69.5	2.3
PCL500-HDI-PEG400 1:2:1	25.2	49.7	2.0
PCL500-HDI-PEG 3000 1:2:1	86.4	175.2	2.0

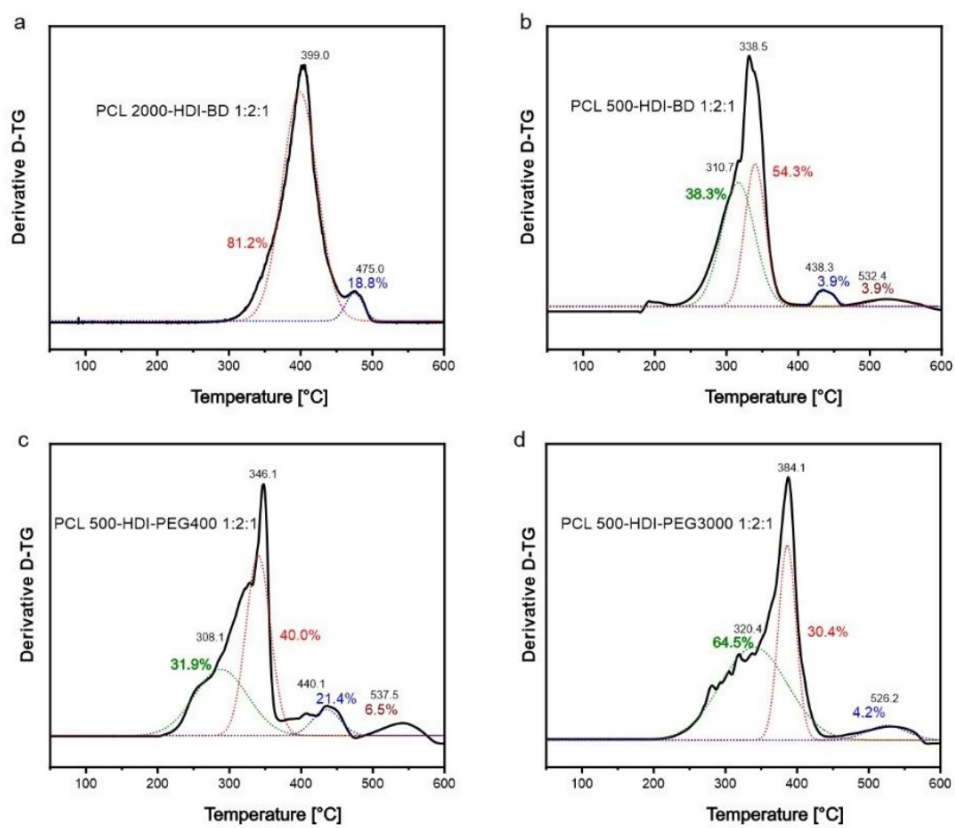


Figure S2. Derivative thermogravimetry gaussian fitting results of a) PCL2000-HDI-DB 1:2:1; b) PCL500-HDI-BD 1:2:1; c) PCL500-HDI-PEG400 1:2:1; d) PCL500-HDI-PEG3000 1:2:1.

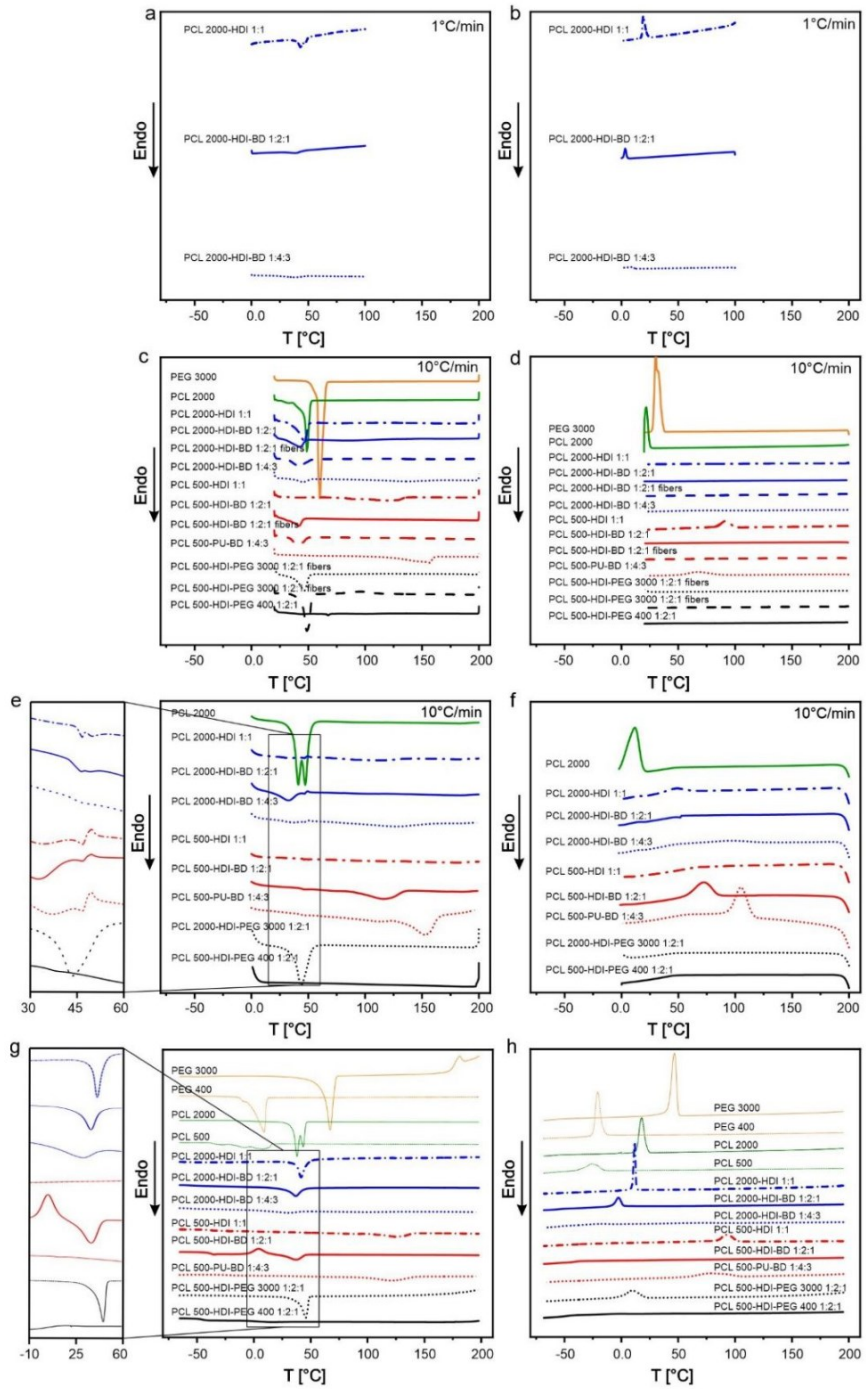


Figure S3. Thermal properties of PCL-PU_s copolymers: 1 °C/min: a) DSC first heating; b) DSC first cooling; 10 °C/min c) DSC first heating from 0 °C to 200 °C; d) DSC first cooling from 200 °C to 0 °C; e) DSC second heating from 0 °C to 200 °C; f) DSC first cooling from 200 °C to 0 °C; g) DSC second heating from -70 °C to 200 °C; h) DSC first cooling from 200 °C to -70 °C.

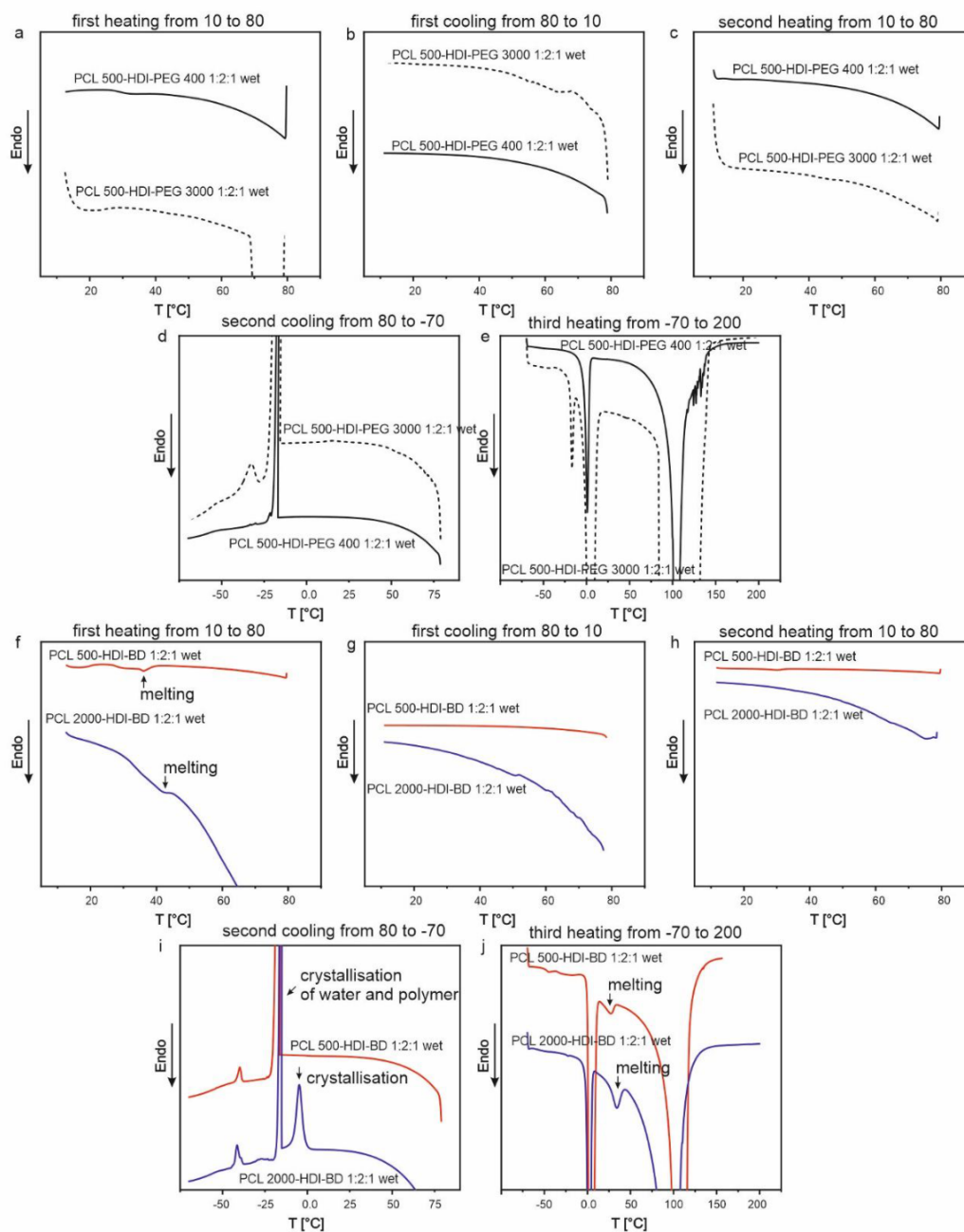


Figure S4. Thermal properties of wet PCL-HDI-PEGs a) DSC first heating from 10 °C to 80 °C; b) DSC first cooling from 80 °C to 10 °C; c) DSC second heating from 10 °C to 80 °C; d) DSC second cooling from 80 °C to -70 °C; e) DSC third heating from -70 °C to 200 °C. Thermal properties of

wet PCL-HDI-BDs f) DSC first heating from 10 °C to 80 °C; g) DSC first cooling from 80 °C to 10 °C; h) DSC second heating from 10 °C to 80 °C; i) DSC second cooling from 80 °C to -70 °C; j) DSC third heating from -70 °C to 200 °C.

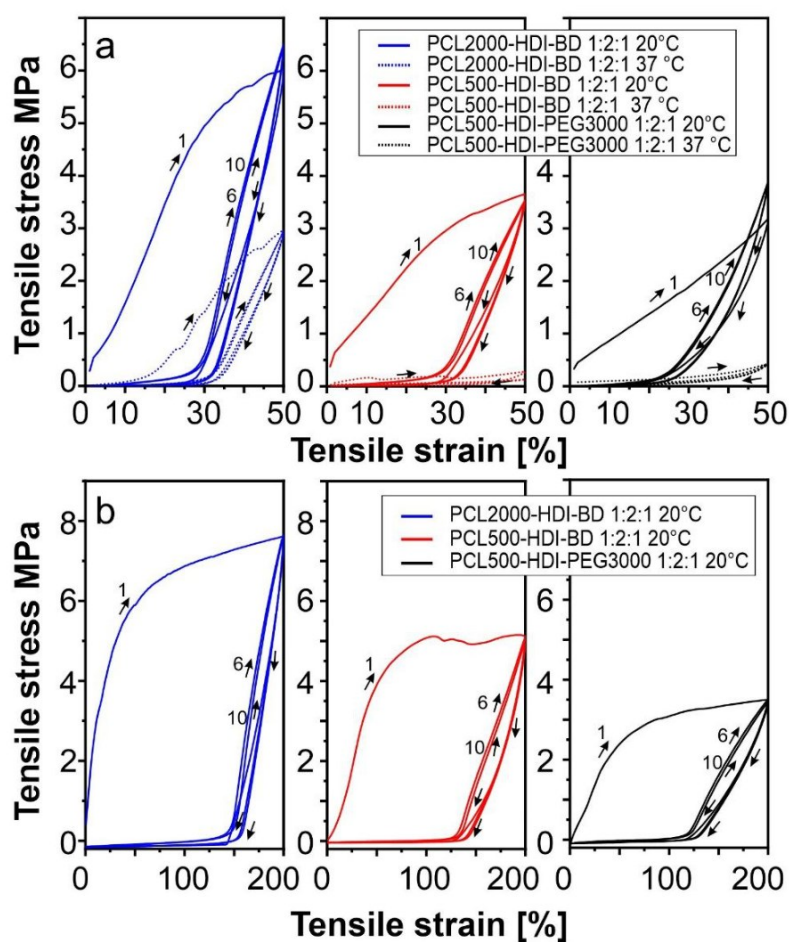


Figure S5. Tensile stress versus tensile strain curves of polymers that form fibers at 20 and 37 °C;

a): cycles to 50% strain; b) cycles to 200% strain.

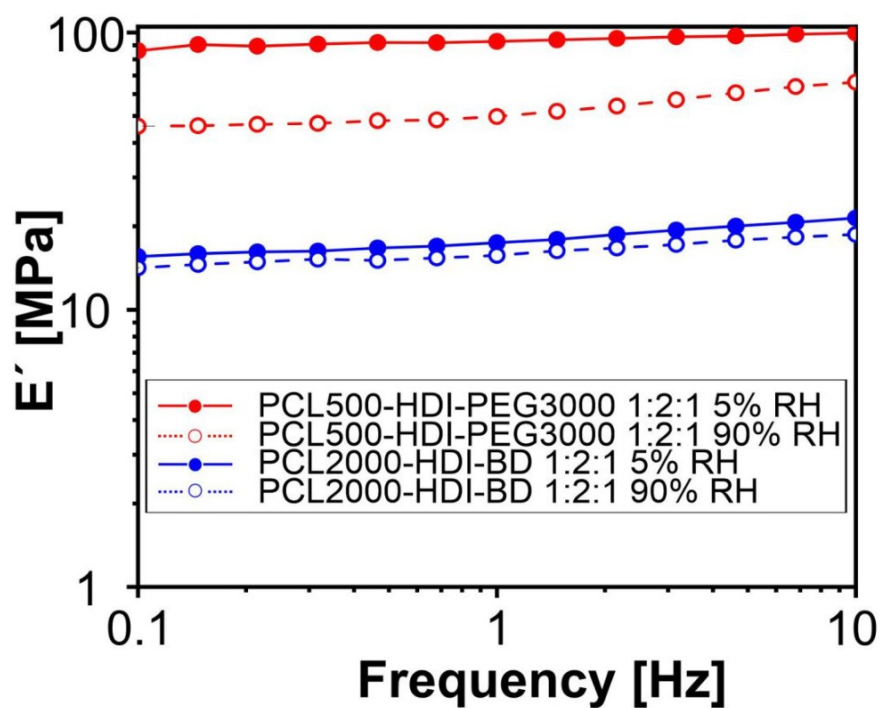


Figure S6. Mechanical properties of polymer obtained in air with different humidity.

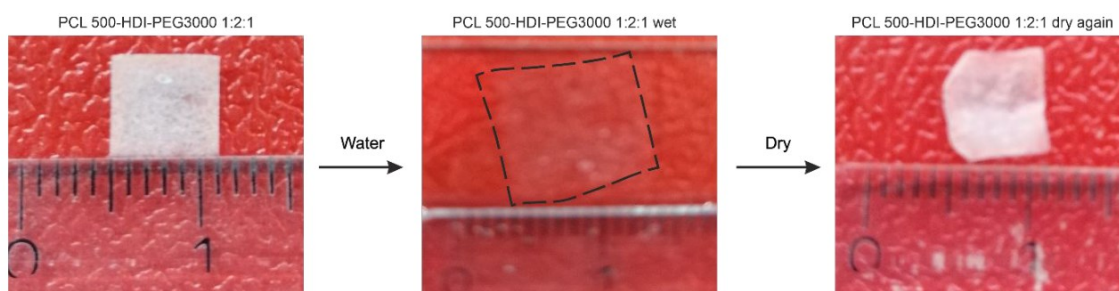


Figure S7. Effect of water immersion of a film of PCL500-HDI-PEG3000 1:2:1.

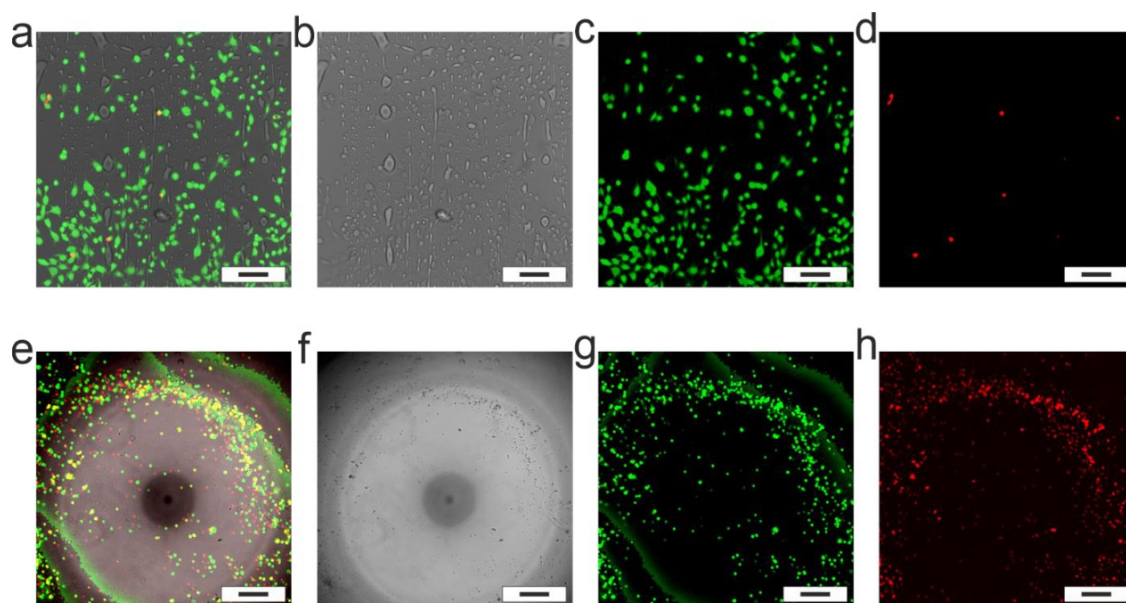


Figure S8. C2C12 myoblasts cell culture a-d) viability at day 1 of cells (Live/Dead assay) on PCL500-HDI-BD 1:2:1 touch-spun fibers. Red - dead cells; green - live cells. Scale bars 50 μm ; e-h) viability at day 1 of cells (Live/Dead assay) on PCL500-HDI-PEG3000 1:2:1 touch-spun fibers. Red - dead cells; green - live cells. Scale bars 500 μm . The cell culture experiment was discontinued due to melting of polymer fibers.

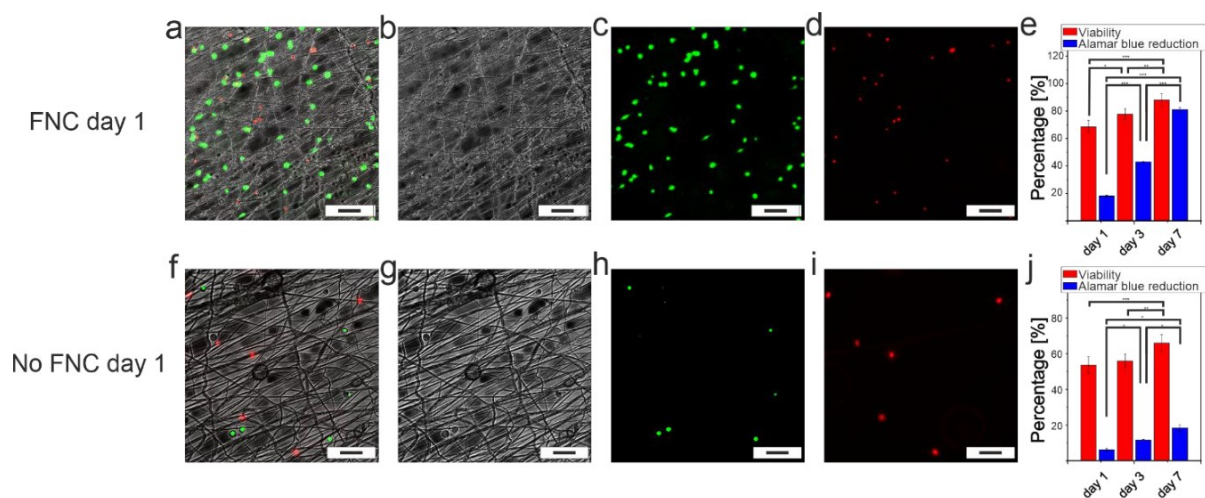


Figure S9. C2C12 myoblasts cell culture a-d) viability of cells (Live/Dead assay) on PCL2000-HDI-BD 1:2:1 touch-spun scaffolds coated with FNC. Red - dead cells; green - live cells at day 1 of culture; e) quantification of cell viability and cell metabolic activity after 1, 3, and 7 days of culture measured by Alamar Blue Assay. f-i) viability of cells (Live/Dead assay) on PCL2000-HDI-BD 1:2:1 touch-spun scaffolds non coated with FNC. Red - dead cells; green - live cells at day 1 of culture; j) quantification of cell viability and cell metabolic activity after 1, 3, and 7 days of culture measured by Alamar Blue Assay. * $p \leq 0.05$; ** $p \leq 0.01$; *** $p \leq 0.001$; f-i) . Scale bars 100 μm .

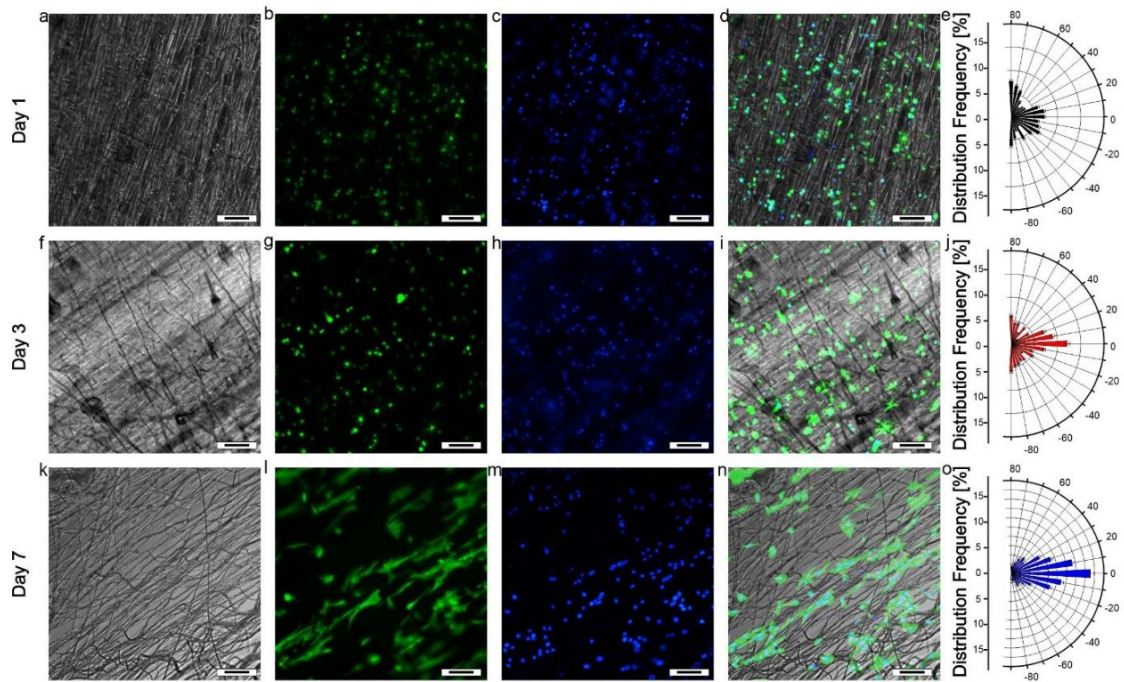


Figure S10. C2C12 myoblasts cell culture a-d) cell nuclei alignment on PCL2000-HDI-BD 1:2:1 touch-spun scaffolds at day 1. e) quantification analysis of cell nuclei alignment at day 1. f-i) cell nuclei alignment on PCL2000-HDI-BD 1:2:1 touch-spun scaffolds at day 3. j) quantification analysis of cell nuclei alignment at day 3. k-n) cell nuclei alignment on PCL2000-HDI-BD 1:2:1 touch-spun scaffolds at day 7. o) quantification analysis of cell nuclei alignment at day 7. Scale bars 100 μm .

Corrections Manuscript 2

Soft elastic fibrous scaffolds for muscle tissue engineering by touch spinning

Page 61. NMR The nuclear magnetic resonance spectra of soluble synthesized PCL-PU were obtained using a Bruker Avance 500 spectrometer (Bruker BioSpin GmbH, Silberstreifen, Germany) (500.16 MHz for ^1H). ^1H NMR chemical shifts (δ) were reported in parts per million (ppm) relative to tetramethylsilane (TMS), with the residual solvent peak used as an internal reference using DMSO- d_6 . (500 MHz, DMSO- d_6 , δ): 7.03 (s), 3.81 (s), 2.92 (s), 1.64 – 1.42 (m), 1.42 – 1.09 (m) corresponding to the polyurethane part, shifts 3.97 (t, $J = 6.5$ Hz); 2.26 (t, $J = 7.3$ Hz) corresponding to polycaprolactone 1.64 – 1.42 (m), 1.42 – 1.09 (m) overlapping PCL and Polyurethane parts and 3.51 (s) corresponding to the PEG protons.

Manuscript 3

Fibrous scaffolds for muscle tissue engineering based on touch-spun poly(ester-urethane) elastomer

*Juan Uribe-Gomez, Dennis Schönfeld, Andrés Posada-Murcia, Michel-Manuel Roland,
Anja Caspari, Alla Synytska, Sahar Salehi, Thorsten Pretsch and Leonid Ionov*

Wiley Online Library – Advanced Science News- Macromolecular Bioscience

Published on: January 10, 2022

DOI: 10.1002/mabi.202100427

Fibrous Scaffolds for Muscle Tissue Engineering Based on Touch-Spun Poly(Ester-Urethane) Elastomer

Juan Uribe-Gomez, Dennis Schönfeld, Andrés Posada-Murcia, Michel-Manuel Roland, Anja Caspari, Alla Synytska, Sahar Salehi, Thorsten Pretsch, and Leonid Ionov*

Development of fiber-spinning technologies and materials with proper mechanical properties is highly important for the manufacturing of aligned fibrous scaffolds mimicking structure of the muscle tissues. Here, the authors report touch spinning of a thermoplastic poly(1,4-butylene adipate)-based polyurethane elastomer, obtained via solvent-free polymerization. This polymer possesses a combination of important advantages such as 1) low elastic modulus in the range of a few MPa, 2) good recovery ratio and 3) resilience, 4) processability, 5) nontoxicity, 6) biocompatibility, and 7) biodegradability that makes it suitable for fabrication of structures mimicking extracellular matrix of muscle tissue. Touch spinning allows fast and precise deposition of highly aligned micro- and nano-fibers without use of high voltage. C2C12 myoblasts readily align along soft polymer fibers and demonstrate high viability as well as proliferation that make proposed combination of polymer and fabrication method highly suitable for engineering skeletal muscles.

1. Introduction

The development of approaches for regeneration of tissues is vitally important for future progress of medicine.^[1–4] In the conventional tissue engineering approach, cells are deposited onto a supporting complex 3D structure—scaffold.^[5] In order to be effective, this engineered 3D structure must be as close as possible to the native extracellular matrix (ECM).^[6] ECM is formed by proteoglycans and polysaccharides, which form gel-like structures and ensure aqueous environment for cells, as well as by collagen and elastin, which form fibers and, in this way, provide suitable mechanical properties for tissues and a proper structural environment for cells. Collagen is a crystalline protein, which forms nearly nonstretchable fibers with very large elastic modulus in the order of gigapascals.^[7] On the contrary, elastin is a soft amorphous cross-linked protein

with elastic modulus in the order of megapascals (1–2 MPa) and could be extended to 100%, and often up to 200% before breaking.^[8,9] Together, collagen and elastin ensure the J-like shape of the stress–strain curve of soft tissues, with elastic modulus in the range of tens of kilopascal at small strain and an elastic modulus of 1 MPa at 50% of extension as well as the reversibility of deformation.^[8] Thus, the development of materials and methods for the fabrication of fibrous architectures mimicking the fibrous structure of ECM is highly important.

To this end, various microfabrication techniques such as photolithography,^[10] melt-electro writing (MEW),^[11,12] electrospinning,^[13] touch spinning,^[14] and their combinations have been utilized to fabricate biomimetic micro/nanoscale structures, primarily using biologically relevant materials.^[15,16] For example, to the fabrication of aligned fibers, electrospinning can be used with various collectors, such as two parallel bars (a relatively slow process) and a rotating drum (a faster process).^[17–19] In contrast to randomly collected fibers in electrospinning, MEW technique allows deposition of uni-axially aligned fibers in a programmed way.^[20–22] However, MEW is a relatively time-consuming process with an average fabrication rate of 50 mm s⁻¹ and limited maximal speed of the linear actuator.^[22–26] Consequently, polymers with high melting points have to be exposed to high temperatures for long periods of time in extruders, which may influence the polymer properties and structures. An alternative fiber fabrication technique introduced

J. Uribe-Gomez, A. Posada-Murcia, M.-M. Roland, L. Ionov
 Faculty of Engineering Sciences and Bavarian Polymer Institute
 University of Bayreuth
 Ludwig Thoma Str. 36A, Bayreuth 95447, Germany
 E-mail: leonid.ionov@uni-bayreuth.de

D. Schönfeld, T. Pretsch
 Fraunhofer Institute for Applied Polymer Research IAP
 Geiselbergstr. 69, Potsdam 14476, Germany

A. Caspari, A. Synytska
 Leibniz-Institut für Polymerforschung Dresden e.V.
 Hohe Str. 6, Dresden 01069, Germany

A. Synytska
 Fakultät Mathematik und Naturwissenschaften
 Technische Universität Dresden
 Mommsenstrasse 4, Dresden 01064, Germany

A. Synytska
 Bayerisches Polymerinstitut – BPI
 Universität Bayreuth
 Universitätsstraße 30, Bayreuth 95440, Germany

S. Salehi
 Department of Biomaterials
 University of Bayreuth
 Prof.-Rüdiger-Bormann Str. 1, Bayreuth 95447, Germany

 The ORCID identification number(s) for the author(s) of this article can be found under <https://doi.org/10.1002/mabi.202100427>

DOI: 10.1002/mabi.202100427

by Minko is touch spinning; the technique is based on touching and pulling polymer solutions or melts by a rapidly rotating rod, which draws fibers one by one upon its rotation.^[27–29] The main advantages of touch spinning over MEW or electrospinning are that touch spinning allows much faster deposition of aligned fibers due to the rapid rotation of the motor and it does not require any voltage source that makes it safer for use. Recently, we showed that the aligned touch-spun fibers are promising scaffolds for muscle tissue engineering and they support the alignment of muscle cells.^[14]

Common thermoplastic polymers, such as polycaprolactone (PCL) or polylactide (PLA), have a high elastic modulus in the order of hundreds of MPa (340 MPa for PCL) with a melting temperature of 60 and 160 °C, respectively. In addition, they are significantly harder than cells and tissues. On the other hand, certain polyurethane copolymers may be characterized by a lower stiffness, which makes them also interesting candidates for soft tissue engineering applications.^[14,26] The yield point of polymers is, for example, affected by strain rate and temperature. Therefore, deformation conditions have to be closely considered in line with an application environment. A significant advantage of segregated polyurethane copolymers is that their thermomechanical properties can be tailored by varying the individual building blocks and the ratio of hard to soft segments. Typical strains, which may occur during deformation when stimulating the formation of muscle tissues in an engineered environment, are ≈20%.^[30] When using PCL or PLA as base materials, large parts of the deformation may become irreversible at such strains, and a mechanical stimulation becomes impossible. To solve this problem, this issue was addressed here by using thermoplastic polyurethane elastomers, which can be processed in melt and solution, they can be soft and demonstrate high reversibility of deformation at large strain values.^[31] According to literature, various thermoplastic polyurethanes have been used to fabricate fibers for tissue engineering applications such as polyurethane-urea,^[32] poly(ester carbonate urethane)urea,^[33] PCL–polyurethane,^[14] and polyurethane-fibrinogen.^[34]

In our previous report, several copolymers of PCL-based polyurethanes were synthesized by two-step polymerization using dimethyl sulfoxide (DMSO) as a solvent.^[14] The main problem of the synthesis was applying anhydrides, due to their toxicity, and providing an inert atmosphere, which is expensive and hard to manage for industrial purposes.^[35] In the current study, we report the synthesis of a poly(ester-urethane) (PEU), where we avoid the use of solvents during preparation. In this case, the reaction occurs at a higher temperature (120 °C instead of 70 °C in solution) that results in a higher molecular weight by one order of magnitude on average.

This work reports on a PEU suitable for biofabrication and capable of forming microfibers. The segmented block copolymer mainly consists of a biodegradable aliphatic polyester, poly(1,4-butylene adipate) (PBA), block-linked to each other by an aromatic polyurethane block. At body temperature, it is softer than most common polyesters ($E \approx 1\text{--}3$ MPa) in comparison with PCL ($E \approx 8\text{--}20$ MPa).^[14] It demonstrates significant reversibility (above 50%) of deformation at 50% elongation, cell viability higher than 85%, and degradation in phosphate-buffered saline (PBS) around 7% per month. Obviously, the solvent-free polymerization approach opens opportunities for the production of

cell and environmentally friendly materials. Therefore, our PEU could be a suitable candidate for muscle tissue engineering.

2. Results and Discussion

2.1. Synthesis and Characterization

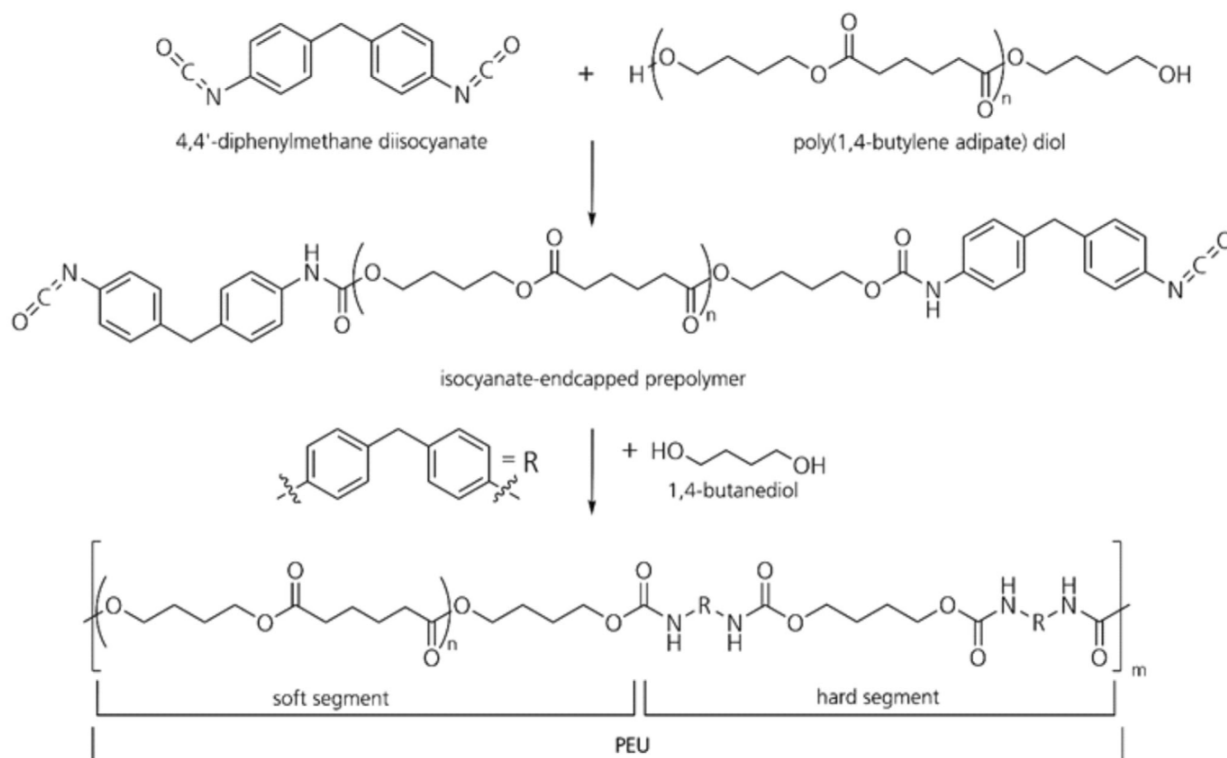
The PEU was obtained in a two-step synthesis process following the prepolymer method,^[35–37] shown in **Scheme 1** and described in detail in our recently published work.^[38] First, 4,4'-diphenylmethane diisocyanate (MDI) and poly(1,4-butylene adipate) diol (PBA-diol) were brought to reaction in order to build up an isocyanate-terminated prepolymer. Afterward, the chains of the prepolymer were extended by adding BD. As a result of using building blocks with bifunctional units, a linear phase-segregated PEU block copolymer was obtained. Herein, the so-called soft segments, which impart elastic properties to the polymer in the amorphous state, were built up by PBA. In turn, the hard segments composed of MDI and BD contribute to the strength of the PEU and provide physical cross-linking to the polymer. The number average molecular weight of the TPU-PBA 25 was determined as $M_n \approx 1.4 \times 10^5$ g mol⁻¹ with polydispersity indices (PDI) ≈ 2.9 (Figure S1 and Table S1, Supporting Information). The block copolymer was characterized by ¹H-NMR and Fourier transform infrared spectroscopy (FTIR) spectroscopy to verify the molecular structure. It is well-known from earlier works that similar polymers exhibit a high degree of reversible deformability up to several hundred percent of strain.^[14,39–42]

The ¹H-NMR spectra show characteristic chemical shift, spin multiplicity, coupling constants, and integration of all the protons of the block copolymer (**Figure 1a**). In general, the peaks at the low field between 10.0 and 7.0 ppm were assigned to the aromatic protons and the N–H in the urethane, confirming the successful reaction. As nuclear magnetic resonance (NMR) spectra show single signals for each part of the block copolymer, it is possible to calculate the ratio between the hard and soft segment using the Equation (1),

$$\text{HSC}\% = \left(\frac{\int \text{HS}}{\int \text{HS} + \int \text{SS}} \right) \times 100 \quad (1)$$

where HS is a hard segment, being the summary of integrals of one aromatic signal and the independent signal of BD; and SS is a soft segment from an individual signal of PBA in NMR. As a result of the calculations taking the signals at 7.07, 3.79, and 2.27 ppm, we obtained 23.9% of hard segment content, which was comparable to the composition expected (25.0%) from the ratio between the monomers used for polymerization.

The FT-IR spectra (**Figure 1b**) shows distinct bands which are specific for the PEU. The bands at 1531 cm⁻¹ and 3328 cm⁻¹ correspond to the N–H bending and N–H stretching of the urethane group, respectively. The band at 1727 cm⁻¹ that corresponds to the free (non-hydrogen-bonded) C=O stretching of the urethane and carbonyl groups, and the absence of a distinct signal at 2280 cm⁻¹ correlated with the presence of freely available isocyanate groups are indicators of complete reaction. There is the band at 1164 cm⁻¹ due to the C–O stretching of the carbonyl group; the bending out-of-plane of O–CO–N shows a band at 673 cm⁻¹. In the range of 3031–2796 cm⁻¹ the asymmetric



Scheme 1. Prepolymer synthesis method for the production of a phase-segregated PUU.

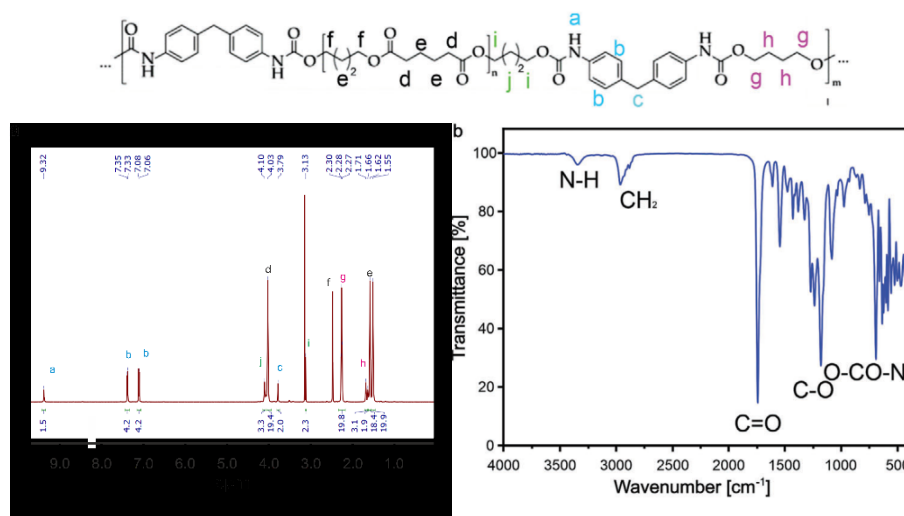


Figure 1. a) NMR spectra and b) FTIR spectra of TPU-PBA 25 block copolymer.

and symmetric C-H stretching is observed, and at 1463 cm⁻¹ the asymmetric C-H bending of CH₂ is observed. Finally, the band located at 1596 cm⁻¹ corresponds to the C-C stretching of the aromatic rings and the band at 816 cm⁻¹ corresponds to the C-H bending of the p-disubstituted benzene ring. The principal FTIR signals indicate the urethane linkage in the TPU-PBA 25, which is strong indication for the synthesis of polyurethane copolymers.^[43,44] Thus, both the results from FTIR and NMR

spectroscopy confirm the successful synthesis of the TPU-PBA 25.

Thermogravimetric analysis (TGA) was performed to investigate the composition and thermal degradation of the polymer (Figure 2a). Pure Desmophen 2505 (PBA diol) was used as a reference sample. First, we noticed that while pure monomer demonstrates single-stepped thermal degradation with the maximum at ~410 °C, the copolymer demonstrates clear three steps: maxima

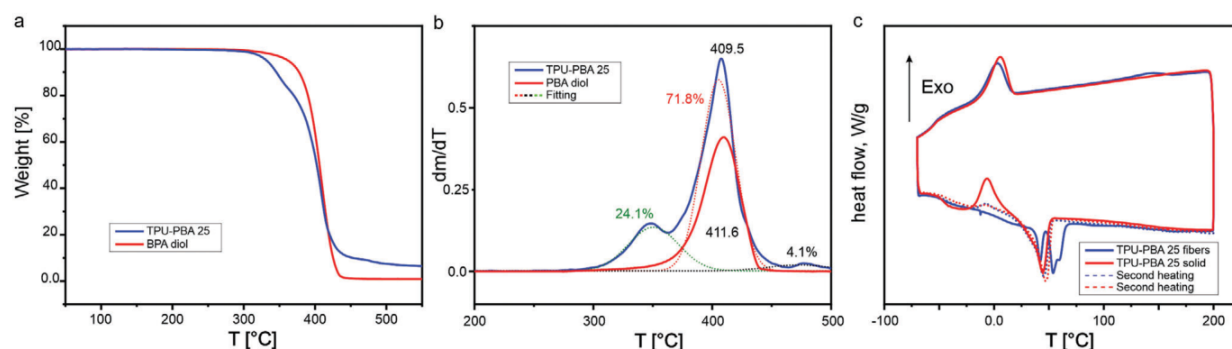


Figure 2. Thermogravimetric analysis: a) TGA from 50 to 550 °C under nitrogen atmosphere, mass loss of TPU-PBA 25, and PBA diol. b) dm/dT of TPU-PBA 25 and PBA diol. c) DSC from -70 to 200 °C at 10 °C min^{-1} of TPU-PBA 25.

Table 1. Quantitative summary of DSC data.

Polymer	T_g [°C]		T_m [°C]		ΔH [J g ⁻¹]		X_c^b [%]	
	1st heating	2nd heating	1st heating	2nd heating	1st heating	2nd heating	1st heating	2nd heating
PBA diol*	-42.0	-57.0	21	6, 30	89.3	17.5	66.14	55.0
TPU-PBA 25	-45.6	-42.3	-6.8 ^{a)}	-7.2 ^{a)}	15.9	0.9	28.2	19.3
			44.1	47.0	22.2	25.2		
TPU-PBA 25 fibers	-46.0	-47.5	42.1	-7.2 ^{a)}	3.6	2.6	10.7	17.7
			54.1	44.9	10.8	21.3		

* Data from Rogulska et al.^[47] ^{a)} From cold crystallization peaks. ^{b)} The percentage crystallinity was calculated as: $X_c = 100\Delta H_m/\Delta H_m^*$ ($\Delta H_m^* = 135$ J g⁻¹ for 100% crystalline PBA).^[48]

at 360, 410, and 480 °C with 24.1%, 71.8%, and 4.1% respectively, of mass loss calculated by the integration of the Gaussian fitting deconvolution (Figure 2b). The amplitude of the low-temperature decomposition step (maximum at 360 °C) in the copolymer appears corresponding to the urethane and chain extender parts (24.1% of the derivative deconvolution), meaning that the high-temperature step is attributed to the soft segment part. The composition obtained from TGA was found to be in very good agreement with the ratio between the monomers used for polymerization, 75.0% in mass of soft segment and 25.0% of the hard segment.

Thermal transitions in the PEU powder and the fibers were studied by differential scanning calorimetry (DSC) (Figure 2c and Figure S2, Supporting Information). At starting temperature of ≈ -70 °C, we found that the polymer exhibits a glass transition at around -50 °C upon both heating and cooling. This is comparable to the thermal behavior of structurally related PEU.^[42,45,46] Powder exhibits cold crystallization at ≈ -5 °C in the first heating cycle that was not observed in the case of fibers. Both powder and fibers have a melting peak at ≈ 45 °C, which is due to the melting of soft domains.^[47] The fibers show a second melting peak during the first heating with a maximum at ≈ 50 – 55 °C that could be attributed to the melting of ordered domains. The fibers and powder polymer start to crystallize upon cooling at ≈ 5 °C. In the second heating cycle, both fibers and powder show identical behavior. The crystallinity degree of the obtained copolymer is very low: 19.3% and 17.7% in powder and fibers, respectively

(Table 1). Thus, a similar trend was observed as recently verified for re-extruded PBA-based TPU, namely that the reprocessed polymer exhibits a slightly lower crystalline content.^[46]

Meanwhile, PBA diol, which was used as a reference, showed two melting transition temperatures at 30.0 and 53.0 °C during the second heating with a total enthalpy of fusion of 74.0 J g⁻¹ corresponding to a crystallinity percentage of 55.0%. The DSC of the copolymer showed a single melting endothermic signal observed between 40 and 50 °C. The introduction of PBA chains in the segmented PEU was accompanied by a restriction of chain movements, thus reducing the affinity of PBA to crystallize (Figure S3 and Table S2, Supporting Information).

2.2. Mechanical Properties

Next, the mechanical properties of the TPU-PBA 25 were characterized using dynamic mechanical analysis (DMA) (Figure 3a) and cyclic tensile testing at room temperature and cell culture temperature (37 °C) (Figure 3b). It was found that the storage modulus of the copolymer in film and fibers in the measured range (from 0.1 to 10 Hz) is almost independent of frequency. Humidity at 20 °C slightly decreases the elastic modulus of the films from 17 to ≈ 10 MPa. An increment in the temperature from room temperature to 37 °C causes a dramatic decrease of the modulus of films from 17.2 to 2.7 MPa. Fibers are much softer than films at room temperature—elastic modulus of

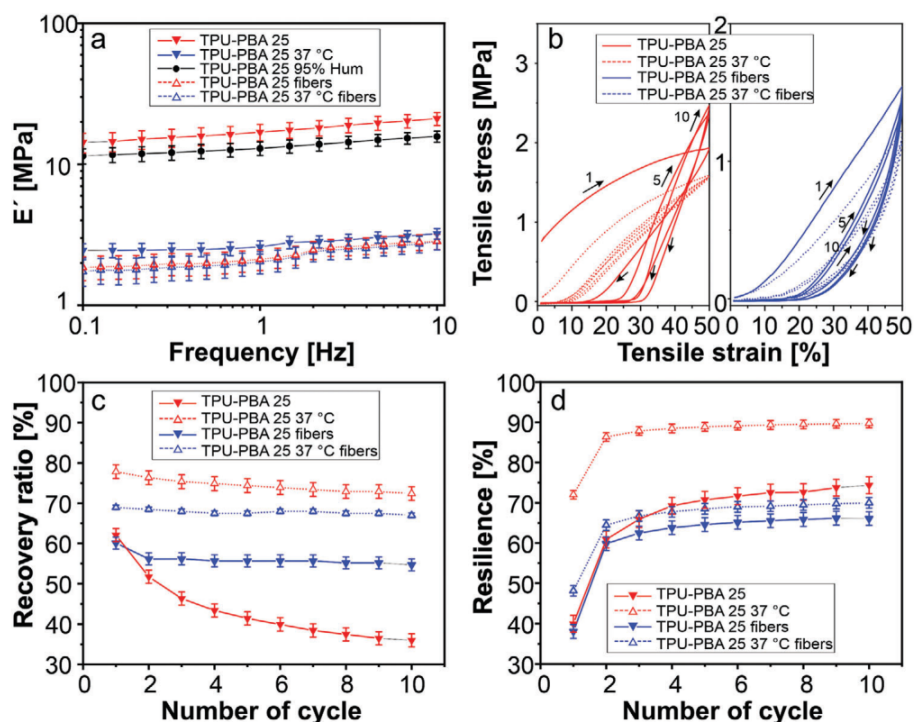


Figure 3. Mechanical properties of TPU-PBA 25. a) DMA frequency sweep, b) representative tensile test curves (cycles 1, 5, and 10 are shown), c) film and fibers recovery ratio, and d) resilience.

Table 2. Summary of mechanical properties from stress–strain cycles of TPU-PBA 25.

Polymer	E'	E'	E'	E'
	[DMA] [MPa]	(cycle 1) [MPa]	(cycle 5) [MPa]	(cycle 10) [MPa]
TPU-PBA 25	17.2	14.7	12.4	11.1
TPU-PBA 25 37 °C	2.7	3.9	2.5	2.3
TPU-PBA 25 95% Hum	13.3	Was not measured		
TPU-PBA 25 fibers	2.3	1.4	1.1	0.8
TPU-PBA 25 fibers 37 °C	2.2	1.0	0.5	0.3

fiber is ≈ 2.3 MPa, and it almost does not change upon heating (Table 2). As the fibers of the copolymer are very soft, the measurement of its modulus at 95% humidity was technically impossible (Figure 3b).^[49,50]

A cyclic tensile test was performed to investigate the mechanical properties in dynamic loading–unloading circumstances to evaluate the deformation reversibility of the polymer at a larger amplitude of deformation. Films and touch-spun fibers of TPU-PBA 25 were cyclically stretched to up to 50% and allowed to relax to their initial length (Figure 3b and Figure S4, Supporting Information) while recording stress. It was found that the stress–strain behavior is nearly linear in the first stretching cycle at small deformation. From the subsequent cycles in films at 20 °C, the stress–strain curves have a J-like shape showing a partial reversible deformation; when the temperature increases, this

J-like shape is shifted to lower strains, increasing the recovery ratio (Figure 3c). In the case of second and further cycles from fibers at both temperatures, this J-like shape was not observed, showing an increase in the recovery ratio at 37 °C; meaning that the TPU-PBA 25 block copolymer has the ability to recover to its initial shape partially after releasing the applied force. Thus, after the first cycle, the film of the polymer partially underwent plastic and irreversible deformation, which is clear from the character of decrease of the recovery ratio in comparison to the first cycle. In the case of fibers, for which cycles were performed at 37 °C, the recovery ratio is higher and does not show any dramatic decrease, meaning that a plastic deformation is considerably lower than in the previous case. The polymer film at 37 °C can recover over 75% of its length with respect to the initial state. The recovery ratio of the fibers increases from $\approx 55\%$ to 70% upon heating to 37 °C which is due to the significant softening of the polymer.

Resilience, which is a measure of a material's ability to deform reversibly without energy loss,^[51] increases during the strain–stress cycling and with an increment of temperature. The resilience was evaluated for TPU-PBA 25 in films and fibers (Figure 3d). As it can be seen, all the tested samples lost the majority of the energy during the first cycle. In subsequent cycles, the energy loss decrease indicated by the resilience increase. The reason for the increment in the resilience during cycling can be explained as follows: during first stretching entanglement decoupling occurs. This may be associated with the reorientation and breaking of molecular chains, same as hardening effects associated with crystallization processes. As a matter of fact, the polymer assumes a new state of equilibrium, which does not change

significantly after the second deformation.^[52,53] Consequently, if the TPU-PBA 25 is used after several mechanical training cycles, we can presume constant deformation properties under cyclic loading–unloading deformation conditions.^[54] It is in particular the PBA segment, which provides the elastic behavior to the PEU as long as it is in an amorphous state. Beyond reversibility of deformation after first stretching, a J-shaped stress/strain curve was witnessed. This observation is important, since it allows for mimicking mechanical properties of natural tissues.

We compared the mechanical properties of touch-spun fibers obtained in this contribution with previously reported PCL2000-HDI-BD 1:2:1 (Figure S5, Supporting Information). The main difference between PCL and PBA-based copolymers is the character of stress–strain curves obtained in the cycling stretching experiment (Figure S5a, Supporting Information). The character of recovery of stretched PCL-based copolymer is independent of temperature. In turn, PBA-based copolymer shows different ways to recover at 37 °C in both fibers and films, meaning an increment in the elastomer character of the material. During the first stretching, films and fibers of both materials at room temperature show a nonrecoverable deformation, and the recovery ratio decreases in subsequent cycles in the range of 5–20% evident in the decreasing behavior of the recovery ratio graphs during the first cycles, behavior that is not dramatic or not evidenced when the temperature increases (Figure S5b, Supporting Information). Nevertheless, fibers of PCL-based copolymer show a higher recovery ratio at 37 °C— $\approx 85\%$. By contrast, fibers of PBA-based copolymer have a recovery ratio of $\approx 70\%$ at the same conditions. The higher recovery ratio of the PBA-based copolymer is observed in the films at the 37 °C, and corresponds to $\approx 80\%$. The resilience of both polymers is close to each other with the exception of the fibers of TPU-PBA 25 on fibers at 37 °C that shows a resilience around 25% higher (Figure S5c, Supporting Information). This experiment clearly shows the advantage of PBA over PCL-based copolymer, which, as we showed in the previous study, has several advantages over commonly used thermoplastic polymers such as PCL.^[14]

2.3. Fiber Properties

In this study, scaffolds made by aligned fibrous were prepared by touch spinning *N,N*-dimethylformamide (DMF)-acetone polymer solutions. In order to optimize the touch-spinning parameters, three different concentrations were tested at three different rotational speeds at three different pressures. Uniform blob-free fibers were obtained from the three tested speeds (Figure 4a–c). The fiber orientation and diameter were evaluated by testing ten samples from each parameter (Figure 4d–i). It was found that the alignment of the fibers is directly affected by the pneumatic pressure applied to extrude the solutions. The increase in amplitude of the Gaussian distribution (decrease of alignment) is directly proportional to the pressure (Figure S6, Supporting Information); the same effect was evidenced by the increment in the concentration. Speed of rotation may have twofold effect: 1) increase of the speed results in small reduction in the fiber diameter and 2) bars hit the drop forming a spray producing lower number of fibers at the high concentration of polymer. The dis-

tribution of the fiber alignment and diameter is directly affected by the bridges formed between the fibers during the processing (Figures S7 and S8, Supporting Information). After the complete analysis of the results in terms of fibers diameter and alignment, we determine that touch-spun fibers produced from the solution with low concentration (10%), high speed (1800 RPM), and low pressure (0.13 bar) show a high alignment of fibers with the smallest diameter. These fibers were chosen for further experiments and can be representative ECM for skeletal muscle tissue.

PBA is an aliphatic polyester and is a biodegradable polymer.^[54] These copolymers are expected to be biodegradable, and degradation must be provided by hydrolysis of ester groups.^[43,55–57] In order to prove this, we tested the real-time degradation of touch-spun fibers of TPU-PBA 25 in PBS. In this study, the hydrolytic degradation of the fibers was done by immersion in 3× PBS incubated for up to 4 weeks at 37 °C. It was found that the polymer losses about 7% in mass at week 4 (Figure 5b).^[58] As it is revealed by scanning electron microscopy (SEM) (Figure 5a), the surface on the fibers becomes smoother after three weeks of degradation. We have also studied the change of surface charges by zeta potential of the copolymer upon its degradation (Figure 5c). For this, we performed measurements on touch spun fibers of the copolymer before and after the degradation in the PBS. The pH dependence of the fibers looks nearly similar for the fibers before and after degradation. The curves show a strong change of zeta potential in the range from pH 3 to pH 7 and plateau values with high zeta potentials around -50 mV at alkaline pH. The isoelectric point of the control sample is around pH 3.3. This is slightly acidic. For the degraded fibers, this value is shifted toward 3.8 with minor higher absolute values in the acidic plateau region. This could be an indication of a change in surface chemistry, for example, less functional groups and more hydrophobicity. This change can be explained by a decrease in the surface density of the carboxyl groups, which is due to the hydrolysis and elimination of PBA fragments^[58]—it is expected that the aromatic urethane parts with linked diol shall stay nondegraded.^[26] It was not observed that degraded polymer fibers change their shape upon exposure to liquid stream during zeta potential measurements (Figure 5d). Thus, these studies confirmed our expectation about biodegradability of PBA-PU block copolymer.

2.4. Cytotoxicity

Next, we have performed in vitro cytotoxicity tests based on the ISO 10993-5:2009 using two cell lines, fibroblasts and myoblasts. Indirect contact tests such as extract tests (Figure 6) and agar test (Figure S9, Supporting Information), allow analyzing the interaction of any leachable subproducts or dissolved polymer fragments with the cell monolayer without direct contact with the material. We observed normal morphology of both cell types after being incubated with TPU-PBA 25 fibrous scaffolds while they had a layer of agarose as an interface (Figure S9, Supporting Information). Their morphology had no significant difference compared to the negative control (high-density polyethylene film [HDPE]) and blank (cells cultured in a tissue culture plate with-

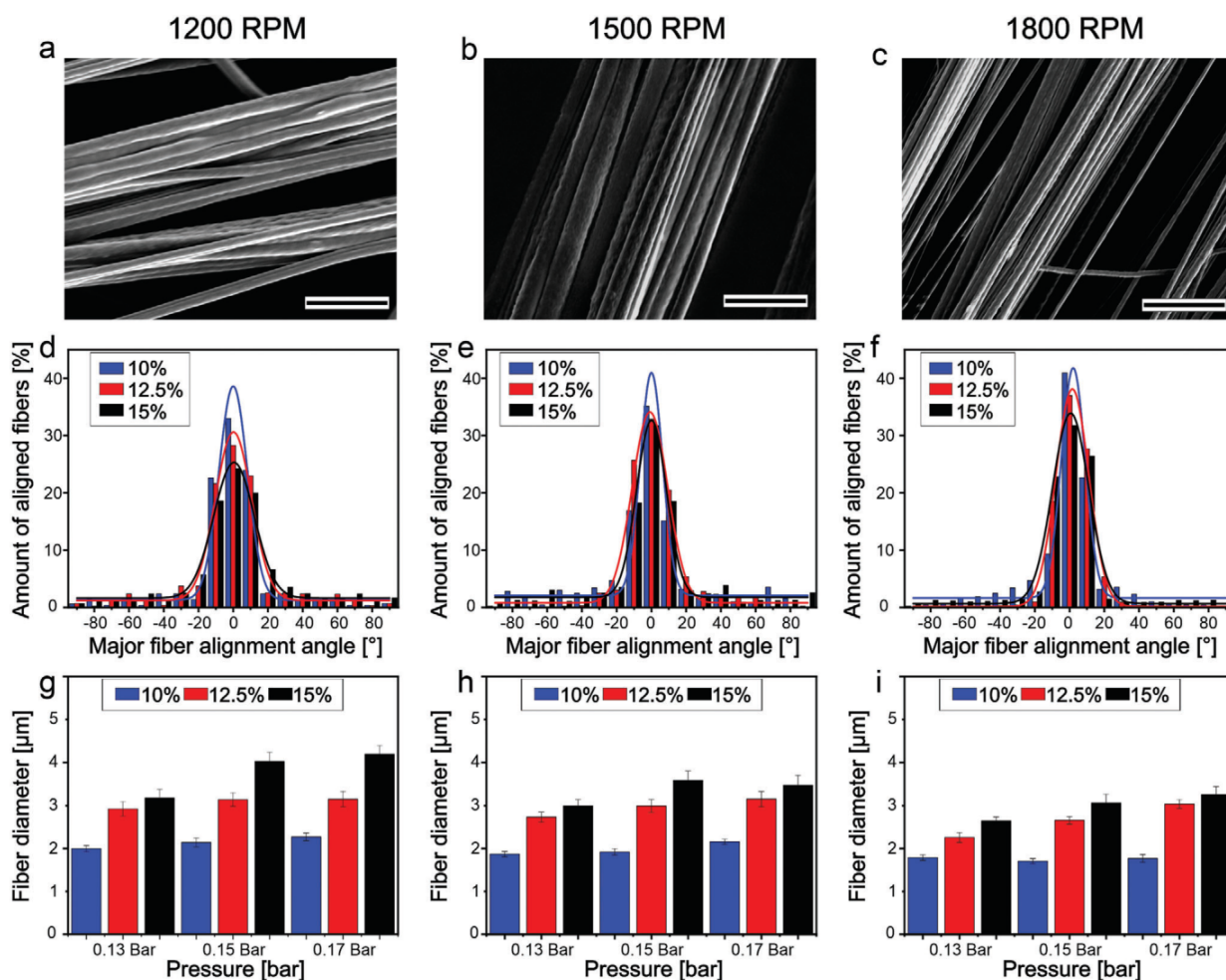


Figure 4. TPU-PBA 25 fibers properties, a–c) SEM pictures of touch-spun fibers at different RPM. d–f) Major angle fiber alignment from different concentrations at 0.13 bar. g–i) Diameter of fibers from different concentrations at different pressures. Scale bars = 10 µm.

out any contact with materials), while the positive control clearly caused changes in the morphology of both cell lines from adherent and spread cells to the round shape and detached cells. Cells exposed to the zinc-diethylthiocarbamate (ZDEC), the positive control, were less spread compared to the cells in the negative and blank control. Moreover, most of the cells were detached, a sign of necrotic cells. Thus, the polymer is biocompatible.

Further, cells after 24 h contact with the extract of materials and controls were analyzed by using Alamar blue, live/dead staining, and fluorescent imaging. These tests also showed intact and normal cell morphology after being exposed to the extracts of the TPU-PBA 25 fibrous scaffolds, negative, and blank control; while, cells in contact with the extract of positive control (ZDEC) did not survive, and no image could be taken from the dead cells as they were washed away during the staining. Quantitative analysis of CellTiter-Blue assay and live/dead assay (Figure 6d,h) confirmed high viability percentage of cells (nearly 100%) for TPU-PBA 25 fibrous scaffolds.

2.5. Cell Proliferation and Alignment

Finally, we performed cell culture studies on the TPU-PBA 25 fibrous scaffold with a fiber diameter 1.7 µm and 81.0% of alignment. For this, proliferation, cell viability, and nuclei alignment were quantified on scaffold with initial cell density of 150.000 cells cm⁻². The results showed that after 7 days of culture, only a few cells adhered to the fibers. In order to improve and compare cell adhesion, the scaffolds were treated with FNC (fibronectin mixture). The metabolic activity and viability of the cells were studied on coated, noncoated scaffolds and treated cell culture plates (Figure S10, Supporting Information). It is clear from the results that the cell's metabolic activity and viability are high in the cell culture plates and increase with time. On the other hand, the nontreated scaffolds present the lowest metabolic activity and viability but are not significantly different from the coated ones. The major difference between the scaffolds is the number of cells attached to the surface, being higher

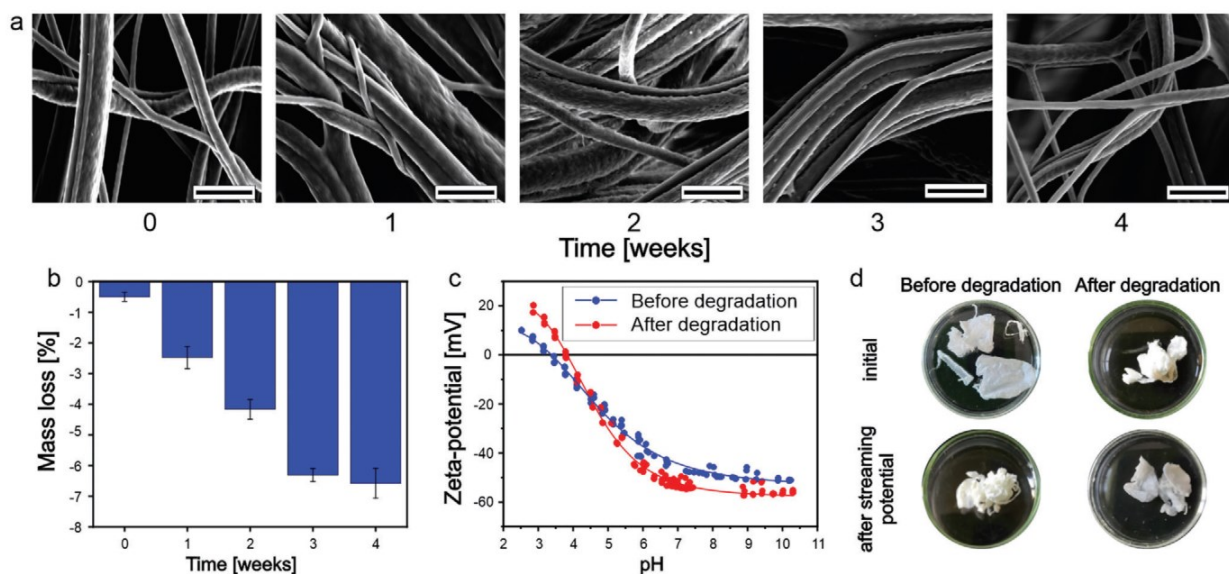


Figure 5. Degradation test of TPU-PBA 25: a) Morphology of touch spun fibers after 0, 1, 2, 3, and 4 weeks immersed in PBS solution at 37 °C. b) Mass loss of touch spun fibers during 4 weeks of degradation. c) Zeta potential of TPU-PBA 25 fibers before and after degradation test. d) Images of fiber bundles before and after degradation test and, before and after exposure to a liquid stream of zeta potential measurements. Scale bars = 10 μ m

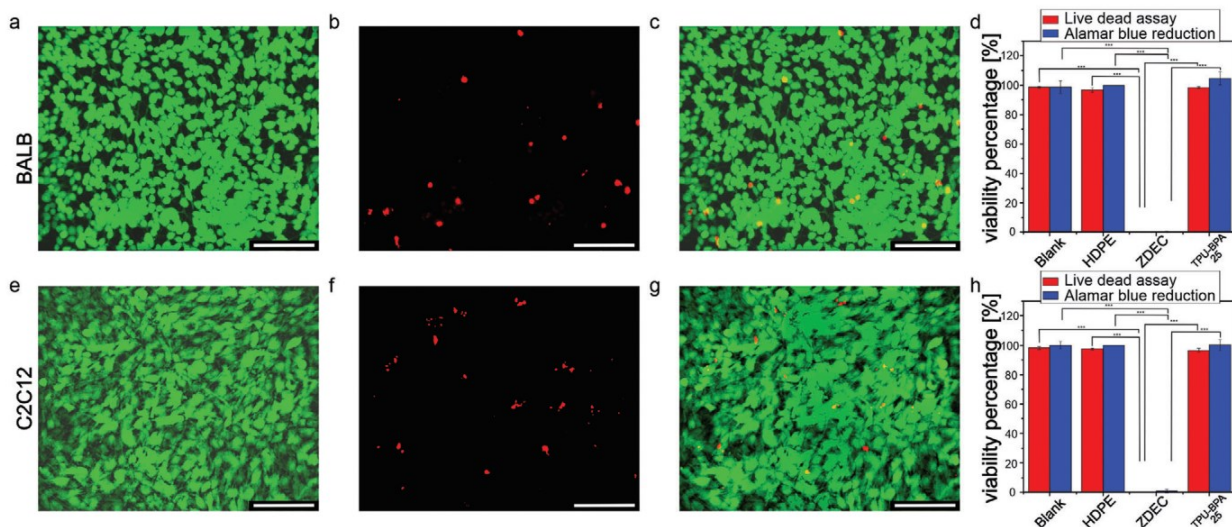


Figure 6. Qualitative and quantitative analysis of the cytotoxicity of the TPU-PBA 25 fibrous scaffold on fibroblasts and muscle cells. a–c) Fluorescent images of fibroblasts and e–g) myoblasts, taken after 24 h exposure to extract of TPU-PBA 25 fibrous scaffolds. Live/dead assay shows green (live) cells stained with calcein AM, and red (dead) cells stained with ethidium homodimer. Quantitative measurement of cell viability using CellTiter-Blue cell viability assay and live/dead assay for d) fibroblasts and h) myoblasts. Blank (cells with no contact to materials), HDPE (negative control), and ZDEC (positive control). Data are presented as the mean \pm standard deviation; *** p value \leq 0.001. Scale bar = 150 μ m.

on the scaffolds coated with FNC. Moreover, seeded cells distributed and adhered uniformly on the top of the fibrous scaffold (Figure 7a–d). Additionally, cells begin to align along and on the top the fibers. Interestingly, in concordance with our previous work,^[14] it was found that cells proliferate and reaches 86% of viability after 7 days in culture that is lower than that measured in our previous PCL-based polyurethanes fibers produced

by touch spinning^[14] but higher than our previous studies on scaffolds produced by melt electrowriting.^[26] Cell proliferation is also faster on the coated scaffolds than noncoated ones (Figure 7e).

Cell alignment on TPU-PBA 25 fiber scaffold, coated and non-coated with FNC, was quantified after staining cell nuclei and the actin filament. Staining experiments verified the tendency of

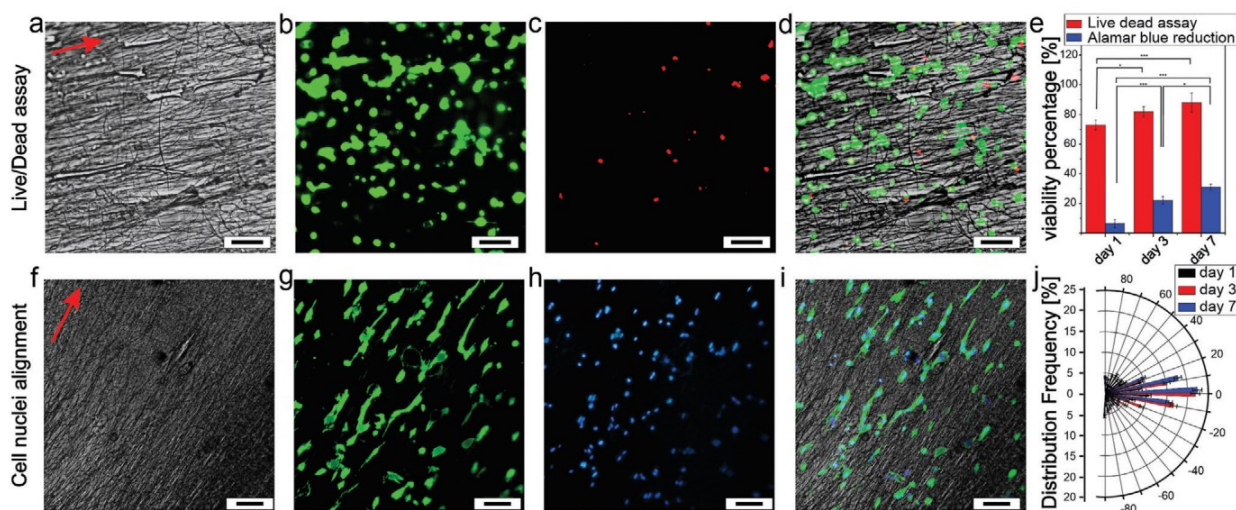


Figure 7. C2C12 myoblasts cell culture. a–d) Live/Dead assay on TPU-PBA fiber scaffolds. Green—live cells and red—dead cells; at day 7 of culture. e) Quantification of cell viability and cell metabolic activity after 1, 3, and 7 days of culture measured by Alamar Blue assay. f–i) Cell nuclei alignment on TPU-PBA fiber scaffolds at day 7 of culture. j) Quantification analysis of cell nuclei alignment. * $p \leq 0.05$; ** $p \leq 0.01$; *** $p \leq 0.001$. Scale bars = 100 μm .

the cells to grow in the direction of the fibers and on top of the scaffold (Figure 7f–i and Figure S11, Supporting Information). It was found that the nuclei cell alignment increases with time during cell incubation: on day 1 $\approx 25\%$ of cells are aligned, on day 4 $\approx 50\%$ of cells are aligned, and after 7 days in culture $\approx 56\%$ of cells are aligned, showing statistically significant ($p \leq 0.001$) between all the time points for the cells cultured on coated scaffolds. On the other hand, the noncoated scaffolds show similar results in terms of percentage of alignment, 25%, 40%, and 51% for days 1, 4, and 7, respectively. Even though there are no major differences between the alignment on the coated and noncoated scaffolds, the number of cells attached to the scaffolds coated with FNC is three times higher than that on noncoated scaffolds. It must be noted that if the angle formed by the cells with the main orientation of the fibers was in the range of -10° and 10° , the cells were considered aligned. Notably, cell alignment is not that high as the alignment of fibers (Figure 7j). This deviation can be explained by distance between fibers allowing the cells to form bridges in the gaps between the fibers them and change the orientation. The cell alignment improved after 7 days of culture due to the fact that cells prefer to grow following the directionality of the fibers and in the spaces in between them, instead of forming bridges between two or more fibers (Figure 7j). Also, they prefer to elongate along the fibers to form connections with other cells.

3. Conclusion

In this work, we report an approach for the fabrication of highly aligned microfibrillar scaffold. Therefore, a new thermoplastic polyurethane elastomer with soft segments made from PBA was synthesized and touch spinning technique was used to prove the suitability of the copolymer for muscle tissue engineering. In this regard, a promising combination of mechanical and thermal properties could be verified at human body temperature as evidenced by highly reliable elastomeric properties after the first loading–unloading cycle. The reported polymer demon-

strates superior mechanical properties compared with PCL-based polyurethanes previously reported, and is characterized by an excellent biocompatibility that enables its use for fabrication of fibrous scaffolds allowing high cell alignment required for regeneration of such anisotropic tissues as muscle tissue.

4. Experimental Section

Materials: MDI (Fisher Scientific), 1,4-butanediol (BD, Alfa Aesar), molecular sieves (pore size of 4 Å, Alfa Aesar), Desmophen 2505 (hydroxyl-terminated PBA-diol [$M_n = 4000 \text{ g mol}^{-1}$, Covestro Deutschland AG]), DMSO (Sigma-Aldrich), DMF (Sigma-Aldrich), acetone (Sigma-Aldrich), ethylenediaminetetraacetic acid (EDTA, Sigma-Aldrich), calcium chloride dehydrate (Sigma-Aldrich), Dulbecco's phosphate buffered saline (DPBS, Sigma-Aldrich), Dulbecco's Modified Eagle Medium (DMEM, Merck), penicillin–streptomycin (Pen/Strep, Gibco), gentamycin sulfate (Sigma-Aldrich), fetal bovine serum (FBS, Merck), FBS Gold Plus (Serena), GlutaMAX (Gibco), 4-(2-hydroxyethyl)-1-piperazineethanesulfonic acid (HEPES, Carl Roth), Trypsin/EDTA (0.05%, Sigma-Aldrich), Trypan-Blue reagent 0.4% (Sigma-Aldrich), calcein-AM (Thermo Fisher Scientific), ethidium EthD-1 (Thermo Fisher Scientific), phalloidin DyLight 488 (Thermo Fisher Scientific), 4',6-diamidino-2-phenylindole (DAPI, Thermo Fisher Scientific), Alamar Blue HS Cell Viability Reagent (live/dead assay) (Thermo Fisher Scientific), FNC solution (fibronectin, collagen, albumin mixture, Athena Enzyme Systems), and triton X-100 (Sigma-Aldrich) were used as received. The C2C12 myoblast (passage number less than 7) was purchased from ATCC (Manassas, VA). M-MSV-BALB/3T3 fibroblasts were purchased from the European Collection of Authenticated Cell Cultures (Public Health England). Agarose NEEO ultra quality was purchased from Roth. HDPE (Hatano Research Institute) and polyurethane film containing ZDEC (Hatano Research Institute) were used as negative and positive controls in ISO Standard tests 10993-5.

Synthesis of TPU-PBA 25: The prepolymer method was applied to synthesize a PBA-based PEU (Scheme 1). Therefore, 0.037 mol of PBA-diol was melted and dried in a vacuum oven at 80°C overnight. At the beginning of the synthesis, the PBA-diol was heated to 120°C under nitrogen flow and stirring. Afterward, 0.157 mol of molten MDI was added. After 90 min of continuous stirring, the isocyanate-encapped prepolymer was converted to PEU by adding 0.120 mol of BD. At the same time, the stirring speed was increased, and changes in viscosity were followed with an IKA

Eurostar 60 control from IKA-Werke GmbH & Co. KG (Staufen, Germany). As soon as the melt viscosity increased significantly, corresponding to a rise in torque by a factor of five, the polymer melt was poured onto a plate, which was covered with polytetrafluoroethylene. Finally, the obtained PEU was cured for 120 min in a convection oven at 80 °C, before it was ground to granules.

Nuclear Magnetic Resonance Spectroscopy: The NMR spectra of TPU-PBA 25 were obtained using a Bruker Avance 500 spectrometer (Bruker BioSpin GmbH, Silberstreifen, Germany) (500.16 MHz for ¹H). ¹H NMR chemical shifts (δ) were reported in parts per million (ppm) relative to tetramethyl silane, with the residual solvent peak used as an internal reference using DMSO-d₆, 500 MHz, DMSO-d₆, δ = 9.32 (s, 2H), 7.34 (d, J = 8.0 Hz, 6H), 7.07 (d, J = 8.4 Hz, 6H), 4.10 (s, 4H), 4.03 (s, 26H), 3.79 (s, 3H), 3.13 (s, 3H), 2.28 (s, 28H), 1.71 (s, 4H), 1.66 (s, 3H), 1.62 (s, 26H), 1.55 (s, 28H).

Fourier Transform Infrared Spectroscopy: FTIR spectra were measured in transmittance mode using a Bruker Tensor 27 (USA) spectrometer with spectral data spacing of 4 cm⁻¹ from 400 to 4000 cm⁻¹. The main bands in these spectra were stretching vibrations of NH groups in the 3500 to 3000 cm⁻¹ range; the symmetric and asymmetric stretching vibrations of -CH₂ groups (ν = 2950 and 2820 cm⁻¹). The characteristic stretching vibration of carbonyl group C=O (ν = 1728 cm⁻¹) and C-N stretching (ν = 1531 cm⁻¹) confirmed the presence of urethane groups; also, the absence of distinct signal at 2280 cm⁻¹ associated with the presence of freely available isocyanate. The stretching vibration of the C-O-C bond (ν = 1596 cm⁻¹) and the stretching bands from the C-O bond of the ester group (ν = 1220 and 1165 cm⁻¹) corresponded to the PBA part of the copolymer.

Gel Permeation Chromatography: Gel permeation chromatography was used to determine the molecular weight (number average molecular weight [Mn], weight average molecular weight [Mw]) and PDI using an instrument with 2 PSS-GRAM gel columns (particle size = 10 μ m) with porosity range from 100 to 3000 Å (PSS, Mainz, Germany) together with a refractive index detector (Agilent Technologies). DMF (HPLC grade) with lithium bromide (5 g L⁻¹) was used as a solvent (for dissolving polymer and as eluting solvent) with a flow rate of 0.5 mL min⁻¹, toluene (HPLC grade) was used as an internal standard. The calibration was done with narrowly distributed polystyrene (homopolymers, PSS calibration kit). An injection volume of 100 μ L was used for all the measurements. The samples were dissolved in DMF and filtered through a 0.22 μ m PTFE filter before analysis.

Differential Scanning Calorimetry: The thermal behavior of the copolymer was investigated using DSC (DSC3, Mettler Toledo, USA). DSC measurements were performed by loading 5–7 mg of the polymers in a closed aluminum crucible. Three different scans were performed. In the first one, the sample was scanned in three steps: 1) heating from -70 to 200 °C to eliminate any thermal history, keeping at 200 °C for 5 min, 2) cooling down to -70 °C and keeping at -70 °C for 5 min, 3) heating to 200 °C with temperature rates of 10 °C min⁻¹. The second one: 1) heating from -70 to 70 °C and keeping at 70 °C for 5 min, 2) cooling down to -70 °C, keeping at -70 °C for 5 min, and 3) heating to 70 °C with a temperature rate of 10 °C min⁻¹. The third one: 1) heating from 20 to 200 °C and keeping at 200 °C for 10 min, 2) cooling down to 20 °C, keeping at 20 °C for 10 min, and 3) heating to 200 °C again with a temperature rate of 1 °C min⁻¹.

Thermogravimetric Analysis and Degradation Test: TGA (TGA 2 STAR System, Mettler Toledo [USA]) was performed from 30 to 550 °C at a heating rate of 10 °C min⁻¹ under a nitrogen atmosphere. A real-time degradation test of the TPU-PBA 25 fibers was also performed by testing at various time points such as 1, 2, 3, and 4 weeks in PBS solution at 37 °C. PBS was changed every 3 days to ensure a constant pH during all degradation. Samples were weighted after freeze-drying and characterized by SEM at each time point. Three samples of each time point were tested.

Mechanical Testing: Thin-film of TPU-PBA 25 was cast on a glass slide from 25 wt% solutions in DMF at room temperature. After the film was air-dried at room temperature for 48 h, it was manually removed and placed into a vacuum desiccator for 3 days to ensure complete evaporation of the solvent. Rectangular strips (\approx 10 \times 4 \times 0.4 mm) and fiber scaffolds (\approx 10 \times 2 \times 0.1 mm) were prepared for mechanical tests. Tensile tests were

performed on a DMA (MCR 702 MultiDrive Anton Paar, Austria) equipped with Solid Rectangular Fixtures (SRF5) and a temperature chamber (CTD 600 TDR). During the measurement, static (120 kPa) and dynamic forces (120 kPa) were applied, within a frequency range from 10 to 0.1 Hz, to characterize the elastic properties of the material in extension-deformation mode. The measurements were performed at 20 and 37 °C for fibers and films, separately; the films alone were measured in a humidity controller chamber at 5% and 95% relative humidity.

Cyclic tensile tests of films and fibers were performed using the same configuration of DMA to investigate the sustainability of the copolymer. The samples were loaded and prestretched until a force lecture around 0 N was achieved, then stretched at 1% min⁻¹ to 50% strain and released at 1% min⁻¹ until initial length for 10 consecutive cycles; the samples were tested at 20 and 37 °C. From the recorded tensile strain-stress data, the percentage recovery ratio (R_r) of each cycle was calculated using Equation (2),

$$\%R_r = \left(1 - \frac{\epsilon}{\epsilon_0}\right) \times 100 \quad (2)$$

where ϵ was the residual strain after the unloading steps and ϵ_0 was stretching amplitude, which in the authors' case was 0.5 (50%). The property of materials to absorb energy after elastic deformation was named resilience (R_e) and was calculated using Equation (3),^[43]

$$\%R_e = \left(\frac{W_{\text{unload}}}{W_{\text{load}}}\right) \times 100 \quad (3)$$

where W_{unload} represented the area under the stress-strain curve in the release step, and W_{load} represented the area under the stress-strain curve in the stretch step.

Touch Spinning: Touch spinning was performed in a custom-made touch-spinning device similar to one published by Minko.^[27] The TPU-PBA 25 was dissolved in DMF at room temperature under magnetic stirring for 6 h, and then acetone was added to obtain a ratio of 2:1 DMF:acetone (acetone must be added to enhance the solvent evaporation during processing). The solution concentrations were optimized to yield continuous bead-free fibers with the smallest possible diameters. The final concentrations were 10%, 12.5%, and 15% w/v. The prepared solutions were loaded into a plastic dispenser with an 18-gauge PTFE blunt-end needle (I.D. 0.838 mm). Touch spinning was performed with a rotating rod attached to a wheel/disc and stable-bridged collector, distances of 1.0 mm and 5.0 cm correspondingly; the separation between the parallel bars in the collector was 2.5 cm. Rotational speed applied was 1250, 1500, and 1800 rpm, and feeding air pressure was 0.13, 0.15, and 0.17 bars.

Streaming Potential Measurements: Zeta potential was determined with SurPASS 3 (Anton Paar, Graz, A) by streaming potential measurements. 50 mg of the fibers were fixed with membranes, pore size 20 μ m, in the powder sample holder. This part was inserted in the cylindrical cell equipped with Ag/AgCl electrodes. The permeability index was adjusted to around 100. The electrolyte solution was KCl, C = 10–3 mol L⁻¹. The pressure was changed in the range from 600 to 200 mbar. The measurements were initiated at neutral pH. For pH-adjustment solutions, HCl or KOH (C = 0.1 mol L⁻¹) were used. Fibers before and after real-time degradation were tested.

Scanning Electron Microscopy: SEM (Apreo, Thermo Fisher Scientific, USA) was used to characterize the morphological properties of TPU-PBA 25 fibers before and after the degradation test. Fully dried samples were coated with \approx 1.3 nm platinum to ensure electrical conductivity. The alignment in all the cases follows a Gaussian distribution by using Equation (4), described in Figure S12, Supporting Information.

$$y = y_0 + \frac{A}{w\sqrt{\pi/2}} e^{-2\frac{(x-x_0)^2}{w^2}} \quad (4)$$

Cytotoxicity Test: M-MSV-BALB/3T3 fibroblasts and C2C12 mouse myoblast cells were used to test the cytotoxicity based on ISO Standard

10993-5. Cells were cultured in a growth medium containing DMEM supplemented with 10% FBS Gold Plus, 1% GlutaMAX, 0.1% Gentamycin.

Cells were plated and grown to subconfluency prior to initiating the assays. Cells cultured without any contact with material were used as a blank control (Blank). For all assays, HDPE and ZDEC polyurethane were used as a negative (nontoxic) and positive (toxic) controls, respectively. Following the standard procedure, two indirect culturing methods (agar test and extract) were applied to evaluate whether there was a cytotoxic response to polymers. Samples were sterilized using 20 min UV under a steril bench.

For the agar test, after subconfluency of 75 000 cells/mL fibroblasts or 55 000 cells/mL myoblasts, a layer of autoclaved agarose gel with 37 °C (0.5% in DMEM) containing all supplements was cast on the top of the cell monolayer, and after 1 h of gelation, the sterilized fibrous scaffold (0.5 × 0.5 cm), as well as a same size piece of the positive and negative controls, were laid down on the gel. The materials and cells were incubated at 37 °C and 5% CO₂ for 24 h, after which the morphology changes of the cells were imaged using optical microscopy Leica DMI8 (Leica Microsystems, Germany).

Similarly, for the extract test, both cell lines were plated and grown to subconfluency 24 h before initiating the assay. The sterilized fibrous scaffold, as well as positive and negative controls, was incubated at 37 °C and 5% CO₂ with the 400 µL culture media for 24 h. After 24 h, the cell culture media was replaced with 350 µL of extract media. Cells were then incubated at 37 °C and 5% CO₂ for 24 h prior to cytotoxic evaluation. For the extract test, cytotoxicity of the material was evaluated qualitatively using fluorescence microscopy Leica DMI8 (Leica Microsystems, Germany) and quantitatively through the CellTiter-Blue Cell Viability Assay (Promega) and live/dead assay. The detail of these assays is presented in the Supporting Information.

Cell Culture: C2C12 mouse myoblast cells (with passage number less than 7) were cultured on aligned fibers made of the copolymer with a size of 4.0 cm². Before cell seeding, fibrous scaffolds were fixed in crowns (Scaffdex CellCrown inserts) with an effective internal area of 0.2 cm² and sterilized by washing them with ethanol 70% v/v for 30 min and exposing to UV light for 1 h under the clean bench. To enhance the cell adhesion on fibers, the scaffolds were coated with sterilized FNC solution for 1 h. Fibers without coating were tested as a control. Following the coating, a cell suspension with a density of 10⁶ cell mL⁻¹ was seeded on top to achieve a cell density of 150.000 cells cm⁻² and incubated for 1 h to achieve the initial attachment of the cells. The growth medium for C2C12 cells containing DMEM, FBS serum 10% v/v, Pen/Strep 1%, Glutamin 4.0 mM, and HEPES 20.0 mM was added to the samples and was refreshed every 2nd day.

Live/Dead Assay, Proliferation Rate, and Alignment: The cell viability was analyzed using a live/dead assay and following the manufacturer protocol at different time points: 1, 3, and 7 days after the culture in the growth medium. A staining solution containing green fluorescent calcein AM in DPBS to target the esterase activity within the cytoplasm of living cells and the red fluorescence Ethidium homodimer-1 (EthD-1) was used to indicate dead cells. The samples were covered with the staining solution and incubated for 30 min at room temperature before imaging. After each time point, samples were visualized under the Nikon Eclipse Ti2 fluorescence microscope attached to a DS-Qi2 digital Nikon camera and Nis-D Elements v4.550 software was used for image analysis. The viability of the cells was calculated by counting the number of live and dead cells in ten different images from three different samples.

The proliferation rate of the myoblasts cells cultured on the fibers was measured using Alamar Blue assay after 1, 3, and 7 days of culture. According to the manufacturer's protocol, 10% of reagent was added to the samples with the medium at each time point and incubated at 37 °C for 90 min and stirring gently every 30 min to avoid gradients. The reacted media from each sample was removed and kept on ice in the dark; 100 µL of that was transferred to a 96 well-plate, then its absorbance was measured using a plate reader (Berthold Tech TriStar2S, Germany) at 535 nm of excitation and 590 nm of emission wavelength. The negative control was prepared by mixing 10% Alamar blue in medium, and the positive control was prepared by mixing 10% reduced Alamar Blue in sterile MilliQ water. Three repeats were considered for each composition.

To quantify the alignment of the muscle cells on the fibers after 1, 3, and 7 days in culture, the actin filaments and nuclei were stained using a staining solution of Phalloidin DyLight 488 and DAPI in PBS to target rich regions in adenine and thymine in DNA and to label F-actin in fixed cells, respectively. First, the cell-cultured samples were fixed with formaldehyde (3.7%) solution for 15 min at room temperature. After washing with PBS, the cells were permeabilized with Triton (0.1%) solution for 5 min and washed with PBS. Next, the samples were covered and incubated with staining solution for 30 min at room temperature, followed by imaging using a fluorescence microscope. To determine cell alignment, morphological changes of nuclei were analyzed using ImageJ and orientation J plug-in in ten images from three different samples per day in culture. Nuclei orientation angles $-10^\circ > x < 10^\circ$ with respect to the fibers were considered as aligned.

Statistical Analyses: All results were treated using the software origin version 9.7 and were presented as mean ± standard deviation. All the values were averaged at least in triplicate, and statistical analyses were performed using a Student's *t*-test and one-way analysis of variance. Tukey's test was used to evaluate specific differences in values. A value of $p < 0.05$ was considered significant.

Supporting Information

Supporting Information is available from the Wiley Online Library or from the author.

Acknowledgements

This work was supported by DFG (IO 68/14-1, IO 68/17-1, SA 3575/1-1) and Fraunhofer Cluster of Excellence "Programmable Materials" under project 630507. T.P. wishes to thank the European Regional Development Fund for financing a large part of the laboratory equipment (project 85007031). The authors would further like to thank Prof. Scheibel for providing them access to SEM and Hanin Alkhamis and Samantha Bittinger for proofreading.

Conflict of Interest

The authors declare no conflict of interest.

Data Availability Statement

The data that support the findings of this study are available in the supplementary material of this article.

Keywords

biofabrication, microfibers, poly(ester-urethane), skeletal muscles, touch-spinning

Received: October 26, 2021

Revised: December 17, 2021

Published online:

- [1] M. Ochi, N. Adachi, H. Nobuto, S. Yanada, Y. Ito, M. Agung, *Artif. Organs* **2004**, 28, 28.
- [2] C. Dieckmann, R. Renner, L. Milkova, J. C. Simon, *Exp. Dermatol.* **2010**, 19, 697.

- [3] H.-H. Sun, T. Jin, Q. Yu, F.-M. Chen, *J. Tissue Eng. Regen. Med.* **2011**, 5, e1.
- [4] J. Barthes, H. Özçelik, M. Hindié, A. Ndreu-Halili, A. Hasan, N. E. Vrana, *BioMed. Res. Int.* **2014**, 2014, 18.
- [5] S. Khalil, J. Nam, W. Sun, *Rapid Prototyping J.* **2005**, 11, 9.
- [6] A. D. Theocharis, S. S. Skandalis, C. Gialeli, N. K. Karamanos, *Adv. Drug Delivery Rev.* **2016**, 97, 4.
- [7] E. Gentleman, A. N. Lay, D. A. Dickerson, E. A. Nauman, G. A. Livesay, K. C. Dee, *Biomaterials* **2003**, 24, 3805.
- [8] B. B. Aaron, J. M. Gosline, *Biopolymers* **1981**, 20, 1247.
- [9] H. S. Rapoport, J. Fish, J. Basu, J. Campbell, C. Genheimer, R. Payne, D. Jain, *Tissue Eng., Part C* **2012**, 18, 567.
- [10] S. Miao, H. Cui, M. Nowicki, S.-J. Lee, J. Almeida, X. Zhou, W. Zhu, X. Yao, F. Masood, M. W. Plesniak, M. Mohiuddin, L. G. Zhang, *Biofabrication* **2018**, 10, 035007.
- [11] M. L. Muerza-Cascante, D. Haylock, D. W. Huttmacher, P. D. Dalton, *Tissue Eng., Part B* **2015**, 21, 187.
- [12] N. T. Saidy, F. Wolf, O. Bas, H. Keijdener, D. W. Huttmacher, P. Mela, E. M. De-Juan-Pardo, *Small* **2019**, 15, 1900873.
- [13] S. Agarwal, J. H. Wendorff, A. Greiner, *Adv. Mater.* **2009**, 21, 3343.
- [14] J. Uribe-Gomez, A. Posada-Murcia, A. Shukla, H. Alkhamis, S. Salehi, L. Ionov, *ACS Appl. Bio Mater.* **2021**, 4, 5585.
- [15] J. He, B. Zhang, Z. Li, M. Mao, J. Li, K. Han, D. Li, *Biofabrication* **2020**, 12, 042002.
- [16] J. Ding, J. Zhang, J. Li, D. Li, C. Xiao, H. Xiao, H. Yang, X. Zhuang, X. Chen, *Prog. Polym. Sci.* **2019**, 90, 1.
- [17] P. Katta, M. Alessandro, R. D. Ramsier, G. G. Chase, *Nano Lett.* **2004**, 4, 2215.
- [18] P. D. Dalton, D. Klee, M. Möller, *Polymer* **2005**, 46, 611.
- [19] I. Apsite, J. M. Uribe, A. F. Posada, S. Rosenfeldt, S. Salehi, L. Ionov, *Biofabrication* **2019**, 12, 015016.
- [20] J. Groll, T. Boland, T. Blunk, J. A. Burdick, D.-W. Cho, P. D. Dalton, B. Derby, G. Forgacs, Q. Li, V. A. Mironov, L. Moroni, M. Nakamura, W. Shu, S. Takeuchi, G. Vozzi, T. B. F. Woodfield, T. Xu, J. J. Yoo, J. Malda, *Biofabrication* **2016**, 8, 013001.
- [21] P. D. Dalton, *Curr. Opin. Biomed. Eng.* **2017**, 2, 49.
- [22] T. M. Robinson, D. W. Huttmacher, P. D. Dalton, *Adv. Funct. Mater.* **2019**, 29, 1904664.
- [23] T. D. Brown, P. D. Dalton, D. W. Huttmacher, *Adv. Mater.* **2011**, 23, 5651.
- [24] F. M. Wunner, O. Bas, N. T. Saidy, P. D. Dalton, E. M. D.-J. Pardo, D. W. Huttmacher, *J. Visualized Exp.* **2017**, 130, e56289.
- [25] G. Constante, I. Apsite, H. Alkhamis, M. Dulle, M. Schwarzer, A. Caspari, A. Synytska, S. Salehi, L. Ionov, *ACS Appl. Mater. Interfaces* **2021**, 13, 12767.
- [26] J. Uribe-Gomez, A. Posada-Murcia, A. Shukla, M. Ergin, G. Constante, I. Apsite, D. Martin, M. Schwarzer, A. Caspari, A. Synytska, S. Salehi, L. Ionov, *ACS Appl. Bio Mater.* **2021**, 4, 1720.
- [27] A. Tokarev, D. Asheghali, I. M. Griffiths, O. Trotsenko, A. Gruz, X. Lin, H. A. Stone, S. Minko, *Adv. Mater.* **2015**, 27, 6526.
- [28] S.-J. Lee, D. Asheghali, B. Blevins, R. Timsina, T. Esworthy, X. Zhou, H. Cui, S. Y. Hann, X. Qiu, A. Tokarev, S. Minko, L. G. Zhang, *ACS Appl. Mater. Interfaces* **2019**, 12, 2067.
- [29] D. Asheghali, S.-J. Lee, A. Furchner, A. Gruz, S. Larson, A. Tokarev, S. Stake, X. Zhou, K. Hinrichs, L. G. Zhang, S. Minko, *Nanomedicine* **2020**, 24, 102152.
- [30] C. Mueller, M. Trujillo-Miranda, M. Maier, D. E. Heath, A. J. O'connor, S. Salehi, *Adv. Mater. Interfaces* **2021**, 8, 2001167.
- [31] R. J. Spontak, N. P. Patel, *Curr. Opin. Colloid Interface Sci.* **2000**, 5, 333.
- [32] J. Chen, R. Dong, J. Ge, B. Guo, P. X. Ma, *ACS Appl. Mater. Interfaces* **2015**, 7, 28273.
- [33] Y. Hong, J. Guan, K. L. Fujimoto, R. Hashizume, A. L. Pelinescu, W. R. Wagner, *Biomaterials* **2010**, 31, 4249.
- [34] E. Ergene, B. S. Yagci, S. Gokyer, A. Eyidogan, E. A. Aksoy, P. Y. Huri, *Biomed. Mater.* **2019**, 14, 025014.
- [35] P. Kasprzyk, E. Sadowska, J. Datta, *J. Polym. Environ.* **2019**, 27, 2588.
- [36] S. G. Kim, D. S. Lee, *Macromol. Res.* **2002**, 10, 365.
- [37] I. Yilgör, E. Yilgör, G. L. Wilkes, *Polymer* **2015**, 58, A1.
- [38] D. Schönfeld, D. Chalissery, F. Wenz, M. Specht, C. Eberl, T. Pretsch, *Molecules* **2021**, 26, 522.
- [39] T. Pretsch, I. Jakob, W. Müller, *Polym. Degrad. Stab.* **2009**, 94, 61.
- [40] T. Pretsch, W. W. Müller, *Polym. Degrad. Stab.* **2010**, 95, 880.
- [41] M. Bothe, T. Pretsch, *J. Mater. Chem. A* **2013**, 1, 14491.
- [42] N. Fritzsche, T. Pretsch, *Macromolecules* **2014**, 47, 5952.
- [43] M. Hao-Yang, *J. Mater. Chem. B* **2017**, 5, 4137.
- [44] P. K. Behera, P. Mondal, N. K. Singha, *Polym. Chem.* **2018**, 9, 4205.
- [45] N. Mirtschin, T. Pretsch, *Polymers* **2017**, 9, 98.
- [46] D. Chalissery, T. Pretsch, S. Staub, H. Andrä, *Polymers* **2019**, 11, 1005.
- [47] M. Rogulska, A. Kultys, S. Pikus, *J. Therm. Anal. Calorim.* **2017**, 127, 2325.
- [48] C. Q. Huang, S. Y. Luo, S. Y. Xu, J. B. Zhao, S. L. Jiang, W. T. Yang, *J. Appl. Polym. Sci.* **2010**, 115, 1555.
- [49] D. S. Huh, S. L. Cooper, *Polym. Eng. Sci.* **1971**, 11, 369.
- [50] D. J. Martin, G. F. Meijjs, G. M. Renwick, S. J. Mccarthy, P. A. Gunatillake, *J. Appl. Polym. Sci.* **1996**, 62, 1377.
- [51] J. Gosline, M. Lillie, E. Carrington, P. Guerette, C. Ortlepp, K. Savage, *Philos. Trans. R. Soc., B* **2002**, 357, 121.
- [52] H. Tobushi, H. Hara, E. Yamada, S. Hayashi, *Smart Mater. Struct.* **1996**, 5, 483.
- [53] S. Mondal, H. J. Lian, *Iranian Pol. J.* **2006**, 15, 135.
- [54] A. Lindström, A.-C. Albertsson, M. Hakkarainen, *Polym. Degrad. Stab.* **2004**, 83, 487.
- [55] A. K. Blakney, F. I. Simonovsky, I. T. Suydam, B. D. Ratner, K. A. Woodrow, *ACS Biomater. Sci. Eng.* **2016**, 2, 1595.
- [56] R. Scaffaro, A. Maio, F. Suter, E. Gulino, M. Morreale, *Polymers* **2019**, 11, 651.
- [57] Y. Fu, G. Wu, X. Bian, J. Zeng, Y. Weng, *Molecules* **2020**, 25, 3946.
- [58] R. Al-Itry, K. Lamnawar, A. Maazouz, *Polym. Degrad. Stab.* **2012**, 97, 1898.

Supporting Information

Fibrous scaffolds for muscle tissue engineering based on touch-spun poly(ester-urethane) elastomer

*Juan Uribe-Gomez, Dennis Schönfeld, Andrés Posada-Murcia, Michel-Manuel Roland, Anja Caspari, Alla Synytska, Sahar Salehi, Thorsten Pretsch and Leonid Ionov**

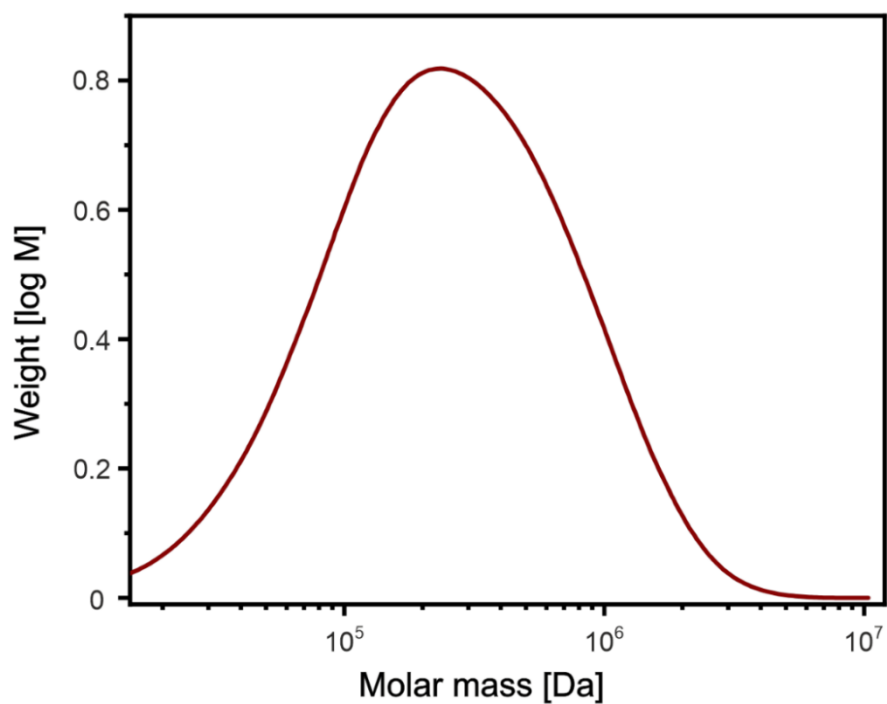


Figure S1. GPC profile of TPU-PBA 25.

Table S1. Mw, Mn, and PDI results from GPC measurements using DMF as the solvent. The unit of molecular weight is g mol⁻¹.

Polymer	Mn ($\times 10^5$)	Mw ($\times 10^5$)	Mz ($\times 10^5$)	PDI
TPU-PBA 25	1.44	4.18	9.93	2.91

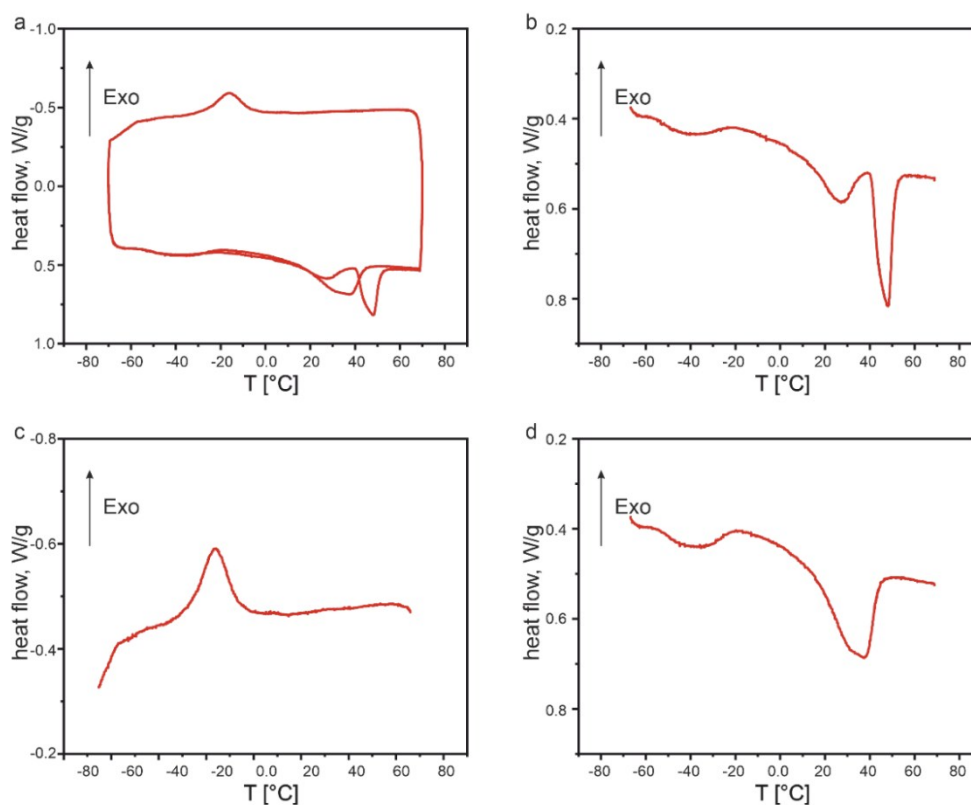


Figure S2. a-d Thermal properties 10°C/min from -70 to 70 °C: a) DSC full scanning; b) first heating; c) first cooling; d) second heating.

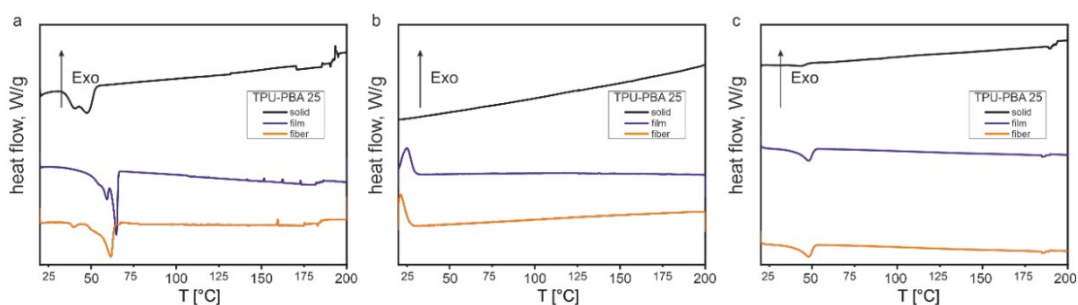


Figure S3. DSC scan of TPU PBA 25 in solid, film and fibers at 1°C/min from 20 to 200 °C: a) first heating; b) first cooling; c) second heating.

Table S2. DSC thermal properties of TPU PBA 25 in solid, film and fibers from 20 to 200 °C at 1 °C/min

TPU PBA	T_m [°C]	Total ΔH [J g ⁻¹]	X_c^b [%]
---------	------------	---------------------------------------	-------------

25						
	1 st	2 nd	1 st	2 nd	1 st	2 nd
	heating	heating	heating	heating	heating	heating
Solid	40.1	43.9	29.4	2.7	21.7	2.0
	47.6					
Film	59.4	48.0	39.7	16.7	29.4	12.4
	64.9					
Fibers	40.5	48.0	1.37	16.5	17.4	12.2
	61.5		22.1			

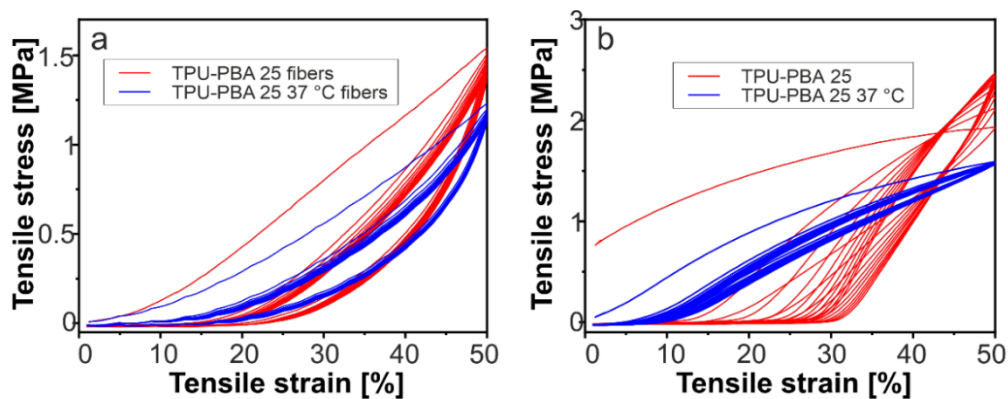


Figure S4. TPU-PBA 25 tensile stress versus tensile strain curves at 20 and 37 °C; a) Fibers; b) Films.

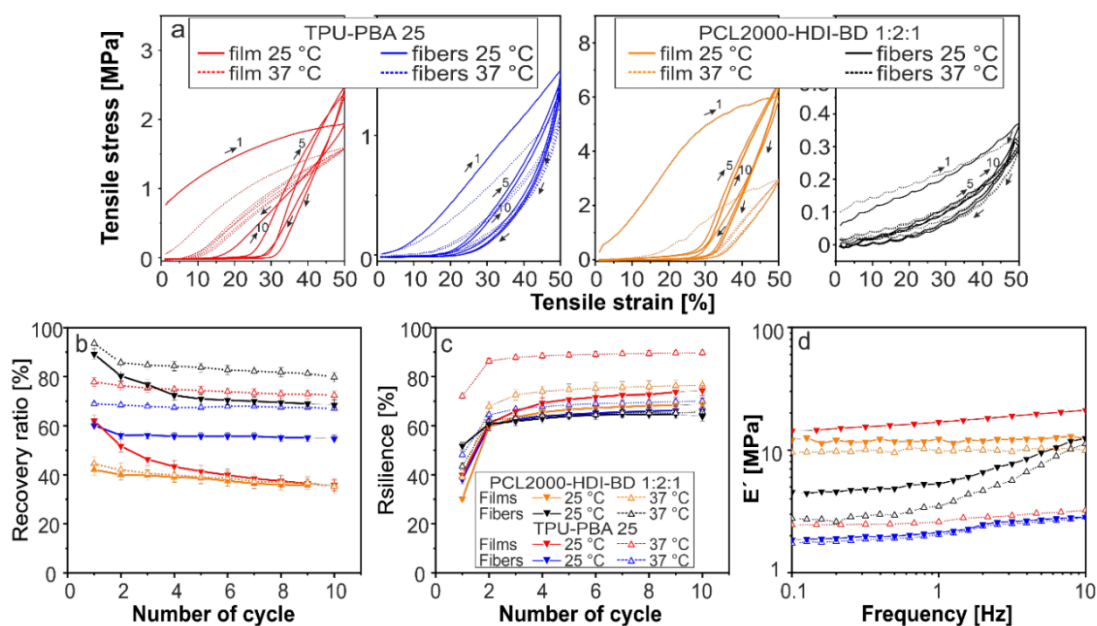


Figure S5. Mechanical properties of TPU-PBA 25 and PCL2000-HDI-BD 1:2:1 a) representative cyclic tensile test curves (1,5 and 10 cycles are shown), b) recovery ratio, c) resilience in ten cycles of loading and unloading, and d) DMA frequency sweep.

Table S3. Mechanical properties of TPU- PBA 25 in comparison with PCL2000-HDI-BD 1:2:1

Polymer	E' (DMA) [MPa]	E' (Cycle 1) [MPa]	E' (Cycle 5) [MPa]	E' (Cycle 10) [MPa]	Minim R.R.	Max resilience
TPU-PBA 25 film 25 °C	17.2	14.7	12.4	11.1	62.0	74.4
TPU-PBA 25 film 37 °C	2.7	3.9	2.5	2.3	72.4	89.7
TPU-PBA 25 fibers 25 °C	2.3	1.4	1.1	0.8	54.7	66.2
TPU-PBA 25 fibers 37 °C	2.2	1.0	0.5	0.3	67.0	70.0
PCL2000-HDI-BD 1:2:1 film 25 °C	12.1	16.8	0.73	0.39	35.7	68.8
PCL2000-HDI-BD 1:2:1 film 37 °C	9.9	9.3	0.33	0.30	35.1	76.5
PCL2000-HDI-BD 1:2:1 fibers 25 °C	6.6	0.56	0.35	0.31	68.5	64.6
PCL2000-HDI-BD 1:2:1 fibers 37 °C	4.8	0.49	0.32	0.29	79.8	65.6

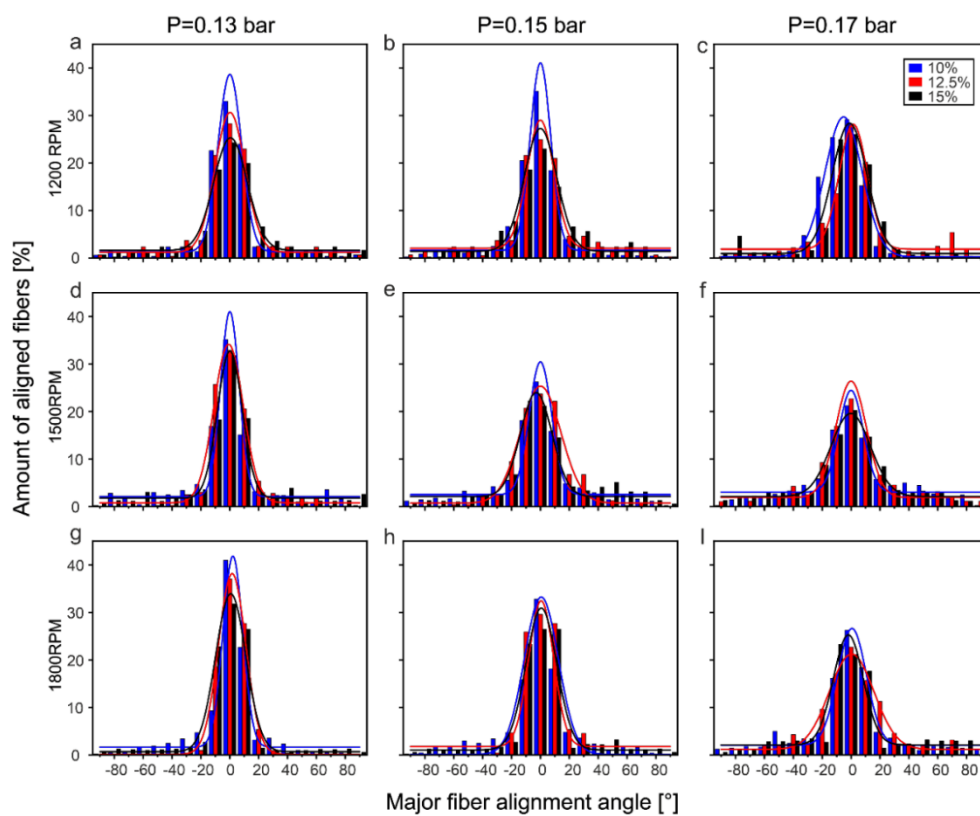


Figure S6. Major fiber alignment of fibers from different concentrations at different speed and pressures.

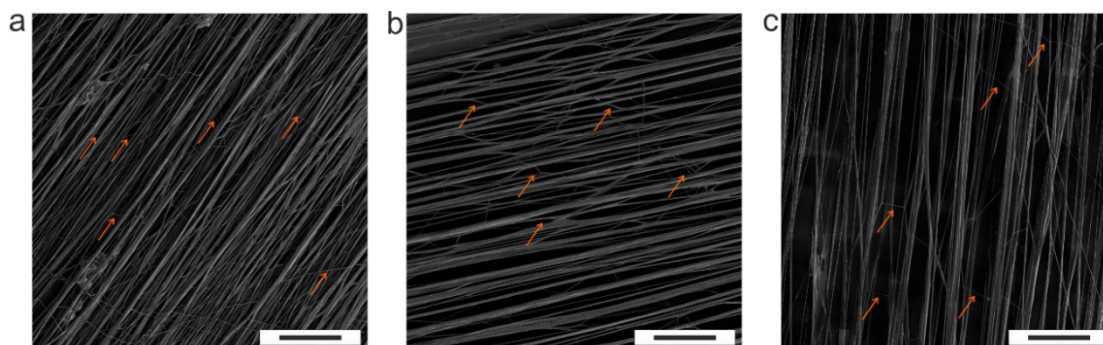


Figure S7. SEM images of touch-spun fibers, pressure 0.15 bar, speed 1500 RPM, a) 10%, b) 12.5 %, c) 15 %. Scale bars 100 μm

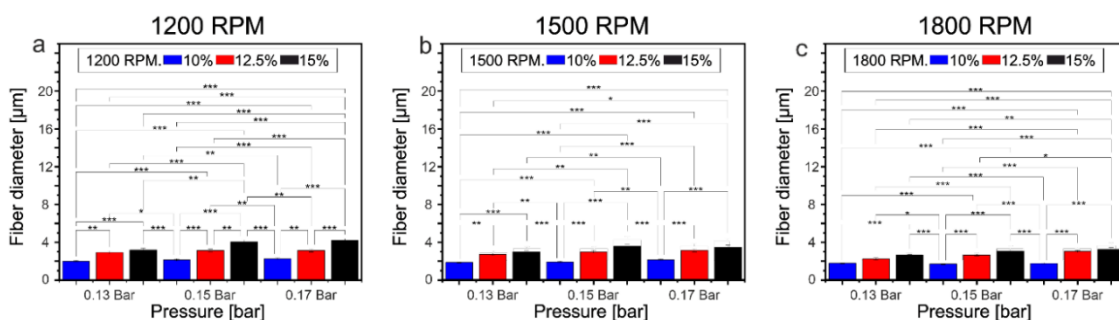


Figure S8. Fiber diameter of fibers from different concentrations at different speeds and pressures with statistics.

In vitro cytotoxicity and cell viability test

CellTiter-Blue Assay

The CellTiter-Blue® Cell Viability Assay (Promega) was used to quantitatively evaluate cell metabolic activity according to the manufacturer's protocols. An initial solution of cell culture medium and CellTiter reagent in a ratio of 10% v/v was prepared, pipetted to each of the samples and incubated at 37°C for ~2.5h. After incubation, 100μl of AB solution from each sample was pipetted on a 96-well plate and the fluorescence was recorded at 560/590nm using a plate reader (Mithras LB 940, Germany). Obtained data were used to calculate the fluorescence absorbance using three replicates for each sample. Relative cell metabolic activity was normalized to the mean of the blank culture media. Samples were evaluated, and the mean cell metabolic activity and standard deviations are reported (n = 3).

Fluorescence Imaging

Live/dead Assay was also performed on cells after the CellTiter-Blue® Assay to qualitatively evaluate their viability. A live/dead solution was prepared with 4 μM of calcein AM and 2.0 μM of ethidium homodimer in PBS. After washing the CellTiter-Blue reagent with DPBS, live dead staining solution was added to cells following by 30 min incubation at room temperature in dark prior to imaging. Next, cells were imaged using the fluorescent

microscope Leica DMI8 (Leica Microsystems, Germany) and minimum 3 pictures were obtained per sample and number of cells was calculated using the manual cell counter Plugin ImageJ. Finally, cell viability was determined by dividing the live cells to the total number of cells.

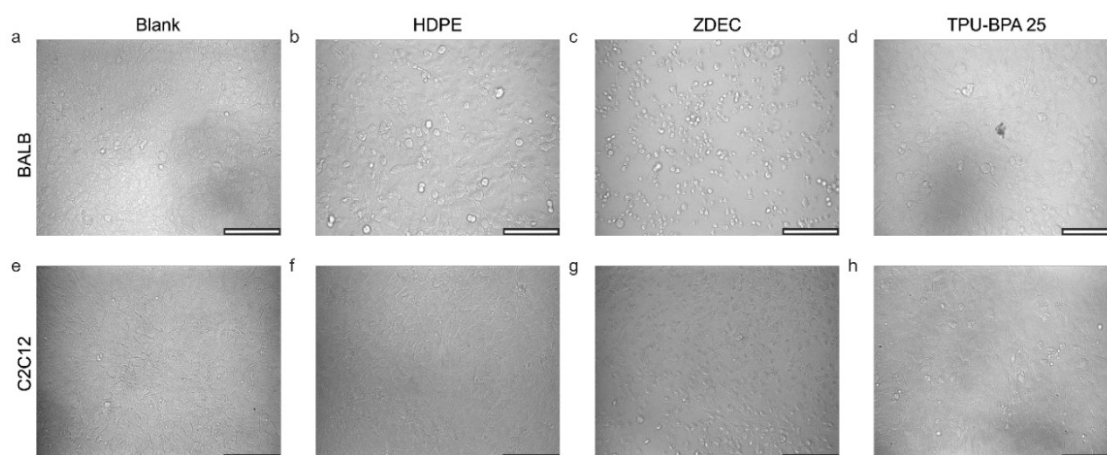


Figure S9. Fibroblasts and myoblasts morphology monitored by optical microscopy after 24 h indirect contact with TPU-PBA 25 touch-spun scaffolds a,e) blank, b,f) HDPE, c,g) ZDEC and d,h) TPU-PBA 25 touch-spun scaffolds. Normal morphology of fibroblasts and muscle C2C12 cells was seen in contact with fibrous material as well as negative control HDPE and Blank. Cells in contact with ZDEC are round shape and dead. Scale bar 15μm.

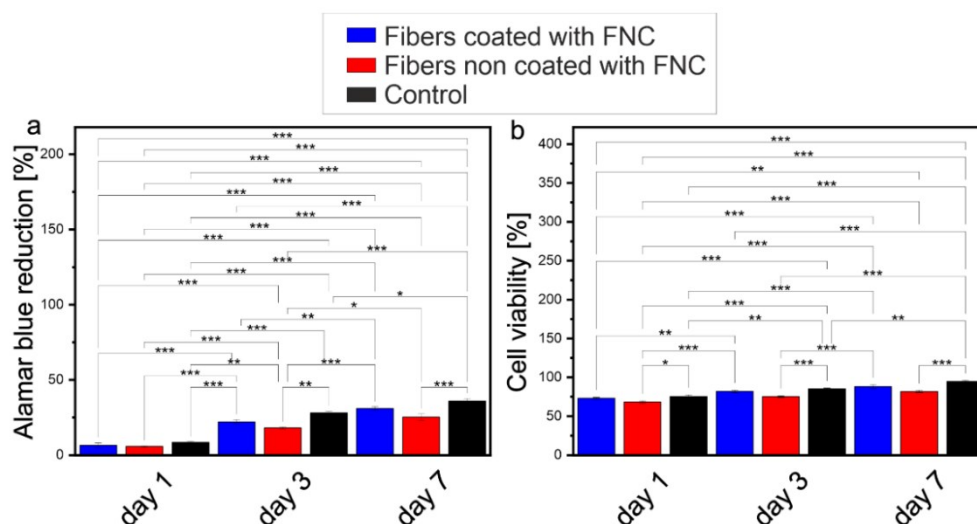


Figure S10. C2C12 myoblasts cell culture results on TPU-PBA 25 touch-spun scaffolds coated and non-coated with FNC and control, on treated cell culture plates a) quantification of

cell metabolic activity after 1, 3, and 7 days of culture measured by Alamar Blue Assay; b) quantification of cell viability (Live/Dead) after 1, 3, and 7 days of culture. * $p \leq 0.05$; ** $p \leq 0.01$; *** $p \leq 0.001$; f-i).

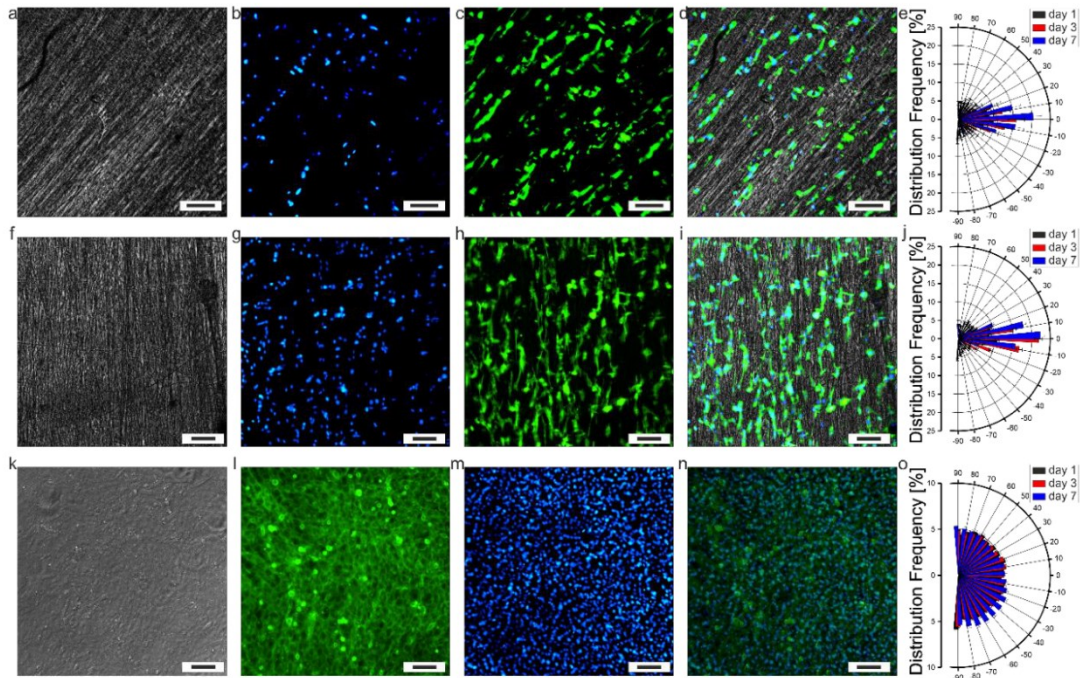


Figure S11. C2C12 myoblasts cell culture cell nuclei alignment a-d) on TPU-PBA 25 touch-spun scaffolds non coated with FNC at day 7; e) quantification analysis of cell nuclei alignment at 1, 3, and 7 days of culture. f-i) on TPU-PBA 25 touch-spun scaffolds coated with FNC at day 7; j) quantification analysis of cell nuclei alignment at 1, 3, and 7 days of culture. k-n) control, on treated cell culture plates at day 7; o) quantification analysis of cell nuclei alignment at 1, 3, and 7 days of culture. Scale bars 100 μm .

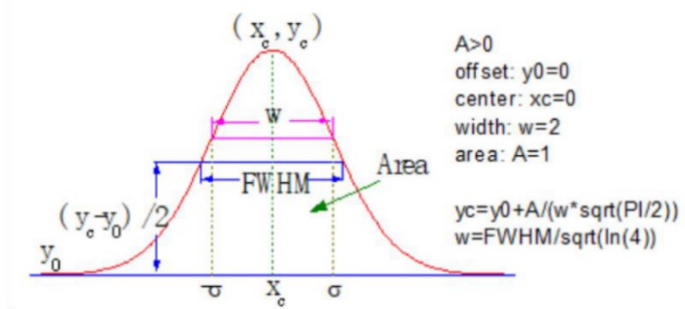


Figure S12. Gaussian fitting parameters.

Corrections Manuscript 3

Fibrous scaffolds for muscle tissue engineering based on touch-spun poly(ester-urethane) elastomer

Page 87. NMR integral position.

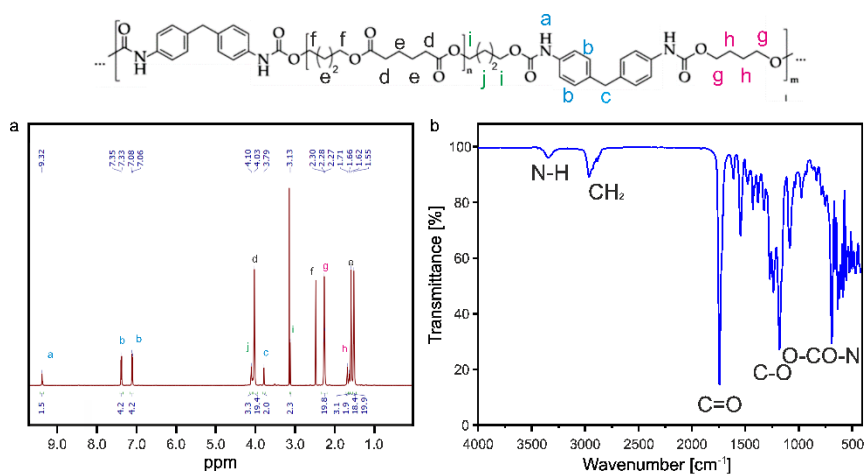


Figure 1: a) NMR and b) FTIR spectra of TPU-BPA-25 copolymer

8. Conclusion

A family of polyurethane-based copolymers were obtained, and some of them were suitable for processing and implementing into fiber production using Melt electrowriting and Touch-spinning techniques. All the obtained Polymers were biocompatible and biodegradable. They show suitable mechanical and physico-chemical properties and provide a suitable environment for cells, mimicking the ECM.

Firstly, the fabrication of shape-changing bilayered scaffolds was achieved using a combination of 3D printing and Melt electrowriting inducing shape transformation. These scaffolds allowed the growth of aligned skeletal muscle cells, providing suitable mechanical properties like the principal components of ECM.

Then, the fabrication of highly aligned soft elastic fibrous scaffolds of a family of polyester–polyurethane soft copolymers based on polycaprolactone with different molecular weights and different chain extenders using touch spinning was achieved. The tested copolymers demonstrated their potential for the engineering of muscle tissue and the construction of highly oriented fiber scaffolds, which was able to support the proliferation and alignment of muscle cells, intended for muscle tissue engineering applications.

Finally, highly aligned fibrous scaffolds that were able to mimic the structure of muscle tissues were designed and constructed by touch spinning a thermoplastic poly(1,4-butylene adipate)-based polyurethane elastomer, obtained via solvent-free polymerization. Cell culture studies proved excellent biocompatibility that enables its use for the fabrication of fibrous scaffolds allowing high cell alignment required for regeneration of anisotropic tissues as muscle tissue.

Acknowledgements

I would like to express my sincere gratitude to:

Prof. Dr. Leonid Ionov, my thesis supervisor, who gave me guidance and advice to fully comply with this project.

Dr. Sahar Salehi for her constant support and guidance in everything related to cell culture, her advice and collaboration in all the papers, as well as for her friendship. (I will miss you)

Prof. Dr. Thorsten Pretsch for his collaboration and guidance during the third paper. On this note, I would also like to thank Dennis Schönfeld for the collaboration and friendly support.

Andrés Posada for his constant help and support during the whole process. And also, for being el amigo borracho.

Diana Marcela Rodríguez porque, aunque esté perdida la esperanza y perdida la ilusión lo seguiremos intentando.

Hanin Alkhamis for her being her and making my life better.

Mi familia, mis padres Ignacio Uribe y María Piedad Gómez por su apoyo y amor, a mis hermanos Pedro Pablo- e Ignacio Uribe Gómez en la distancia por el apoyo. A mi abuela María Eugenia Brunasso, profundo amor y respeto.

Laura Milena Pedraza, por su constante apoyo siempre.

To the group members of Ionov Lab: Arpan Biswas, Indra Apsite, Amit Shukla, Gissela Katherine Constante Ibarra, Aastha Lall, Mairon Trujillo and Katharina Bauer

Especial thanks to David Sonnleitner for his friendship and support.

A mis amigos y a las personas que de alguna manera me apoyaron y creyeron en mis sueños, especialmente a Sergio González, Ricardo Duplat, José Eduardo Rueda, Camilo Navarro, Diana Martínez y Wii, entre otros. A la Universidad Nacional de Colombia sede Bogotá por todo lo aprendido en mi pregrado y maestría.

Final thanks to all the collaborators who made it possible to conduct necessary experiments for publications: Anja Caspari, Alla Synytska, Martin Dulle, Madeleine Schwarzer, especial thanks to Prof. Dr Thomas Scheibel and his group for providing Ionov's group with equipment and support at the beginning of this project and Prof. Seema Agarwal for the GPC measurements and her valuable comments and corrections on this document.

Especially to Elise Liensdorf, whose sense of humor is an oasis in the desert of my life. Her corrections and insight into my final doctoral piece were in a word, priceless. Her personal sacrifice is second to none, and the kindness of her actions are forever etched into my heart. ♡

To each and every single one of you, I am forever grateful and indebted to all of you.

(Eidesstattliche) Versicherungen und Erklärungen

(§ 9 Satz 2 Nr. 3 PromO BayNAT)

Hiermit versichere ich eidesstattlich, dass ich die Arbeit selbstständig verfasst und keine anderen als die von mir angegebenen Quellen und Hilfsmittel benutzt habe (vgl. Art. 64 Abs. 1 Satz 6 BayHSchG).

(§ 9 Satz 2 Nr.3 PromO BayNAT)

Hiermit erkläre ich, dass ich die Dissertation nicht bereits zur Erlangung eines akademischen Grades eingereicht habe und dass ich nicht bereits diese oder eine gleichartige Doktorprüfung endgültig nicht bestanden habe.

(§ 9 Satz 2 Nr. 4 PromO BayNAT)

Hiermit erkläre ich, dass ich Hilfe von gewerblichen Promotionsberatern bzw. –vermittlern oder ähnlichen Dienstleistern weder bisher in Anspruch genommen habe noch künftig in Anspruch nehmen werde.

(§ 9 Satz 2 Nr. 7 PromO BayNAT)

Hiermit erkläre ich mein Einverständnis, dass die elektronische Fassung meiner Dissertation unter Wahrung meiner Urheberrechte und des Datenschutzes einer gesonderten Überprüfung unterzogen werden kann.

(§ 9 Satz. 2 Nr. 8 PromO BayNAT)

Hiermit erkläre ich mein Einverständnis, dass bei Verdacht wissenschaftlichen Fehlverhaltens Ermittlungen durch universitätsinterne Organe der wissenschaftlichen Selbstkontrolle stattfinden können.

.....
Ort, Datum, Unterschrift